ESL-TR-88/06-04

DETERMINATION OF THE TRANSIENT RESPONSE CHARACTERISTICS OF THE AIR-SOURCE HEAT PUMP DURING THE REVERSE CYCLE DEFROST

Final Report
(DRAFT)

ASHRAE PROJECT
479-TRP

June 1988

Dennis L. O'Neal
N.K. Anand
Kurt T. Peterson
Steven Schleising

Energy Systems Laboratory
Department of Mechanical Engineering
Texas A & M University

GLOSSARY OF TERMS

AMCA	Air Movement and Control Association
ARI	Air Conditioning and Refrigeration Institute
ASHRAE	American Society of Heating, Refrigerating and Air Conditioning Engineers
ASME	American Society of Mechanical Engineers
btu	British thermal unit
cfm	Cubic feet per minute
COP	Coefficient of performance
DB	Dry bulb
DOE	Department of Energy
DP	Dew point
EEV	Electronic expansion valve
FSO	Full scale output
lbma	Pounds mass of dry air
NBS	National Bureau of Standards
ORF	Orifice
pt	point
RH	Relative humidity
SAE	Society of automotive engineers
SHSC	Superheat/subcooling
T-accum	Accumulator temperature
TC	Thermocouple
Tsat	Saturation temperature
TXV	Thermal expansion valve
wg	Water gauge

TABLE OF CONTENTS

CHAPTER 1

INTRODUCTION

The residential air-source heat pump is an air conditioning unit that has been modified to transfer heat in two modes. During the summer, the heat pump performs the same job as an air conditioner. In the winter, the heat pump extracts heat from the cold outside air and releases the heat inside the living space. The popularity of the heat pump has come from the fact that it can transfer over three times the energy that it consumes and save the consumer utility dollars over electric resistance heating.

The increasing costs of electricity during the seventies and the threat of Federal efficiency standards encouraged manufacturers to improve the efficiency of heat pumps as well as other residential appliances. Research in the 1970's led to the development of steady state heat pump computer design models that have been used to greatly improve the heat pump's steady state efficiency. While the understanding of steady state performance has greatly improved, the heat pump transient effects, which include cycling, frosting of the outdoor coil, and defrosting of the outdoor coil, are much more difficult to characterize and are still not well understood.

The objectives of this research were to: (1) characterize the reverse cycle defrost of the air-to-air heat pump and (2) examine the effect of different expansion devices on the performance of the heat pump during the defrost cycle.

The investigation consisted of a literature review and an experimental phase. In the literature review, relevant literature on the defrost cycle and transient performance was summarized. During the experimental phase, a test setup was constructed which contained a nominal 3-ton capacity residential air-to-air heat pump. Refrigerant temperature and pressure measurements were made throughout the system as well as refrigerant flow rates, air-side capacity, compressor/outdoor fan power and refrigerant level in the accumulator. Modifications were also made on the heat pump to allow for easy switching of defrost cycle expansion devices without shutting the system off. System parameters and testing procedures were documented to ensure the

experimental results were reproducible. Selection of the expansion device for the focus of this research was done after receiving input from an advisory committee from The American Society of Heating, Refrigerating, and Air-conditioning Engineers (ASHRAE).

A literature review was performed to identify the present state of research in the area of transient heat pump performance and establish the need for further research. A summary of the literature is contained in Chapter 2. Chapter 3 presents a complete description of the experimental setup and procedures used to collect the required data. The results of the research are presented in three parts starting with the analysis of the base case test in Chapter 4. Chapter 5 contains the comparison of TXVs with different response times. Chapter 6 provides a description of the performance using orifices of different diameters. The analyses in Chapters 4 through 5 included the "macro" features of the heat pump such as power usage, capacity and cycle times and a more detailed analysis of system characteristics such as temperature and pressure fluctuations, suction and discharge pressures, and refrigerant flow. Finally, conclusions and recommendations from this research are presented in Chapter 7.

CHAPTER 2

LITERATURE REVIEW

One of the key features of the reverse cycle defrost is that it is a transient process that occurs in the heat pump. Because of the general lack of relevant literature directed at the reverse cycle defrost, it was decided to also examine other literature that may deal with the transient startup of both heat pumps and air conditioners. The available literature was divided into five general categories: (1) Performance Measurement, (2) Transient Performance, (3) Cycling Losses, (4) Frosting Performance, and (5) Defrost Performance. Each topic is discussed below.

Performance Measurement

Heat pump efficiency is measured by taking the usable heating effect and dividing it by the work input. This is called the Coefficient of Performance(COP)[1]. Until 1979, published heat pump heating performance was based solely on the capacity and COP measured at the operating conditions of 47^{o}F and 17^{o}F outside temperature with an indoor temperature of 70^{o}F[2]. This rating method enabled all heat pumps to be compared on a common basis. However, there was no provision for comparing heat pumps on a seasonal energy basis, which would include cycling, frosting, and defrosting losses.

During the mid and late 70's the National Bureau of Standards(NBS)[3] conducted extensive tests on residential heat pumps. Their tests revealed two transient effects that significantly degrade heat pump performance: (1) cycling effects and (2) frosting effects on the outdoor coil. The NBS work led to the development of a new rating procedure that included transient losses due to both cycling and frosting/defrosting losses.

Several researchers have run experimental tests on heat pumps to determine the amount of degradation caused by transient characteristics. Baxter, et al[4], arrived at the degradation losses from cycling and frosting/defrosting of 20% and suggested it could be as high as 40% in warm weather. Wildin, et al[5], arrived at losses from defrosting of 2 to 5%, while Goldschmidt and Hart[6] found losses of 5% for cycling and less than 3% for frosting.

Finally, Bittle and Goldschmidt[7] found a 1 to 2% loss from frosting and a 2 to 17% loss for cycling. There is a wide variation in results. Bittle[7] concluded that the contradictions in the available data can not be resolved without more information from each of the individual investigations.

Transient Performance

A typical heat pump heating cycle during startup, frosting, defrosting, and defrost recovery is shown in Figure 2.1 [8]. The performance approaches steady state for a short period, but its overall operation is far from steady state. Baxter and Moyers[8] monitored a resident for eight winter months. They divided the seasonal energy consumption into the separate steady state and transient components of the heat pump cycle as shown in Table 2.1. They showed that

Table 2.1 - Breakdown of seasonal energy use in the air-to-air heat pump in Reference 8.

Condition	% Energy Use
Steady state	74.3
Transient state	25.7
* Defrost cycle w/o temp.	10.2
* Cycling (Start-up)	8.5
* Frosting of coil	3.7
* Off-cycle parasites	3.3

over 25% of the energy used for heating the house was used during transient conditions when the heat pump performance was low. Figure 2.2 is a plot showing how each of the transient losses affect the COP of the heat pump at different outdoor temperatures. The plot shows how the shape of the COP curve changes as each individual transient effect is considered. The top straight line is the COP

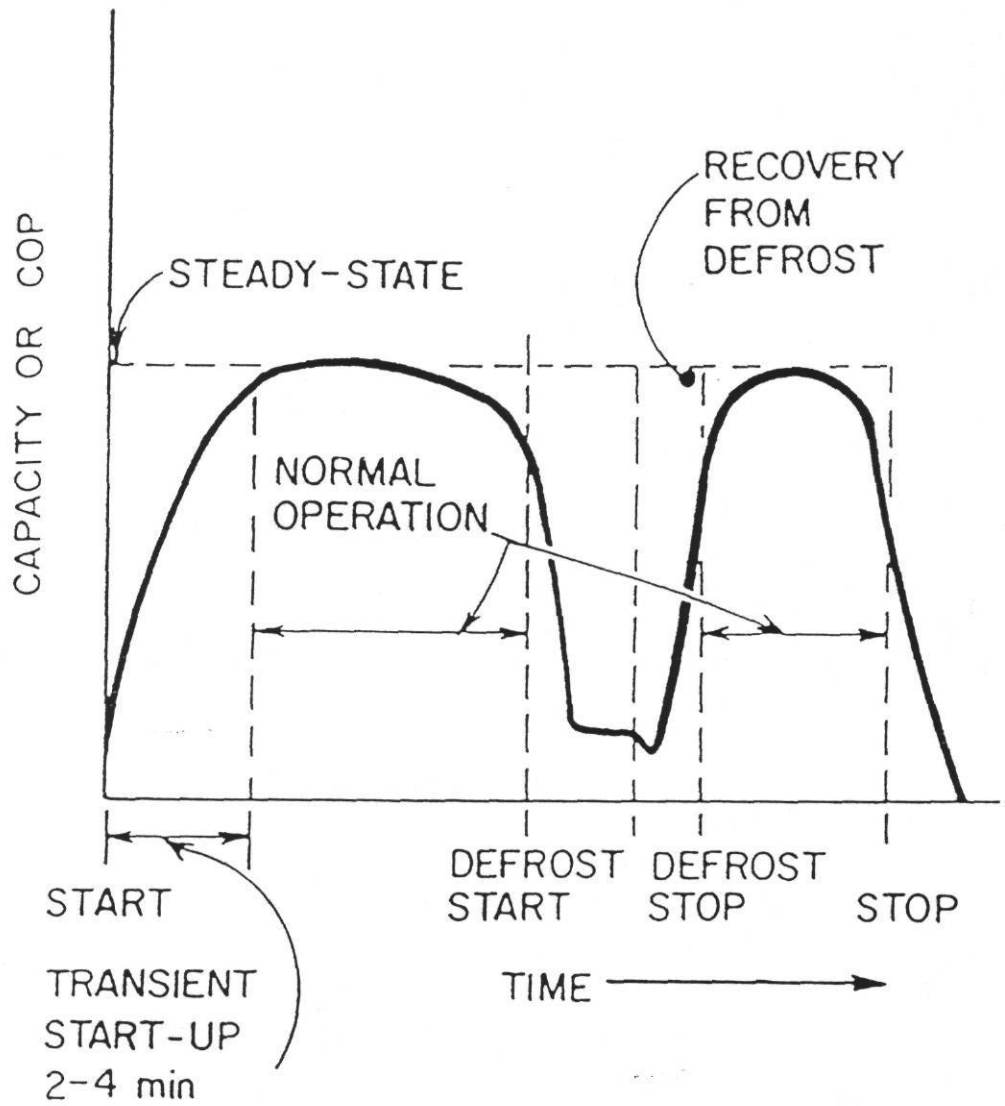

Figure 2.1 - Typical heat pump heating cycle with a defrost [8]

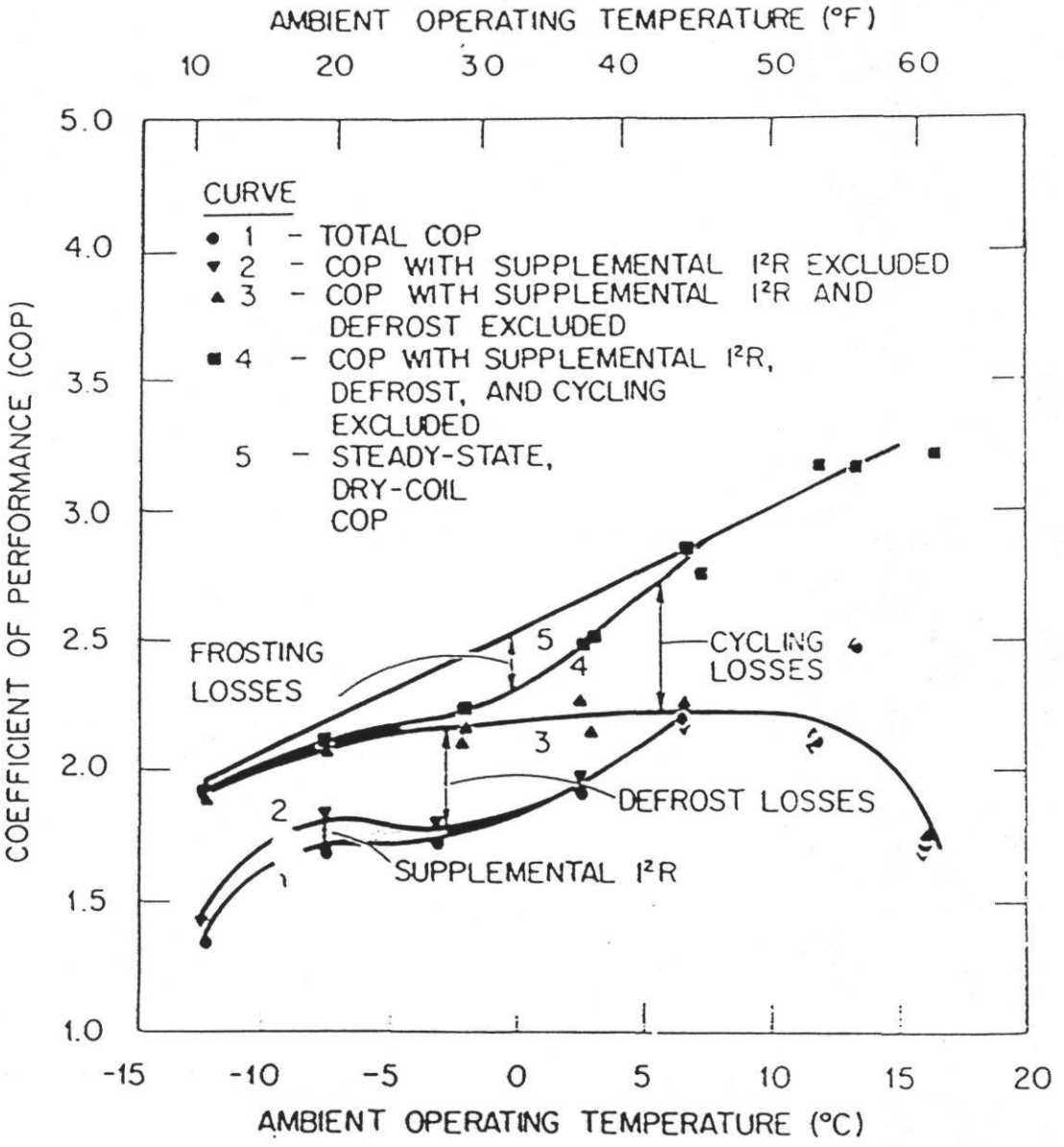

Figure 2.2 - Effect of transient losses on the heating COP of a heat pump [8]

curve for a steady-state dry coil. Frosting losses decrease the COP in the temperature range from about 15°F to 40°F. Cycling losses increase as the outdoor temperature increases and the unit becomes oversized for the heating load. Finally, as the temperature drops below 40°F, defrosting causes further losses.

Cycling Losses

Efficiency losses occur in a heat pump during startup and shutdown. Examining the sources of losses during startup may provide some understanding of the losses that occur during the defrost cycle after the reversing valve has been engaged.

One of the major variables affecting these losses is the location of the refrigerant in the system either right before startup or shutdown. When a heat pump is running at steady state, the refrigerant is not equally distributed throughout the system. The location of the refrigerant depends on the outdoor and indoor ambient conditions, the amount of refrigerant charge in the unit, and the components used in the system. For instance, in the heating mode for those units containing a suction line accumulator, some investigators have found that over 60% of the refrigerant is located in the condenser and accumulator[9],[10].

As the unit shuts down, the pressure is allowed to equalize through the compressor and the TXV. During the winter months, the outdoor coil is much colder than the indoor coil so most of the refrigerant migrates to the outdoor coil. A recent study by Mulroy indicated that when the unit is restarted, the refrigerant fills the accumulator and is trapped there as the accumulator slowly dispenses it back into the system[11]. He concluded that[11]:

> "...for units allowing migration of refrigerant during the off-cycle and which have accumulators, the primary source of cyclic performance loss after the first minute of operation is the result of refrigerant being trapped in the accumulator. The [heat pump] unit will not reach steady state until the accumulator level has been reduced to its steady state value..[Page 815-6]"

Mulroy's results indicated that during the summer, the warmer outdoor temperatures help boil off the refrigerant from the accumulator[11]. However, during the heating season, the colder outdoor temperatures cause the unit to take over 20 minutes before it reaches steady state after startup. Because the accumulator can store a relatively large mass of refrigerant, it effectively creates a thermal lag in the system during startup.

Mulroy[11] eliminated all cycle migration by installing solenoid valves in the refrigerant lines. The unit was able to reach 90% of capacity in about 3 minutes instead of close to 15 minutes when migration was allowed. Young[12] recommended a heat exchanger be attached to the accumulator that would draw heat from the liquid line before the expansion valve and speed up the transient process. A reduction in system volume will also speed up the transient response of the unit as there will be less refrigerant trapped in the accumulator[11].

Frosting Losses

The only reason a heat pump undergoes a reverse cycle defrost is to eliminate frost that has built up on the outdoor evaporator during heating operation. To extract energy from the outdoor air, the outdoor coil must be at a lower temperature than the outdoor air. If the temperature of the coil is below the dew point of the outdoor air and also below $32^{o}F$, then moisture will condense on the coil and freeze. As the frost builds on the coil, the pressure drop across the coil increases. The frost acts as an insulating layer between the cold heat exchanger surface and the relatively warm, moist air. As the pressure drop increases, the airflow produced by the outdoor coil propeller fan decreases. This decrease in airflow reduces the capacity of the evaporator and the capacity of the heat pump. Eventually, the performance of the heat pump is reduced enough that the unit must be defrosted to return the heat pump to peak performance.

Miller[13] found the conditions that will promote frosting of the outdoor coil are when the outdoor temp is between $17^{o}F$ and $40^{o}F$ and the relative humidity is greater then 70%. Figure 2.3 shows typical results of heat pump performance during frosting conditions. At outdoor

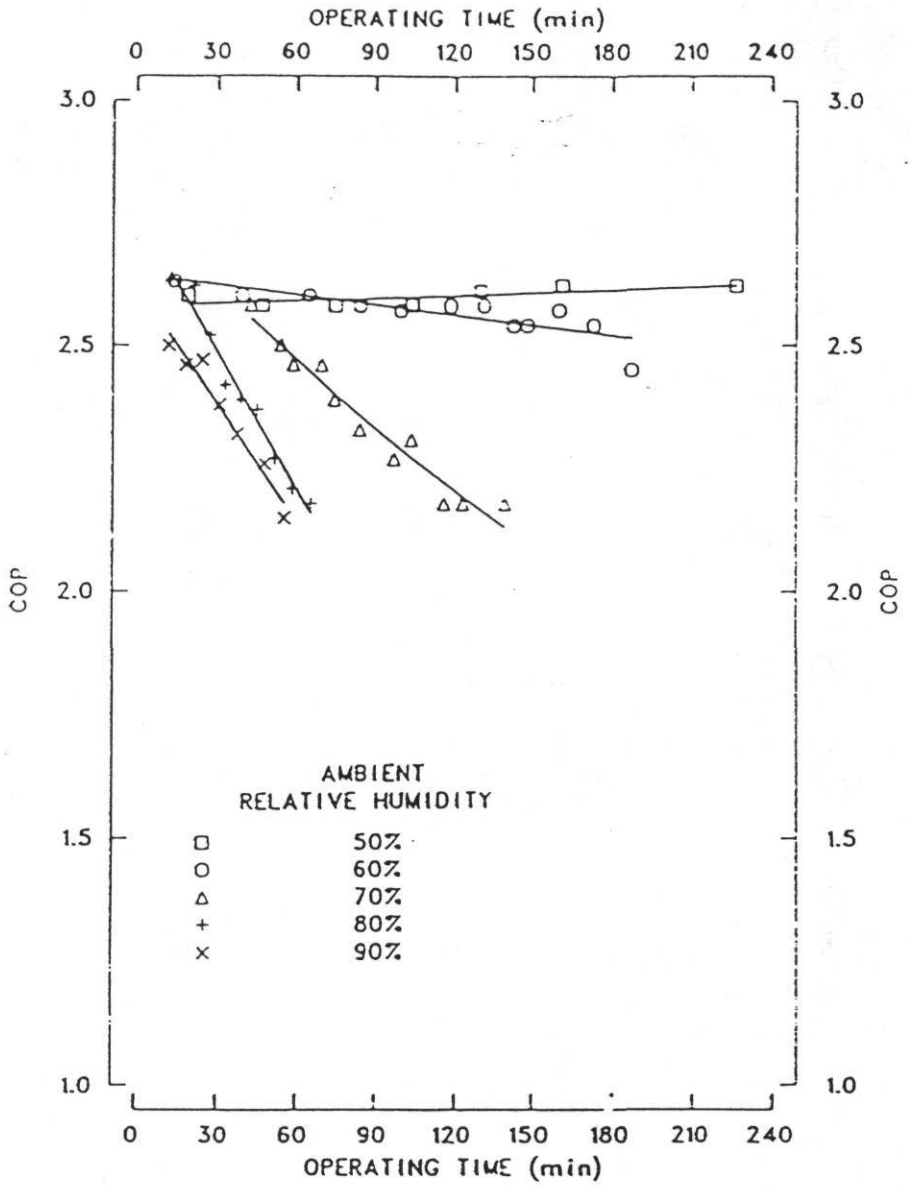

Figure 2.3 - COP of a heat pump measured at 35 F [13]

conditions of 35°F DB, frosting is not evident until the humidity rises to 70% RH and then the frosting rate steadily increases with humidity.

Defrosting Losses

Frost accumulation on the outdoor coil of the heat pump degrades it's performance by insulating the coil and reducing the airflow through the coil. Restoring the heat pump's performance is accomplished with the use of a reverse cycle defrost. The reverse cycle defrost is a procedure that switches the condenser and the evaporator from the heating mode where the outdoor coil is the evaporator to the cooling mode where the outdoor coil is now the condenser. The hot gas which was being pumped into the indoor coil to heat the house is now, during the defrost cycle, pumped into the outdoor coil to melt the frost off of the coil. When the ice is melted from the outdoor coil the heat pump is switched back to heating and resumes normal operation. During the defrost cycle, the heat pump removes heat from the house to melt the ice on the outdoor coil. This cooling effect must be offset by resistance electric heaters which are mounted in the indoor air handler. The electric heaters have a COP of 1, which is typically less than half as efficient as the heat pump, so the overall COP of the heat pump decreases when the heaters are used. Thus, the fewer times and more efficiently the unit can be defrosted, the less energy will be consumed during the defrost cycle.

A recent study on defrost cycle losses was conducted by Young[12]. One of the purposes of his study was developing an "efficient and dependable means of defrosting the outdoor coil..p.671"[12]. He conducted tests on two specially constructed heat pumps. Some of the features of the first heat pump included:

* Nominal heating capacity of 2.5 tons,
* Outdoor coil had fin density of 8 fins/inch,
* Outdoor fan was 3 blade propeller unit, belt driven,
* Electric expansion valve in heating mode,
* Outdoor coil was horizontal,
* Defrost cycle refrigerant control: capillary tubes,
* Condenser outlet had receiver,
* Reversing valve: sliding port,

* Accumulator had heat exchanger (exchanged heat from the outlet of the condenser before expansion device),
* Compressor was indoors,
* Defrost initiation: Demand, based on outdoor fan current.

The second heat pump was a modified version of the first heat pump. The key modifications included:

* Larger compressor (2.75 tons vs. 2.25 tons),
* Outdoor fan was 4 blade propeller unit, direct drive,
* Outdoor coil was at 45°F angle,
* Defrost cycle refrigerant control: large orifice valve,
* Reversing valve replaced with four solenoid valves.

Young claimed that an accumulator heat exchanger enhances the transient response of the heat pump following defrost reversal or system startup[12]. However, nowhere in his paper were data provided on how much it improved the transient response of the unit during the defrost cycle. Data on how much faster the accumulator emptied, effect on defrost time, energy use, etc. would have been useful. The heat exchanger may be one area for further investigation.

An important piece of equipment affecting the length of the defrost cycle in Young's study was the defrost cycle expansion device. By installing a larger defrost orifice than the normal cooling mode capillary tubes, he was able to produce a 30% reduction (almost 1 minute) in defrost cycle time[10]. Young did not give any data on the size of the capillary tubes or orifice he used. The larger orifice almost eliminated the suction pressure drop at the beginning of the defrost cycle and allowed a higher mass flow rate and heat delivery to the outdoor coil. He recommended the installation of a separate expansion device for reverse cycle defrost rather than using the cooling mode device.

Young also found that the common sliding port reversing valve degraded the performance of his first heat pump by as much as 10%. These losses occured from both heat and mass leakage from the high side to the low side of the system. It was not apparent from the study whether this valve was exceptional or typical of reversing valves. He was able to eliminate the losses by installing multiple solenoid valves in the second heat pump.

For the heating mode, Young[12] used an electric expansion device that was opened wider during the recovery period following defrost. This shortened the recovery time to steady state by 50%.

Both of the units that Young tested were significantly different than most heat pumps currently found on the market. For instance, one unit had a horizontal outdoor coil and the other had a 45 degree angle tilt. Most manufacturers use a vertically mounted outdoor heat exchanger. This difference meant that his units probably drained water from the melted frost faster than current models. His outdoor coil had only 8 fins/inch which was significantly less than the 14 to 20 typically found on units sold today. Because of the wider fin spacing, one would expect Young's units to go longer before defrosting. Thus, it appears that caution should be used when trying to extend his results to units currently made by many U.S. manufacturers.

Young's paper provided some excellent ideas on ways to improve performance during the defrost cycle. However, in general he did not quantify how each piece of hardware affected system dynamics during the defrost cycle.

Another recent study of the heat pump reverse cycle defrost was published by Miller[10]. His purposes included: (1) gaining a better understanding of the physical processes that occur during the frost/defrost cycle and (2) quantifying the losses during the cycle. All of Miller's work was conducted on a single heat pump whose primary characteristics included:

* 2.75 Ton nominal capacity,
* Split system,
* Plate fin heat exchanger,
* Liquid line- suction line heat exchanger (only active during heating cycle)
* Suction line accumulator,
* Outdoor coil fin density of 14 fins/inch,
* Demand defrost initiation (based on 0.51 inches WG pressure drop across the outdoor coil),
* Capillary tube expansion during defrost cycle and heating mode,
* A-frame style Indoor coil with 3 tube rows,
* Sliding port reversing valve.

Miller collected system data such as instantaneous capacity and power as well as component data such as

instantaneous temperatures and pressures at different locations throughout the system. While he collected data at a variety of outdoor temperatures and humidities, most of his published frosting/defrost data was at an outdoor air temperature of 35°F and relative humidity of 70%. While the data at those conditions may be useful from a qualitative perspective, it would have been more useful if data had been published for the DOE/ARI heavy frosting tests which are at 35°F and 80% relative humidity. Another possible limitation of his data was that the unit used capillary tubes for the expansion device. Many of the units currently manufactured use either thermal expansion valves or orifices.

For the 35°F, 70% relative humidity conditions, Miller's heat pump ran approximately 2 hours before defrost was initiated[10]. His defrost cycle lasted approximately 7 minutes (Figure 2.4). At defrost initiation, Miller estimated that 50% of the refrigerant was in the indoor coil. However, he based this estimate on previous steady state weight measurements and not measurements made immediately before defrost initiation. Also, conditions were not specified for his previous weight measurements. Pressure measurements across the capillary tubes indicated that there was no refrigerant flow in the system for approximately 1.5 minutes after defrost initiation. The units capacity dropped close to zero in the first 30 seconds, then increased about 4000 Btu/hr for approximately a minute, then decreased until reaching a maximum cooling capacity at 6.5 minutes (Figure 2.5). He stated that after 30 seconds of defrosting, the indoor coil held only low-pressure vapor. Miller's unit took approximately 5 to 6 minutes to completely melt the frost from the outdoor coil.

While he published the temperature exiting the outdoor coil, it was not clear from his paper whether this temperature was the average of all the circuits leaving the coil, or the temperature of the circuit used to determine when defrost should be terminated. Some manufacturers monitor the temperature on a specific circuit (usually the bottom) on the outdoor coil to determine when the defrost cycle should be terminated. For Miller's unit, defrost was terminated when the exiting refrigerant temperature from the outdoor coil reached 75°F

Trask[14] recommended taking the accumulator out of the line between the reversing valve and compressor and mounting it between the reversing valve and the outdoor coil. A check valve mounted at the accumulator would channel the refrigerant through the accumulator in the heating mode, but

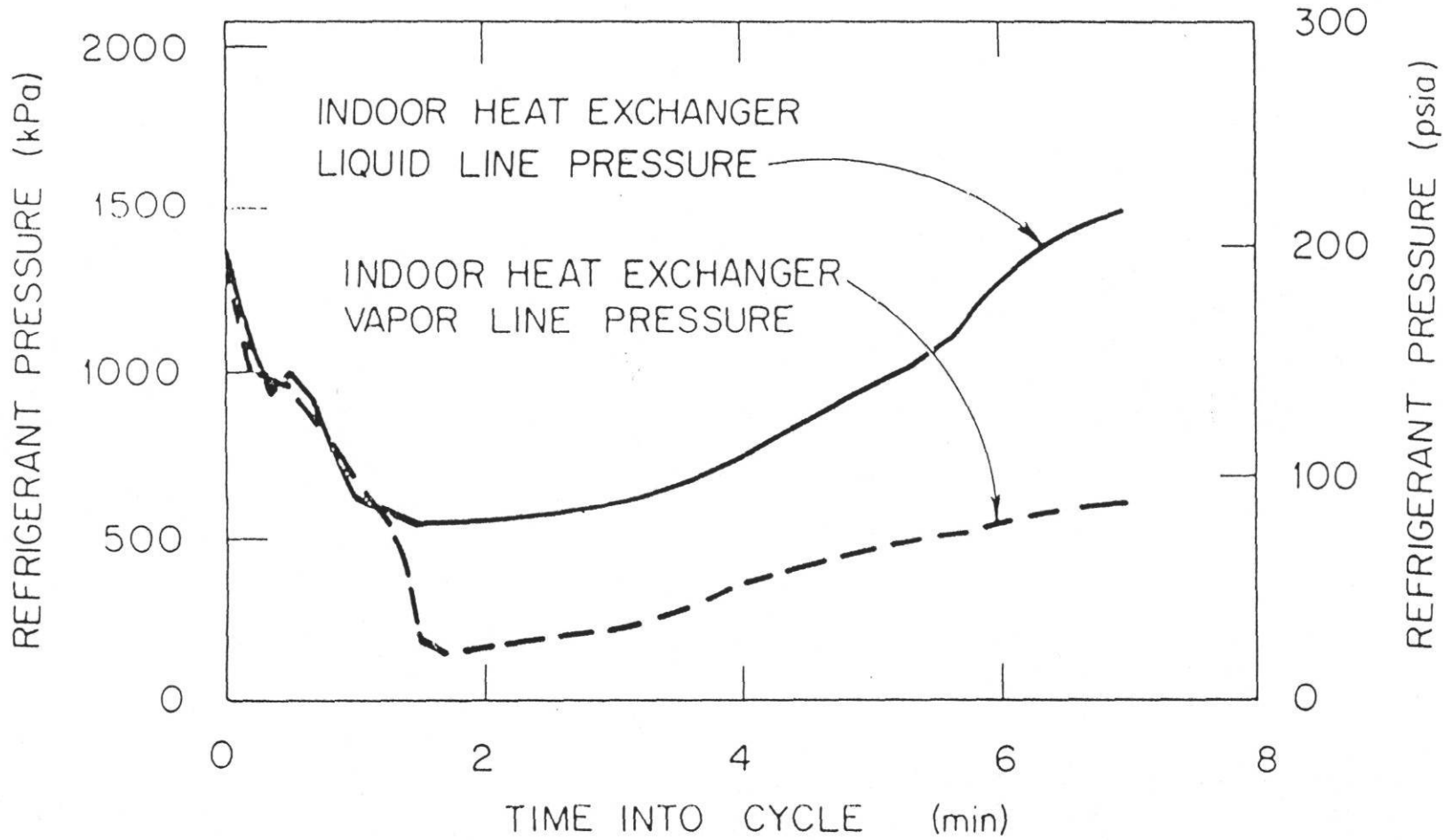

Figure 2.4 - Pressure drop across the capillary tubes for Miller's heat pump during the defrost cycle [10]

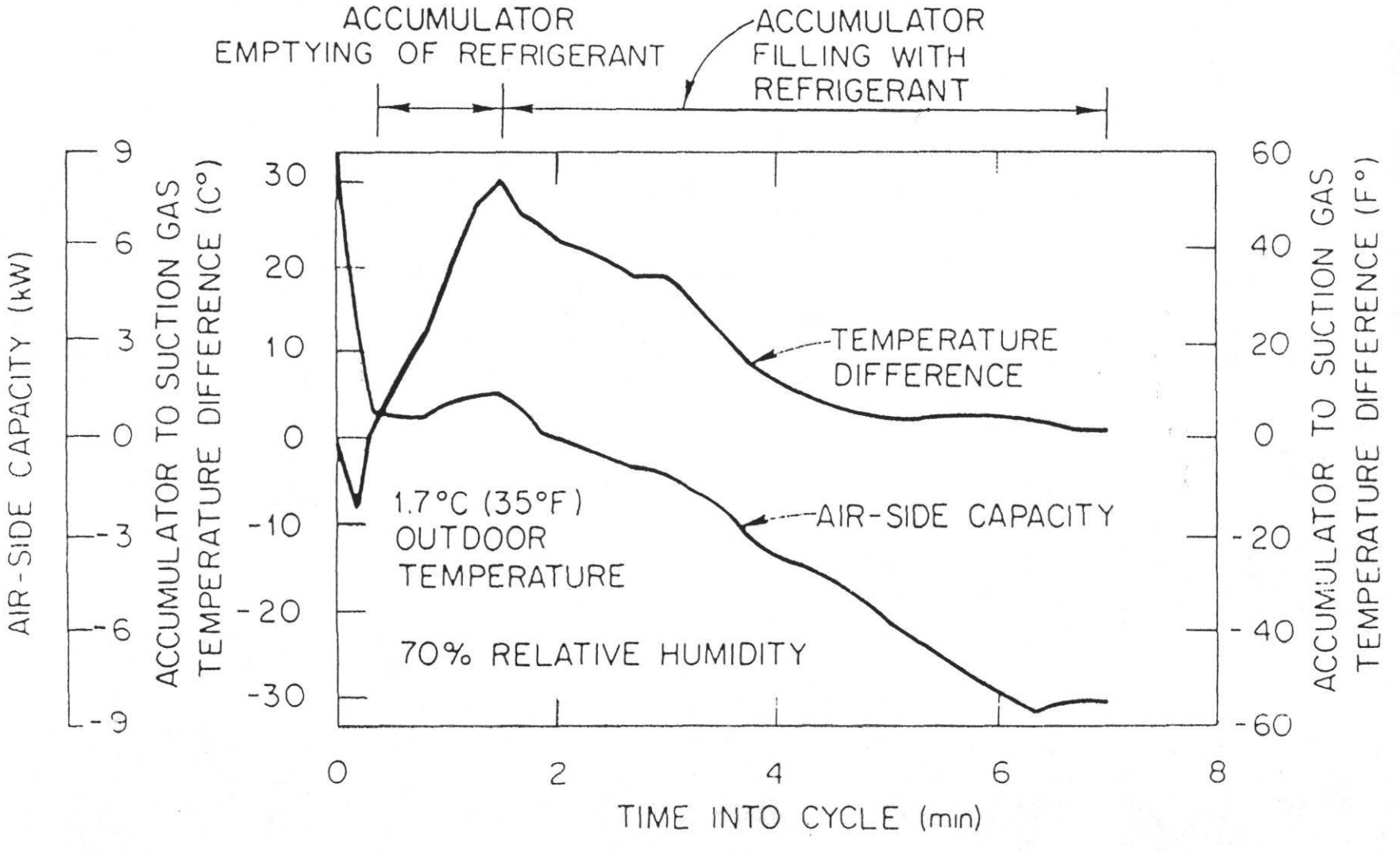

Figure 2.5 - Capacity and accumulator to suction gas temperature difference for Miller's heat pump during the defrost cycle [10]

upon defrost initiation, the hot gas would bypass the accumulator and go directly into the compressor. He claimed this would keep the refrigerant from being cooled down by the accumulator and allow more heat directly into the outdoor coil. As the pressures in the indoor coil drop below 40 psi, Trask recommended using a constant pressure valve to bypass the cooling TXV, allowing refrigerant to flow freely to the indoor coil. Trask claimed the valve would help prevent the large accumulation of refrigerant in the outdoor coil and the subsequent flushing of refrigerant into the accumulator.

Currently, there are two basic methods of controlling when and how long the heat pump is in the defrost mode[15]. These methods are the time-temperature defrost control and the demand defrost control. The time-temperature defrost control is energized when the entering refrigerant to the outdoor coil drops to approximately 30°F. When energized, a timer which can be set for 30,45, or 90 minutes is started and the unit will defrost after each timer interval. After energizing the defrost cycle, the controller senses the leaving refrigerant temperature and terminates the cycle when it rises to approximately 65°F or after ten minutes whichever comes first.

The second control is the demand defrost control which senses the unit's operating conditions and initiates defrost when the conditions indicate heavy frosting. A common demand defrost controller monitors the ambient outside air temperature and the outdoor coil temperature. The manufacturer runs tests on a certain unit and monitors the combinations of air-coil temperatures that occur when defrosting is required. This information is programed into the controller and defrost is initiated when those conditions are met. Termination of the cycle is accomplished in the same manner as the time-temperature defrost.

Baxter and Moyers[8] monitored a residential heat pump with time-temperature defrost controls for two years. They used the temperature and humidity frosting criteria developed by Miller[13] to track the total number of unit defrost cycles and how many of the cycles occurred when there was potential for frosting. The results of their survey showed that 27% of a total of 665 defrost cycles occurred when no frost was on the coil. Baxter and Moyers recommended using demand defrost to cut down on the useless defrost cycles.

Summary

There are many system components and operating conditions that affect the transient characteristics of a heat pump. The suction line accumulator, because of its ability to store large quantities of refrigerant, apparently slows down the startup process. The result is larger transient losses in the system. From the visual observation made by Miller[10], much liquid refrigerant is contained in the accumulator immediately after the reverse cycle defrost. With the accumulator full of refrigerant, the heat pump remains undercharged until the refrigerant is fed back into the system[11]. By the addition of a heat exchanger in the accumulator, Young claimed a reduction in time to get the refrigerant out of the accumulator[12]. The accumulator (or lack of one) appears to be one area for possible further investigation.

Another system component that appears to have a significant effect on performance during defrost was the defrost cycle expansion device[12,14]. In particular, Young found that increasing the expansion device size decreased the defrost time. Miller's unit, which had capillary tubes, experienced no refrigerant flow for approximately 1.5 minutes after defrost initiation. This condition could possibly be due to the size of the capillary tubes. A systematic study of expansion device size and its effect on system performance should be performed.

Two significant limitations to the work published to date are: (1) the uniqueness of each experiment and (2) the general lack of adequate documentation to be able to reproduce the researchers experiment. Young's[12] experiments were conducted on "prototype" laboratory constructed heat pumps. The components (8 fin/inch heat exchanger, liquid receiver, etc.) were constructed in such a manner that they were not typical of current practice in the industry. Unfortunately, even an experiment conducted on a unit more typical of what is currently sold on the market would have unique features that were installed by the manufacturer of the unit. For instance, an experiment on a unit with a suction line accumulator would provide results that may differ from the performance of units that do not use an accumulator. This factor would point toward the need for a series of experiments that would include multiple

units having features used by a majority of industry. This type of study would provide results to separate trends that are equipment specific and those that are generic to the defrost cycle.

The second limitation was mentioned several times in discussing results from various researchers. If a researcher does not adequately document his experiment, it makes it difficult for the next investigator to compare results. Bittle[7] was cognizant of the lack of documentation as she attempted to explain the large variation in results from different investigators.

CHAPTER 3

EXPERIMENTAL APPARATUS

The preceding literature review suggested a need for characterization of the transient response of the air-source heat pump during the reverse-cycle defrost. The objective of the work described in the following chapters was to provide such a characterization by taking performance data from a series of repeatable experimental tests on a test heat pump. These tests were to yield a general representation of factors affecting performance of a typical residential heat pump during frosting/defrosting cyclic operation.

Data required by the experimental study included pressures and temperatures of refrigerant throughout the refrigerant circuit of the test heat pump; flow rate of the refrigerant during testing; flow rate, temperature, pressure, and humidity conditions of air flowing across the heat exchangers of the test heat pump; and power consumption data for the heat pump. To achieve the experimental objective, a test facility was established and experimental procedures developed. Both the test facility and experimental procedure are discussed in detail in this chapter. The experimental procedure included experimental conditions, a refrigerant charging procedure and testing procedure.

Test Facility

A general description of the test facility is first given. The four major components of the facility are then described in detail: the psychrometric rooms, the test heat pump, heat exchanger test sections and data acquisition reduction system.

The test apparatus was located in the psychrometric rooms of the Energy Systems Laboratory at the Texas A&M University Research Annex. The placement of the test equipment within these rooms is shown in Figure 3.1. The psychrometric rooms simulated the indoor and outdoor conditions (temperature and humidity) necessary for heat pump performance testing.

The indoor test section consisted of the indoor coil and the indoor air flow chamber. Conditioned air from the indoor room at 70^{o}F DB and 20% relative humidity(RH), was drawn through the indoor test section by the air flow chamber fan. The air flow chamber, which was used to measure the air flow through the test section, had a damper

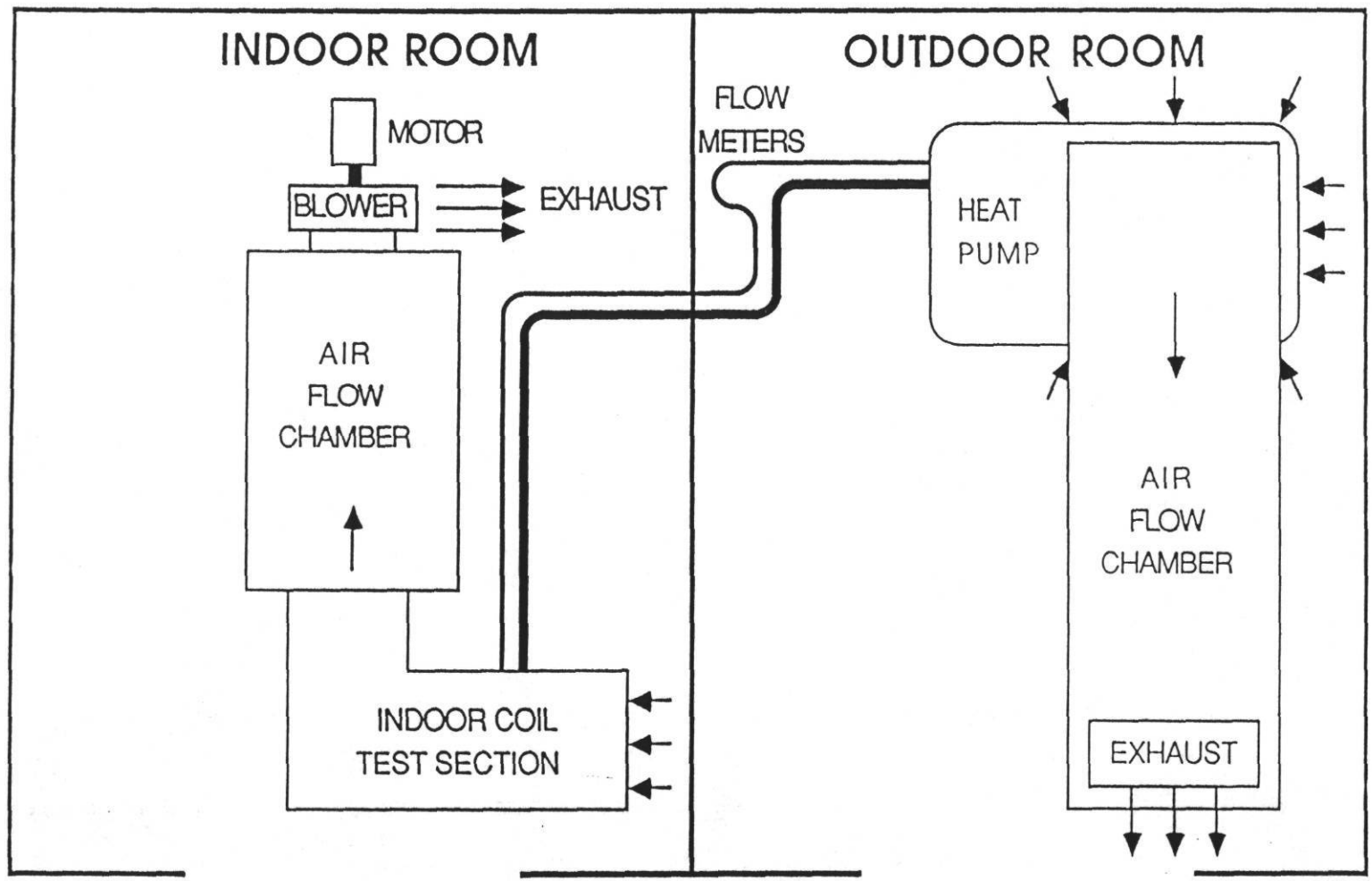

Fig. 3.1 Placement of the Test Heat Pump in the Psychrometric Rooms

mounted on the outlet that was adjustable and was set to maintain a constant air flow of 1250 cfm through the indoor test coil. The air was routed back into the indoor room after leaving the chamber.

The outdoor test section consisted of the compressor, accumulator, outdoor coil, and outdoor air flow chamber. The conditioned outdoor air at 35°F DB and 30°F DP, entered the outdoor coil and was exhausted by the unit fan into the air flow chamber. Air flow was regulated to maintain zero static pressure at the chamber entrance by a set of dampers located in the airflow chamber. The air was then exhausted back into the room.

Psychrometric Rooms

The psychrometric rooms can simulate the various indoor and outdoor conditions required for heat pump performance testing. The rooms were large insulated refrigeration rooms with air blowers to circulate room air through air control ducts in the ceiling of each room. Control of the test conditions in the psychrometric rooms was achieved with a programmable controller which monitored conditions in each room with thermocouple grids and dew point sensors. To correct set-point deviations in the rooms, chilled water cooling coils, electric resistance heaters, and steam humidifiers in the control ducts were used as necessary. A 75-ton capacity chiller and a 300 gallon chilled water storage tank provided the source chilled water for the cooling coils. Four banks of 9900 watt electric heaters in the control air ducts in each room provided resistance heating. Any required dehumidification was done by circulating additional chilled water through dehumidification coils in the air control ducts. Control characteristics of the psychrometric rooms during a typical frosting/defrosting test of the experimental heat pump are shown in Figure 3.2. The figure shows variations in outdoor dry bulb and dew point temperatures and indoor dry bulb temperature. The rise in dew point temperature during the defrost period of the heat pump test (0 to 7.5 minutes in Figure 3.2) was caused by vapor coming from the defrosting outdoor coil of the heat pump. The dew point sampler with which dew point data for the outdoor room was obtained was located near the coil and picks up vapor generated during the defrost (indicated by a rise in dew point temperature). This rise, however, was a local effect, and room conditions remain within testing tolerances.

Test Heat Pump

A nominal three-ton capacity split-system residential air-to-air heat pump was selected for use in characterizing

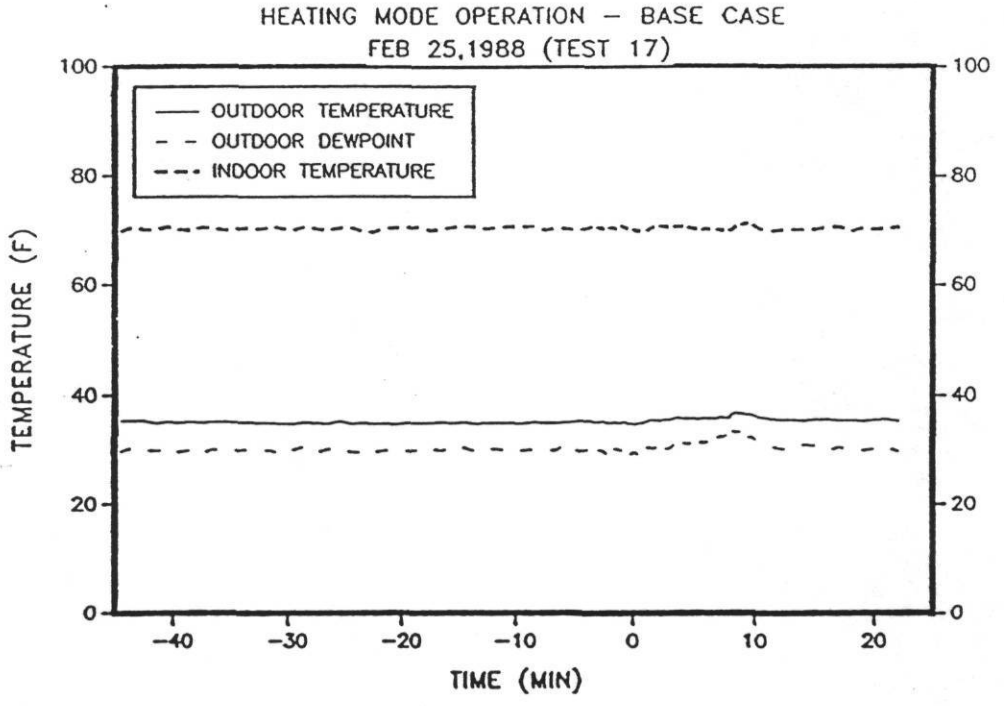

Fig. 3.2 Psychrometric Room Temperature Control Characteristics during a Frosting/Defrosting Test

reverse-cycle defrost transients. The indoor heat exchanger was installed in a galvanized steel air duct in the indoor psychrometric room. The outdoor coil was a free-standing horse-shoe shaped vertical coil placed in the outdoor room. Other heat pump components such as the compressor, accumulator, reversing valve, and electronic controls were also placed in the outdoor room. Each of the major components is described below.

The indoor heat exchanger was a four-row, four-circuit vertical coil with nominal 3/8 inch diameter refrigerant tubes. Fins were wavy and spaced. Each row of the coil had a frontal dimension of 30 inches by 18 inches, and had a rated capacity of three tons. Typical air flow rate across the coil during heating use was 1250 cfm.

The outdoor heat exchanger was a two-row, four circuit vertical coil with nominal 3/8 inch diameter refrigerant tubes. Refrigerant tubing in the coil ran horizontally through vertical wavy fins spaced at twenty fins per inch. Each row of the coil consisted of thirty passes of refrigerant tubing. Figure 3.3 shows the circuit arrangement for the outdoor coil. The surface of the liquid line exit of the lowest circuit in the coil was instrumented with the defrost control sensor used by the heat pump manufacturer. The coil had a frontal dimension of 30 inches by 84 inches. A three-bladed propeller fan was used to pull air through the coil. Typical heating mode air flow rate was 1900 cfm. Air pulled through the coil was exhausted above unit. A drain pan was built to collect defrost water from the outdoor coil during defrost periods. The pan was placed below the coil at a slight incline. Defrost water draining into the pan ran to the lowest side of the pan where a drain hole allowed the water to be collected in a bucket.

Refrigerant tubing between the coils was 3/8 inch in diameter and approximately forty feet long. This section of the refrigerant circuit was referred to as the "liquid line" and contained both the heating-mode and the cooling/defrost-mode expansion devices. In the heating mode, the heat pump outdoor coil was the evaporator. The heating-mode expansion device was a 0.059 inch diameter orifice. This orifice was placed in proximity of the outdoor coil. During cooling and defrost operation of the heat pump, flow of refrigerant in the liquid line was reversed, and indoor coil served as the evaporator for the system. The cooling/defrost mode expansion device was a 2.5 ton capacity thermostatic expansion valve (TXV). This valve was designed to maintain 10^{o}F of superheat in refrigerant leaving the coil. The TXV was placed in proximity of the indoor coil. Additional refrigerant circuitry around the TXV permitted this valve to

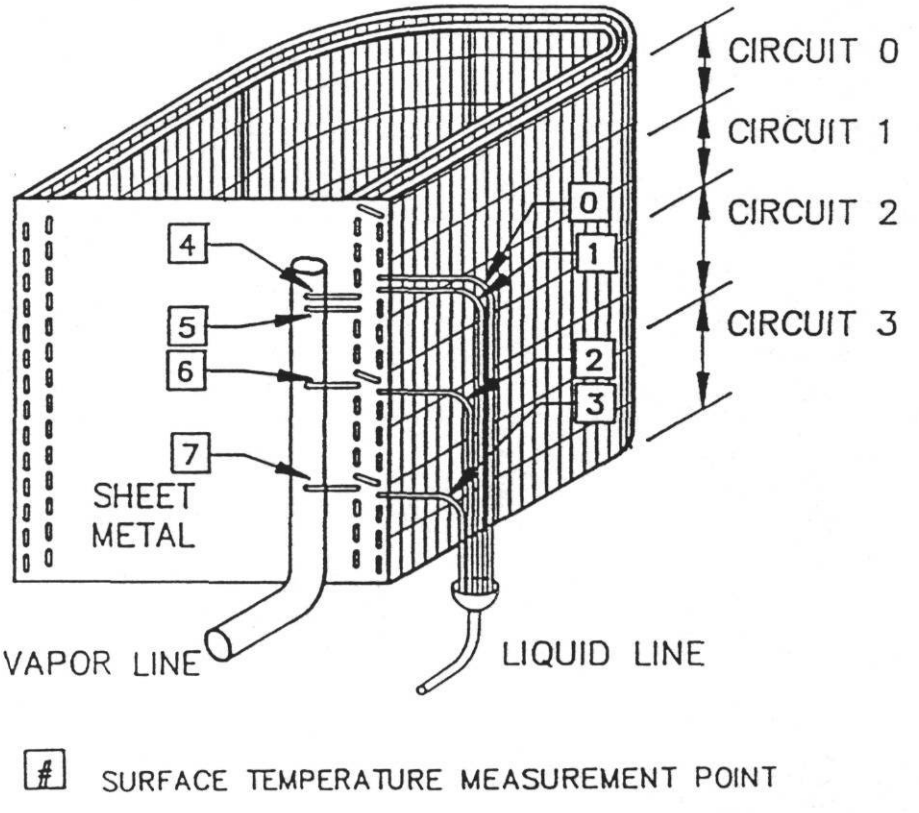

Fig. 3.3 Refrigerant Circuit Arrangement of the Outdoor Coil

be bypassed through a check valve during heating operation. Other equipment in the liquid line included a filter-drier and two paralled mass flow meters used to measure mass rate of flow of refrigerant during testing.

The other major section of refrigerant tubing was referred to as the "vapor line" and included 33 feet of tubing connecting the indoor coil to the system reversing valve and 2 feet of tubing connecting the outdoor coil to the reversing valve as well. This copper tubing was 5/8 inch in diameter. The four-way reversing valve also included ports for the suction and discharge lines of the compressor. This arrangement allowed high pressure refrigerant vapor discharged from the compressor to be directed toward the indoor coil for heating operation and toward the outdoor coil during cooling or defrost operation. Likewise, low pressure refrigerant vapor was pulled by the suction line of the compressor from the outdoor coil during heating and from the indoor coil during cooling or defrost.

The test heat pump system used a three-ton capacity reciprocating compressor to circulate refrigerant through the heat exchanger coils. The compressor was equipped with a suction line accumulator to minimize liquid flow to the compressor during start up and transient operation periods. This accumulator had a liquid refrigerant capacity of approximately eight pounds. When supplied by the manufacturer, the outdoor coil and compressor section of the test heat pump were charged with approximately 11.5 pounds of refrigerant. The accumulator was able to hold 60% of that charge. The accumulator was specially equipped with two bull's eye sight glasses to aid in flow visualization during transient tests of the heat pump. One of these sight glasses was placed 2.5 inches from the top of the accumulator and the other is placed 1.5 inches from the bottom. Total accumulator height was 11 inches.

Electronic controls for the heat pump were attached to a cart with the outdoor coil. The control circuitry was modified to permit manual defrost cycle initiation and termination. Remote switches placed in the control room of the psychrometric test facility allowed switching of the heat pump reversing valve. An additional switch permitted independent control of power to the propeller fan of the outdoor coil. An example of the use of this circuitry was when the automatic defrost control of the test heat pump was manually simulated. Defrost was initiated when an appropriate criteria was reached. To start the defrost, the reversing valve switch was thrown, causing discharge refrigerant to flow from the compressor to the outdoor coil instead of from the compressor to the indoor coil as in the heating mode. At this time, the outdoor coil fan was de-energized as was typically done during a reverse-cycle defrost. To return to heating operation at the end of the

defrost period, the outdoor coil fan was re-energized and the four-way reversing valve was switched to its heating-mode position.

To provide necessary data for transient performance characterization, the refrigerant circuit of the test heat pump was instrumented with flow meters, temperature probes, pressure taps, and surface temperature thermocouples. Figure 3.4 depicts the placement of these instruments in the refrigerant circuit. Table 3.1 provides a description of each of the test points in the refrigerant circuit as well as a description of test points in the heat exchanger test sections.

Refrigerant line pressures were measured at the ten points indicated in Figure 3.4 with 0-300 psig pressure transducers. These integrated circuit diaphragm-style pressure transducers had a stated total accuracy of 1% of full scale output (FSO). However, the transducers used in the experiment were calibrated with a dead weight tester, and a linear least squares fit of the test data was used during data reduction to provide 0.25% FSO accuracy for the transducers. Temperature probes were placed near the pressure transducer taps in the refrigerant circuit to measure refrigerant temperatures at these points. The 1/16 inch diameter probes were constructed as shown in Figure 3.5. The probe tips were far enough into the flow of the refrigerant (approximately eight diameters) to minimize conduction effects to or from the tube surface. Thermocouple wires were placed in the probe wells and surrounded by an oil bath to encourage a uniform temperature throughout the probe tip section. Thermocouples were made with wire taken from a common spool and were cut to a uniform length to minimize output variations caused by variation in wire composition or length.

Refrigerant flow was measured in the liquid line with two parallel mass flow meters. The flow meters contained U-shaped tubes in which flow was determined by Coriolis acceleration and deacceleration effects sensed by the meters' electronics. During frosting/defrosting cyclic operation of the test heat pump, flow through the meters varies from 0 to 11 pounds per minute. The two flow meters were used in parallel to limit pressure loss across the measurement section to a maximum of 10 psi (for the maximum refrigerant flow rate). This pressure drop was less than the 12 psi pressure drip acceptable by ASHRAE Standard 116-83 [18] (12 psi is the equivalent pressure drop for refrigerant at the test conditions experiencing the maximum allowed temperature drop of $3^{o}F$).

Valves shown in the refrigerant circuit diagram were lever-actuated shut-off valves. These ball valves permitted isolation of sections of the heat pump refrigerant circuit

Table 3.1 Description of Test Points

CHANNEL	TYPE	LOCATION
0-3	THERMOCOUPLE	OUTDOOR COIL - INLET (T to B)
4-7	THERMOCOUPLE	OUTDOOR COIL - OUTLET (T to B)
8-10	THERMOCOUPLE	COMPRESSOR - SURFACE (T to B)
11	TC-GRID	OUTDOOR ROOM
12-13	THERMOCOUPLE	ACCUMULATOR - SURFACE (T to B)
14	TC-GRID	OUTDOOR AIR CHAMBER
15	THERMOCOUPLE	CHILLED WATER TEMPERATURE
16-19	TC-PROBE	PROBE IN REFRIG. LINE
20-22	TC-PROBE	PROBE IN REFRIG. LINE
23		----NOT USED----
24-26	TC-PROBE	PROBE IN REFRIG. LINE
27		----NOT USED----
28	TC-GRID	UPSTREAM OF INDOOR COIL (16pt)
29	TC-GRID	DNSTREAM OF INDOOR COIL (16pt)
30-39		----NOT USED----
40-49	PRESSURE TRAN.	REFRIGERANT LINES
50	WATT TRAN.	208 VAC - 1 PHASE
51	FLOWMETER	REFRIGERANT LIQUID LINE
52	DIFF. PRESS.	OUTDOOR AIR CHAMBER (NOZZLES)
53	DIFF. PRESS.	OUTDOOR AIR CHAMBER (INLET)
54	DIFF. PRESS.	OUTDOOR COIL (PRESS. DROP)
55	DEW POINT SENS	UPSTREAM OUTDOOR COIL
56	DEW POINT SENS	DOWN STREAM OUTDOOR COIL
57	FLOW METER	IN PARALLEL WITH #51
58	WATTHOUR TRAN.	COMPRESSOR/OUTDOOR FAN

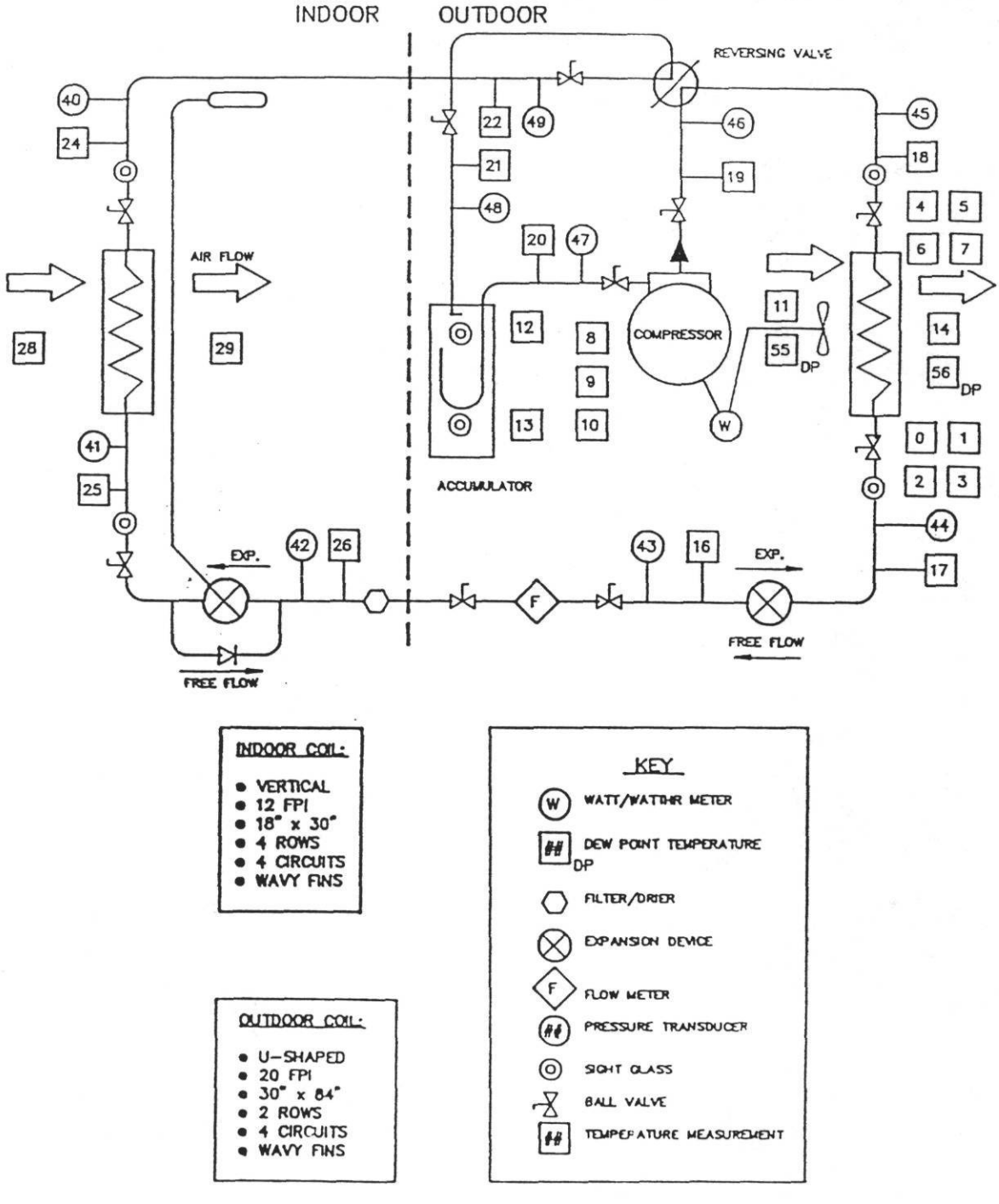

Fig. 3.4 Heat Pump System Schematic

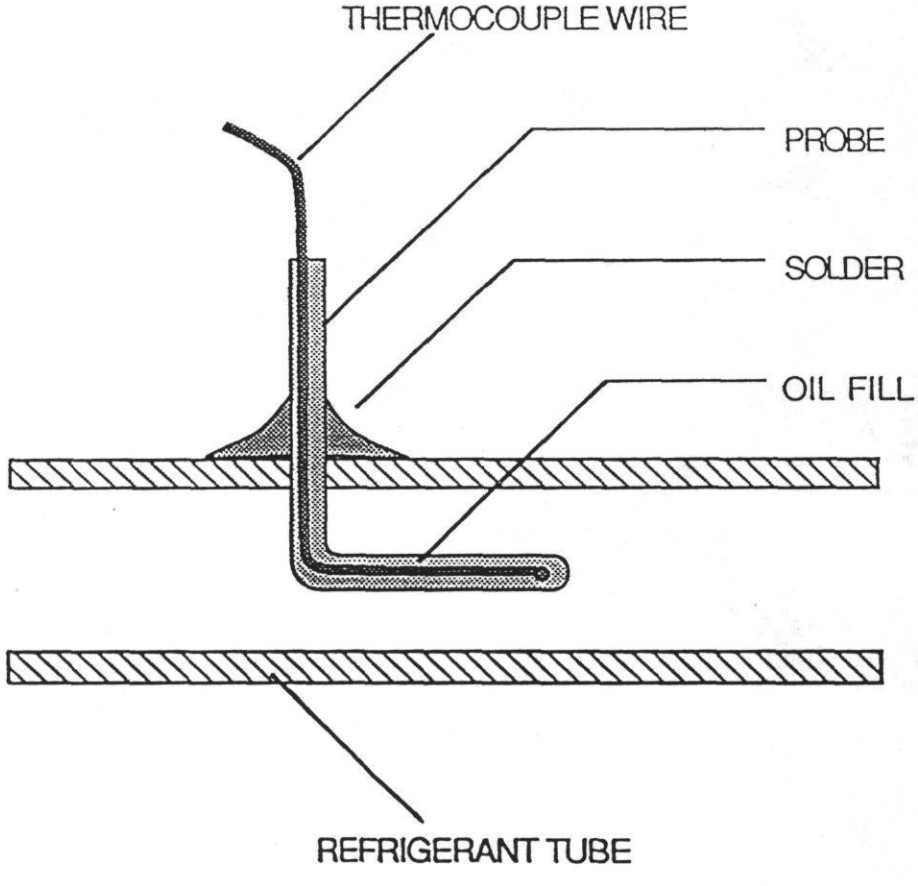

Fig. 3.5 Refrigerant Line Temperature Probe

for leak testing, equipment replacement, and system breakdown. The valves proved to be extremely useful because when a specific section had to be opened, other sections could be isolated, preventing excess refrigerant charge loss. Charging taps in each section of the circuitry allowed purging and charging of the sections independently.

Other points where temperatures were measured on the refrigerant circuit included surface temperatures of the accumulator and compressor and surface temperatures of the liquid and vapor lines going to each of the four circuits of the outdoor heat exchanger. Surface temperature measurements were made with thermocouples constructed from the same wire used in the refrigerant line probes and cut to the same length. Thermocouple junctions used in the surface temperature measurement were fixed to the surface where a temperature measurement was wanted. These junctions are covered with foam insulating tape. All thermocouple signals are transmitted through uniform-length extension wires to the data acquisition system.

Heat Exchanger Test Sections

Test sections were designed and constructed for both the indoor and outdoor heat exchangers to provide air-side performance data for the heat pump tests. The test sections permitted conditioned air from the psychrometric rooms to flow over the respective heat exchanger coils and then return to the rooms. Although the state of air flowing through the test sections was altered by the heat exchanger coils in the sections, the psychrometric rooms have the capacity to re-condition the exhaust air while maintaining set-point conditions. Both of the test sections are discussed in detail in the following paragraphs.

Indoor Test Section

The general layout of the indoor test section is depicted in Figure 3.6. Conditioned air from the indoor psychrometric room was drawn through the 30 by 20 inch insulated duct which contains the indoor coil. This air entered the test section at a control temperature of 70^{o}F and a relative humidity of 20%. The air was pulled through the test section by the booster fan of the downstream air flow chamber. A damper at the booster fan outlet permitted air flow to be adjusted to the level desired for testing.

As air entered the test section, it flowed through a flow straightener. Then it passed over a 16-node thermocouple grid which measured average air temperature across the cross-section. Then the air passed through the indoor heat exchanger coil. Next, the air flowed through a

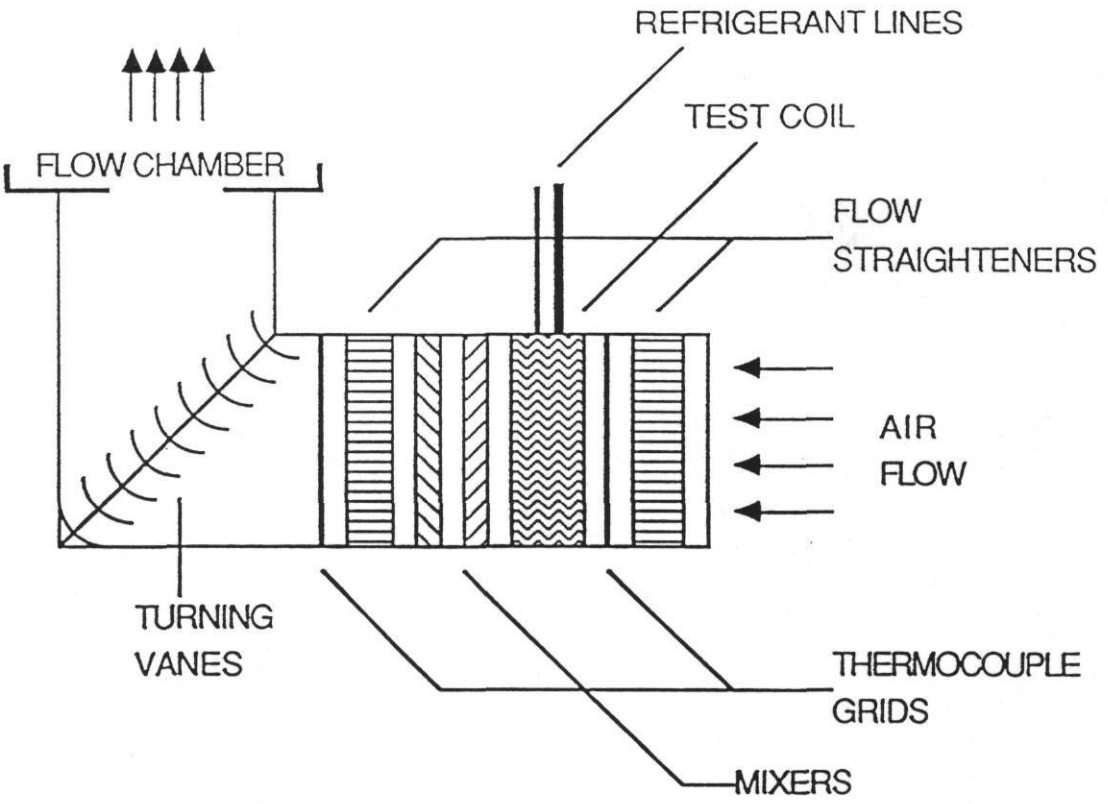

Fig. 3.6 Indoor Heat Exchanger Test Section

set of mixers which removed any temperature stratifications caused by non-uniform heat exchange with the indoor coil of the heat pump. At this point, the air again passed through a flow straightener. A downstream, 16-node thermocouple grid was used to measure air temperature after it is mixed and straightened. Finally, the air entered the flow chamber for flow rate measurement.

Air flow was measured in the flow chamber located downstream from the test section. This chamber is an AMCA 210, figure 15 flow chamber [17]. The chamber contained four ASME flow nozzles (eight, five(2), and three inch diameters) which were used as needed to measure flow rates from 100 to 5000 cfm [17]. Pressure drop across the nozzles was measured with an inclined-tube manometer calibrated to $\pm$0.01 inches water gauge (in wg) with a micromanometer. For the heat pump frosting/defrosting cyclic tests, the two five-inch nozzles were used. Flow was adjusted to give a nozzle pressure drop of 1.3 inches wg. This pressure drop corresponded to 1250 cfm of air through the test section.

Humidity of the indoor psychrometric room air was measured with a dry bulb/wet bulb thermometer test rig placed in the vicinity of the test section. The test rig used a small centrifugal fan to pull air across a dry bulb thermometer and a thermometer whose bulb was wetted with a cotton sock saturated with distilled water. Because dehumidification of air flowing across the indoor coil did not occur, psychrometric properties of downstream were determined with the readings from the upstream air dry bulb and wet bulb temperatures.

Outdoor Test Section

Figure 3.7 shows the components of the outdoor heat exchanger test section. The test section provided data on air flow through the coil as well as air pressure drop through the coil, static pressure downstream of the coil, and dry bulb and dew point temperatures of air entering and leaving the coil. Conditioned air at 35^{o}F dry bulb and 30^{o}F dew point temperature flowed through the coil and was exhausted by the heat pump coil fan into the test section air flow chamber. Air flowing through the chamber was exhausted by the chamber booster fan back into the psychrometric room.

A major consideration in the design of the outdoor heat exchanger test section was that the section had to simulate the normal heating-mode operating environment of the outdoor coil fan. In normal use, this three-bladed propeller fan operated under free flow conditions and exhausted to a zero static pressure ambient. However, measurement of the flow rate of air required placement of a flow chamber at the

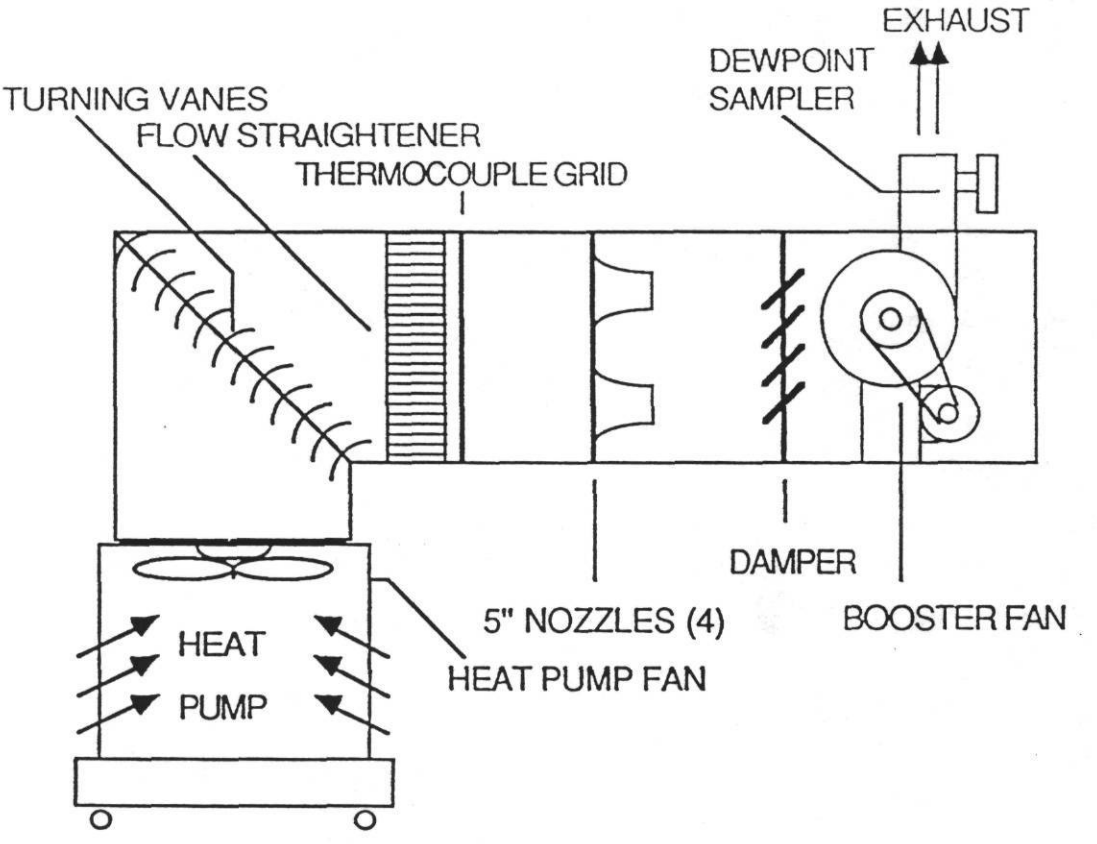

Fig. 3.7 Outdoor Heat Exchanger Test Section

exhaust of the heat pump coil fan. The booster fan of the flow chamber overcame pressure loss in the nozzle section and permitted the coil fan exhaust static pressure to be adjusted to zero. A fixed adjustment could be used for steady state conditions. However, during frosting/defrosting cyclic tests, frost accumulation on the coil changed the system characteristics. This change required a readjustment of booster fan flow rates to maintain the zero static pressure condition. To permit adjustment of the booster fan flow rate, a pneumatically driven damper was placed in the flow chamber. Pressure taps in the flow chamber section downstream of the outdoor coil fan were used to monitor exhaust static pressure. Zero Static pressure were maintained by manually adjusting the damper with a remote control located in the psychrometric test facility control room.

Air temperatures entering the outdoor coil were measured with a five-node grid placed near the coil. Air temperature leaving the coil were measured by a nine-node thermocouple grid in the air flow chamber. This grid was located immediately downstream from a set of flow straighteners. Pressure drop across the flow nozzles was measured with a micromanometer-calibrated, 0 to 2 inches wg differential pressure transducer. Similar transducers were used to measure static pressure and pressure drop across the outdoor heat exchanger coil. Typical heating-mode flow rates through the outdoor coil varies from zero to 500 cfm as the coil accumulates frost.

The dew point temperature of air entering and leaving the outdoor coil test section changed during frosting of the coil because moisture was removed from the air by the frosting coil. An optical mirror dew point psychrometer was used to measure the dew point of the air entering the coil. Figure 3.8 provides a photograph of the air sampler used in the dew point measurement of air entering the U-shaped coil. The sampler was constructed from 1.5 inch diameter PVC pipe. Sampler holes in the pipe were spaced evenly around the coil on the sides of the pipe facing away from the coil. Air was pulled through the sampler holes and into a channel where the psychrometer sensor was located. Then, the air was exhausted by a small blower fan back into the psychrometric room. Sampler holes farthest from the sensor channel was 3/8 inch in diameter. Holes closest to the sensor were 1/8 inch in diameter. The remaining central holes were 1/4 inch in diameter. This graduation of hole size permitted an accurate sampling of air from locations at the far side

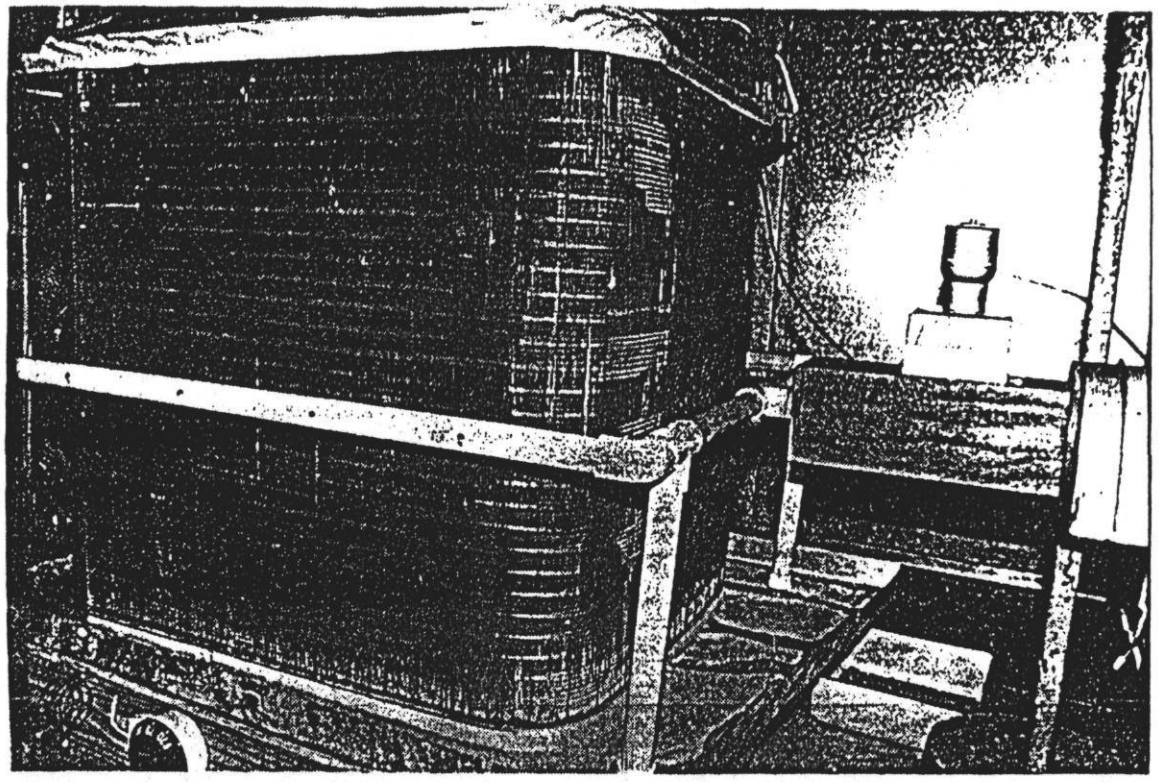

Fig. 3.8 Dew Point Sampler Around the Outdoor Coil

of the sampler where suction pressures were lowest. The dew point temperature of air exiting the coil was measured with a similar dew point psychrometer placed in the exhaust duct of the flow chamber.

Data Acquisition/Reduction

Sensor signals from the test points listed in Table 3.1 were collected and converted to engineering units by the data logger. The data logger handled millivolt and milliamp signals as well as larger voltages and frequency signals. During each frosting/defrosting cyclic test of the heat pump, data processed by the data logger was transferred to an IBM compatible personal computer where it was stored on a 10 megabyte hard disk drive. The maximum collection and storage rate for the 66 data channels used in the frosting/defrosting tests was eight seconds per set. The scan rate was adjustable, so data from frosting periods in the tests was collected every minute while data from the defrost period was collected every ten seconds. A feature of the system was the continual display of run-time data on the computer screen during testing. This data was visually monitored to provide an indication of heat pump performance at any given time during testing. After completion of a test series, all data collected on the hard disk was transferred to a minicomputer for analysis. Data were backed up on floppy disks to help avert possible losses. Command file programs written for minicomputer aided data file manipulation and the plotting of relevant test data. FORTRAN programs were used for refrigerant and moist air property subroutines. These subroutines were used in calculation of air and refrigerant-side heating capacities to provide an energy balance for data validation. Additional calculated properties and performance parameters for each test were plotted for characterization purposes. Plots were produced on pen plotters and laser printers when needed.

A complete listing of equipment used in the testing apparatus is given in Appendix C. All testing instrumentation was calibrated prior to data collection and the accuracies are also listed in Appendix A. In addition, uncertainties associated with various measurements and calculations are discussed in Appendix B.

Experimental Procedure

Once the test facility was completed, an experimental procedure had to be developed. The procedure included testing conditions, refrigerant charging procedure and a testing procedure to ensure repeatable results.

The testing conditions used for the frost/defrost tests were those prescribed for the frost build up test in the Department of Energy (DOE) - Test Procedures for Central Air Conditioners, Including Heat Pumps (1979) [16]. The entering dry bulb temperature for the outdoor coil was 35°F(± 1° during the heating cycle and ± 2° during defrost) with a dew point temperature of 30°F (± 1°) with a maximum wet bulb temperature of 60°F. For this testing, the wet bulb temperature in the indoor room was maintained at approximately 52°F.

The outdoor conditions for the frosting/defrosting cycling test were selected because of the rapid frosting of the outdoor coil at these conditions. The indoor conditions of 70°F DB is specified in the test procedure. A wet bulb temperature of 60°F or less was chosen to provide low enough air humidities to eliminate any condensation on the indoor coil during the reverse cycle defrost.

Refrigerant Charging Procedure

The proper refrigerant charge for the test setup was accomplished during the cooling mode. Charging in the heating mode was not considered because a large amount of refrigerant was stored in the accumulator during normal heating operation. Adding or removing charge during the heating mode would only raise or lower the level of refrigerant in the accumulator and wouldn't affect system characteristics. Though refrigerant charge was not critical during the heating mode, the charge affects the defrost cycle as the unit switches to the cooling mode and the refrigerant is pumped into the outdoor coil to melt the frost.

Factory recommendations called for 14°F of subcooling leaving the condensor (outdoor coil) in the cooling mode. The setup was charged to this level with the outdoor room at 95°F DB and the indoor room at 80°F DB and 57°F WB. This prevented condensation on the indoor coil during the charging procedure.

The first step in the testing session was to set or verify the unit charge at the room conditions mentioned previously. With the refrigerant charge set, the defrost expansion device to be tested was valved into position and the rooms were brought down to testing conditions. This took approximately two hours. Finally, with the rooms at testing conditions, the testing instrumentation was readjusted as necessary and the heat pump started.

After the heat pump was started, the outdoor airflow chamber was adjusted to zero static pressure above the unit. The outdoor chamber damper had to be manually adjusted

throughout the frosting cycle as the air flow changed with varying levels of frost accumulation.

The defrost cycle was initiated manually when the capacity of the heat pump dropped by 20%. The capacity was calculated by measuring the temperature difference and airflow across the indoor coil. Defrost termination was also done manually when the bottom circuit temperature in the outdoor coil rose above 65°F. The outdoor unit fan and chamber fan were both turned off during the defrost cycle. These initiation and termination criteria were selected because they depict a common type of demand defrost control that is currently being used by the manufacturer of this heat pump.

The heat pump was run through 3 to 5 defrost cycles before it reached a point where consecutive defrost times and the amount of defrost water collected were repeatable. One or two cycles were run between test cases for the same reason. At least three consecutive tests were then run for each expansion device or defrost strategy.

As stated previously, the data scans were terminated 15 minutes after the defrost termination. At this time a new scan was begun for the next defrost cycle and the defrost water was collected and recorded. Collecting the water at this time had the advantages of allowing the water to completely drain into the collection pan and making a consistent time of collection for testing.

CHAPTER 4

THE BASE CASE DEFROST CYCLE

This chapter provides a detailed description of the frosting/defrost cycle for the base case test. A description of the base case system is presented first, followed by the overall performance of the heat pump using the base case expansion device and then a more detailed description of the refrigerant dynamics during the frosting/defrost cycle.

Design

To evaluate the effect of various expansion devices and defrost strategies on the frosting/defrost cycle, a base design was developed. The design included an expansion device,a compressor, and defrost termination criteria.

The expansion device used during the base case defrost cycle was a thermal expansion valve (labeled as TXV #57). In selecting TXV #57, nine TXVs of the same model and capacity were tested* for stroke response time. TXV #57 was selected as the base case because it represented the average response time of the group. Table 4.1 provides a brief description of TXV #57.

The base case strategy for defrost termination was then used by the manufacturer of the heat pump. Termination was triggered when the exiting refrigerant temperature of the bottom circuit in the outdoor heat exchanger reached 65°F. This termination scheme is described in detail later in this chapter.

---

* Tests were conducted by the TXV manufacturer.

Table 4.1 - Characteristics of Base Case Defrost Expansion Device - TXV #57.

ITEM	TYPE OR VALUE
NOMINAL CAPACITY	2 1/2 TON
STATIC SUPERHEAT	$6^{O}F$
SYSTEM SUPERHEAT	$10^{O}F$
INLET	3/8" SAE
OUTLET	1/2" SAE
BULB/TXV LINE	5 FEET
BULB FILL	STANDARD RESIDENTIAL A/C and HEATPUMP
PRESSURE EQUALIZATION	BLEED TYPE
CONFIGURATION	STRAIGHT THROUGH
MAXIMUM OPENING	0.0059 $IN.^{2}$
STROKE	0.024 IN.

System Performance of the Base Case

Four operating characteristics were used to measure the overall base case performance using TXV #57 as the defrost expansion device These parameters were the Coefficient of Performance(COP), defrost cycle time, melt time, and drain time. The operating characteristics were averages taken from three consecutive test runs. The average deviations during the tests were +/- 1% for the COP and defrost time, while the deviation was +/- 2% for the melt and drain times. Table 4.2 contains the four operating characteristics for the base case test.

Table 4.2. Heat Pump System Characteristics* for Base Case Test Using TXV #57.

DEFROST EXPANSION DEVICE	INTEGRATED CYCLIC COP	DEFROST TIME (minutes)	MELT TIME (minutes)	DRAIN TIME (minutes)
TXV #57	2.26	8.06	4.22	3.83

* System characteristics are averages taken from three consecutive test runs.

Defrost Time

The defrost time was the time from defrost initiation to defrost termination of the same cycle. For a more accurate comparison of the performance of different expansion devices, the defrost time was divided into two phases, the melt phase and the drain phase. The melt phase started at defrost initiation and ended when the frost on the outdoor coil was melted. At the end of the melt time, the drain phase started and lasted until the cycle was terminated and the melted frost had drained from the coil.

Calculation of COP

The integrated cyclic COP was the ratio of the integrated heating output (measured at the indoor coil) over the integrated energy consumption. The integration was done over a complete frosting/defrost cycle which started at the termination of the previous defrost and ended at the termination of the present defrost.

The heat pump tested did not have a fan matched to the indoor coil. The indoor air chamber provided airflow through the coil. When heat pump tests are conducted without an indoor fan, the test procedure [18] requires corrections for fan power consumption and heating capacity. The correction factor for power usage was 0.365 kW per 1000 cfm airflow through the indoor coil. The correction factor for heating capacity was 1250 Btu/hr/1000 cfm. These correction factors were added to the instantaneous values before integration.

Base Case Energy Balance

To verify the calculations for air-side heating capacity, an energy balance was performed on the indoor coil. Figure 4.1 shows a plot of the refrigerant side and air side capacity for the indoor coil during the base case test. The energy balance was without the correction factors for the indoor fan, since the refrigerant side does not contain the same correction.

The refrigerant side capacity was calculated by multiplying the refrigerant mass flow rate by the change in enthalpy of the refrigerant entering and leaving the indoor coil. The enthalpy of the refrigerant was calculated using subroutines developed by Kartsounes and Erth[20].
The difference in refrigerant and air side capacities was less than 5% during the frosting portion of the cycle. During frost buildup, the heat pump operated under a slow transient process. Thus, there was good agreement between the air side wet refrigerant side capacities. During the defrost cycle, the heat pump underwent a relatively fast transiant process. There was lag between the refrigerant capacity early in the defrost (Figure 4.1). In all tests, the capacity was determined on the air side rather than the refrigerant side.

Description Of Base Case Test

This section provides a detailed description of the frosting /defrost cycle for the base case test. Relevant data(pressure, temperature, capacity, etc.) are plotted and discussed as to their effect on the cycle. Figure 4.2 shows a plot of the power usage(compressor plus outdoor and indoor fans) and capacity for the heat pump with the base expansion device during a complete frosting/defrost cycle. Figure 4.2a shows the complete cycle, while Figure 4.2b provides an expanded plot of the defrost portion of the cycle. Figure 4.2a starts 45 minutes before defrost initiation (-45 minutes), which was approximately 15 minutes after the termination of the previous defrost. Time is equal to 0 minutes at defrost initiation and the plot continues until 25 minutes after defrost initiation (25 minutes). Figure 4.2b starts at 2 minutes before defrost initiation and continues until 18 minutes after initiation of defrost.

Frosting Of The Outdoor Coil
(-45 to 0 minutes)

At the start of Figure 4.2a(-45 minutes), the heat pump had been running 15 minutes since the completion of the previous defrost cycle. At this point, the unit was also running at its maximum capacity of approximately 2.5 tons at 35^{o}F ambient and the accumulator was approximately half full of liquid refrigerant.. Frost was visible on the bottom circuit of the outdoor coil(Figure 4.3) and the air pressure drop through the outdoor coil was just beginning to rise(Figure 4.4a). As the frost continued to grow, the pressure drop across the outdoor coil increased and at -32 minutes, the airflow started to decrease from the maximum of 1900 cfm. The unit's heating capacity was not significantly affected by the frost growth until about -15 minutes, when it began to decrease(Figure 4.2a). At this point, the airflow had fallen to 1500 cfm(Figure 4.4a) and frost was now located mainly on the edges and corners of the coil(Figure 4.5).

After -15 minutes, frost began to spread throughout the coil, until at -8 minutes, frost was visible over most of the surface(Figure 4.6). During those 7 minutes, the air pressure drop through the coil rose to a maximum of 0.15 inches WG at -9 minutes and then abruptly dropped to 0.09 inches WG when the outdoor unit fan motor "stalled" under the high static pressure.(Figure 4.4a). The outdoor unit fan was a 3-blade propeller fan designed to efficiently move large volumes of air but unable to handle large static pressures[21].

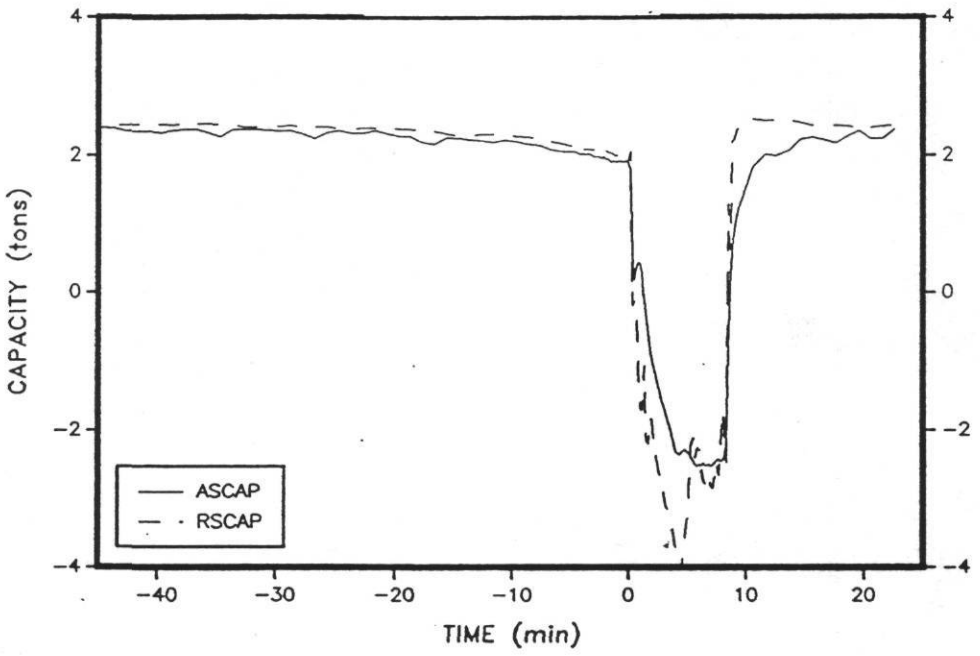

Figure 4.1. Refrigerant-Side/Air-Side Capacity Comparison.

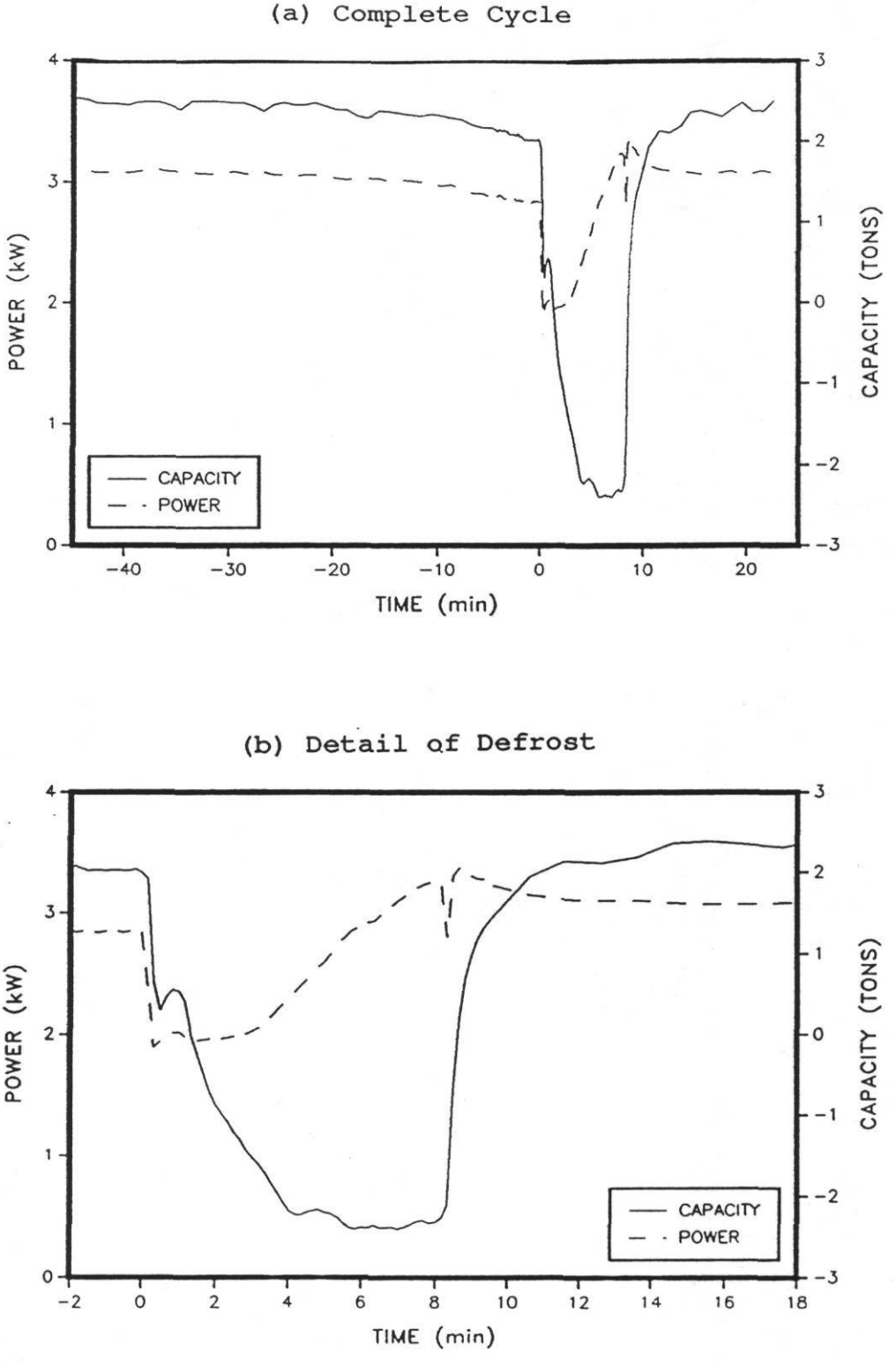

Figure 4.2. Power Usage and Heating Capacity for Base Case.

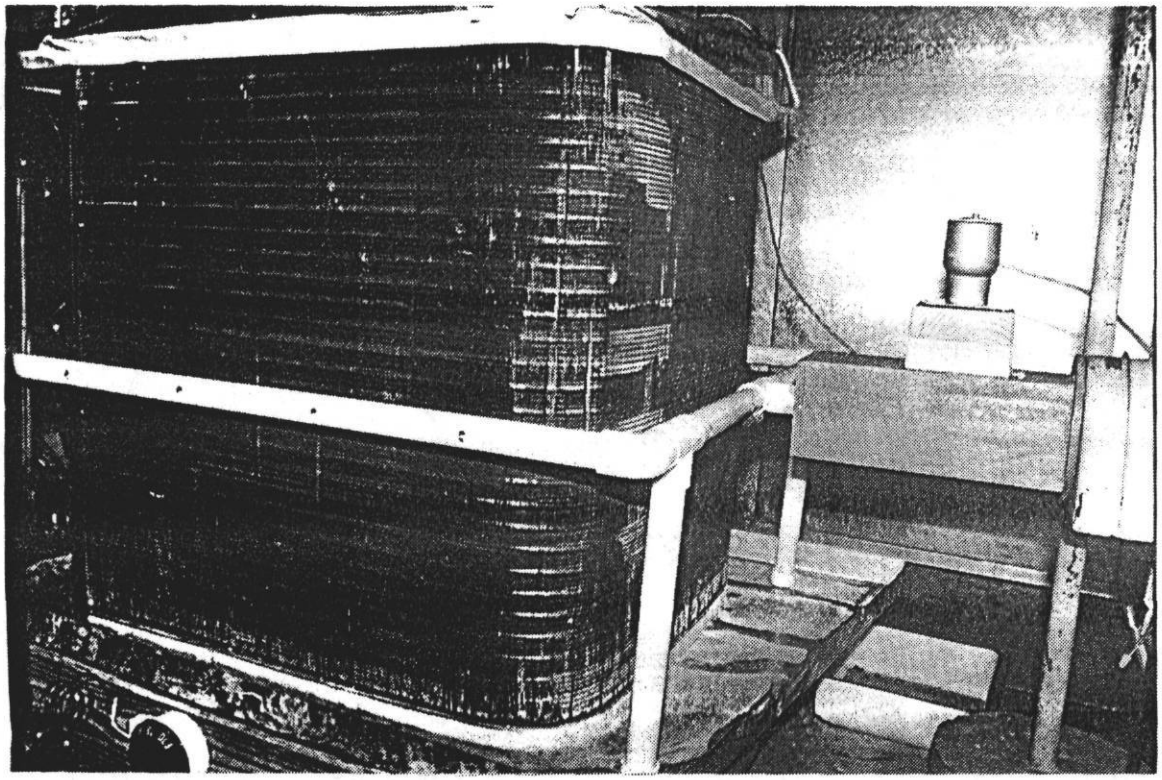

Figure 4.3. Outdoor Coil at 45 Minutes Before Defrost.

(a) Complete Cycle

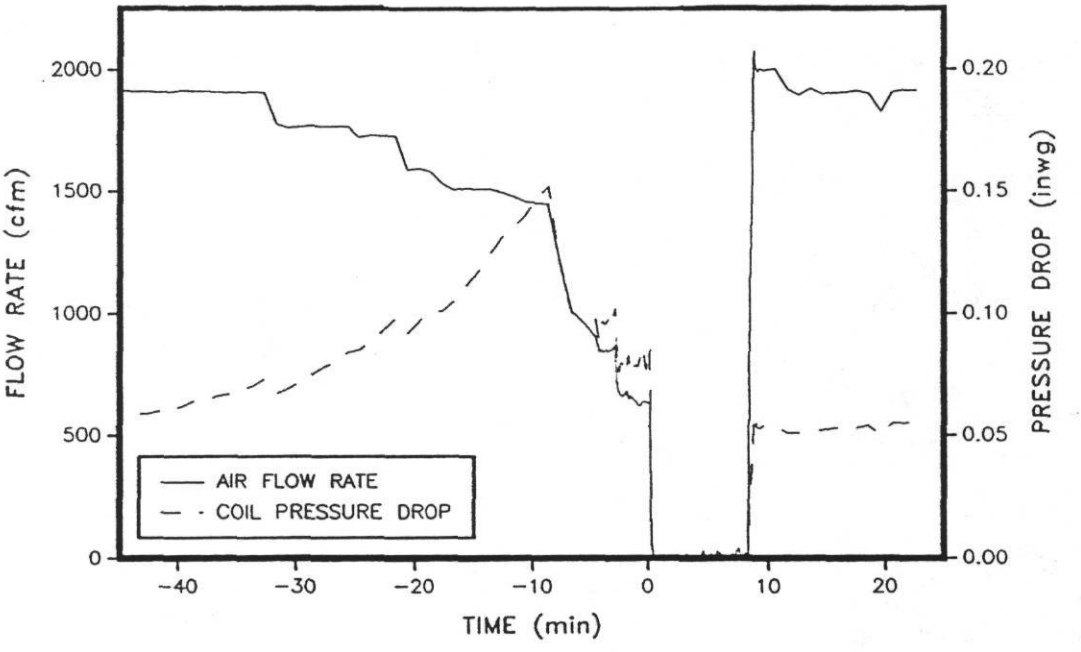

(b) Detail of Defrost

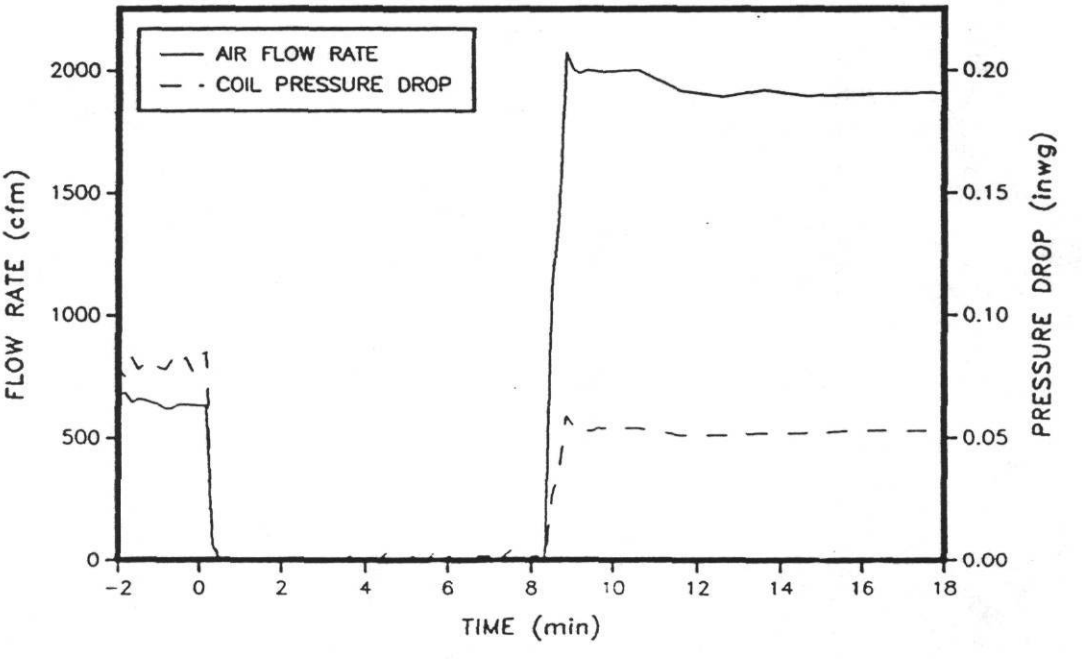

Figure 4.4. Airflow and Pressure Drop Through Outdoor Coil (Base Case).

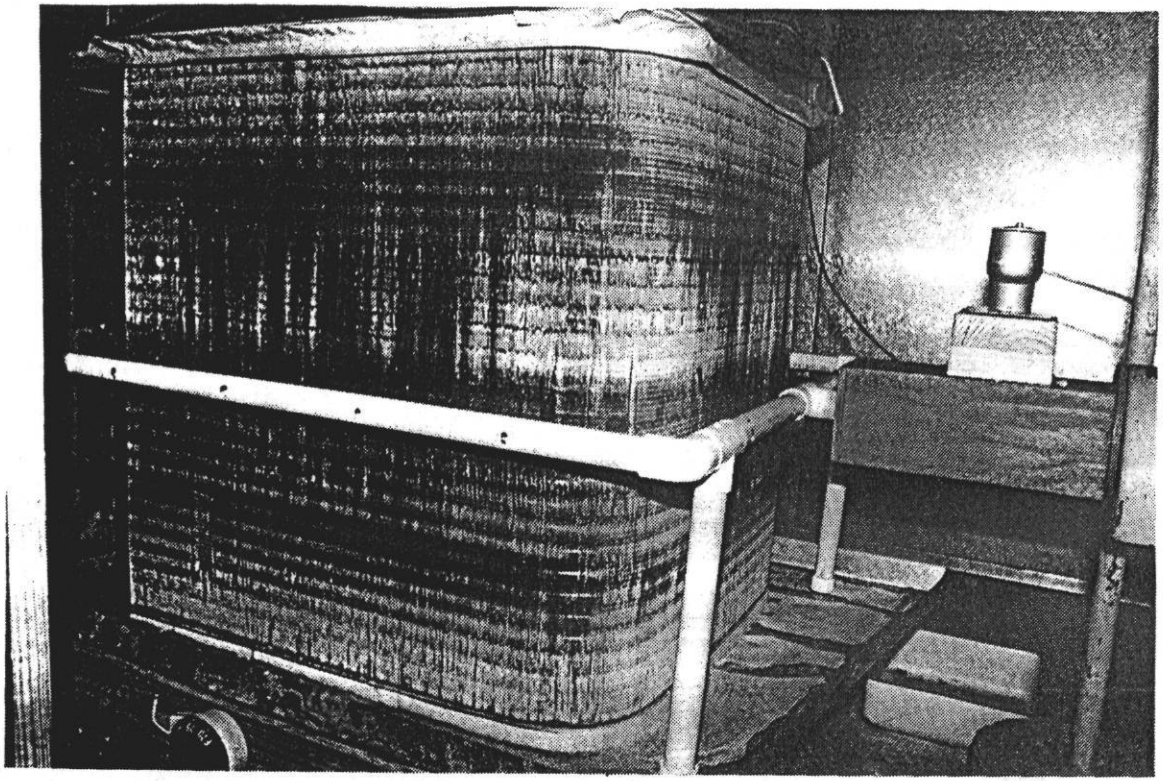

Figure 4.5. Outdoor Coil at 15 Minutes Before Defrost.

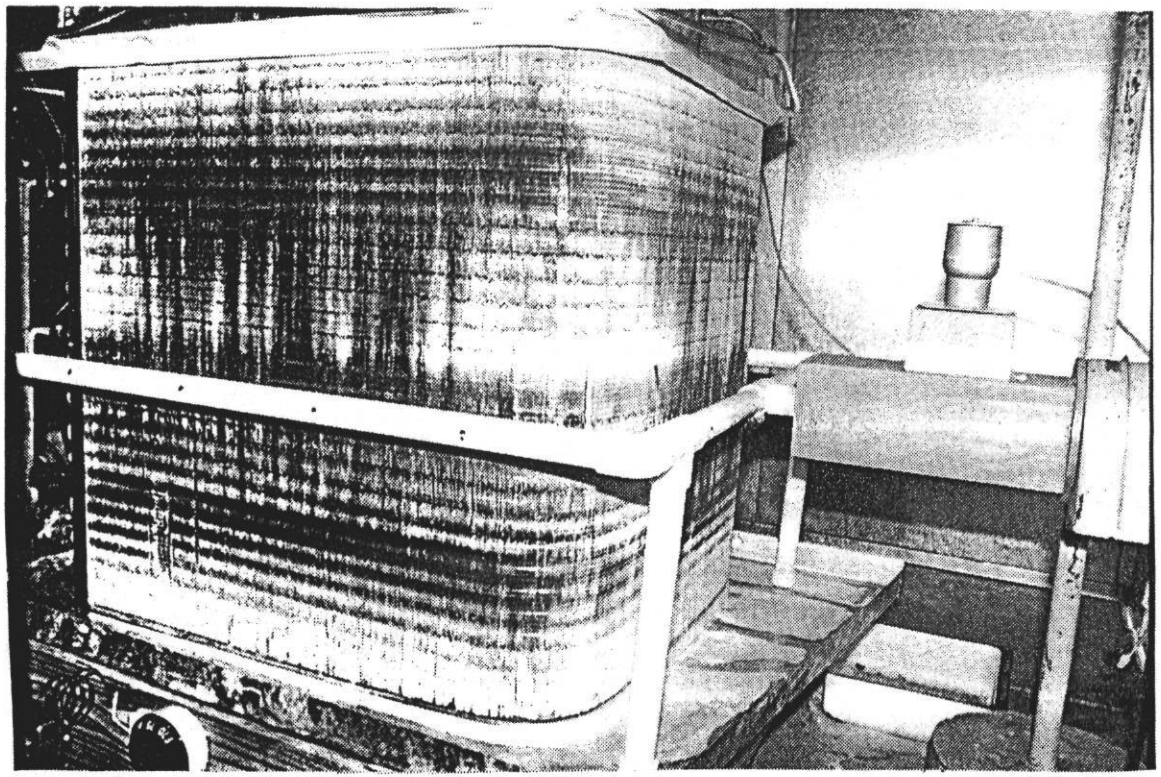

Figure 4.6. Outdoor Coil at 8 Minutes Before Defrost.

(a) Complete Cycle

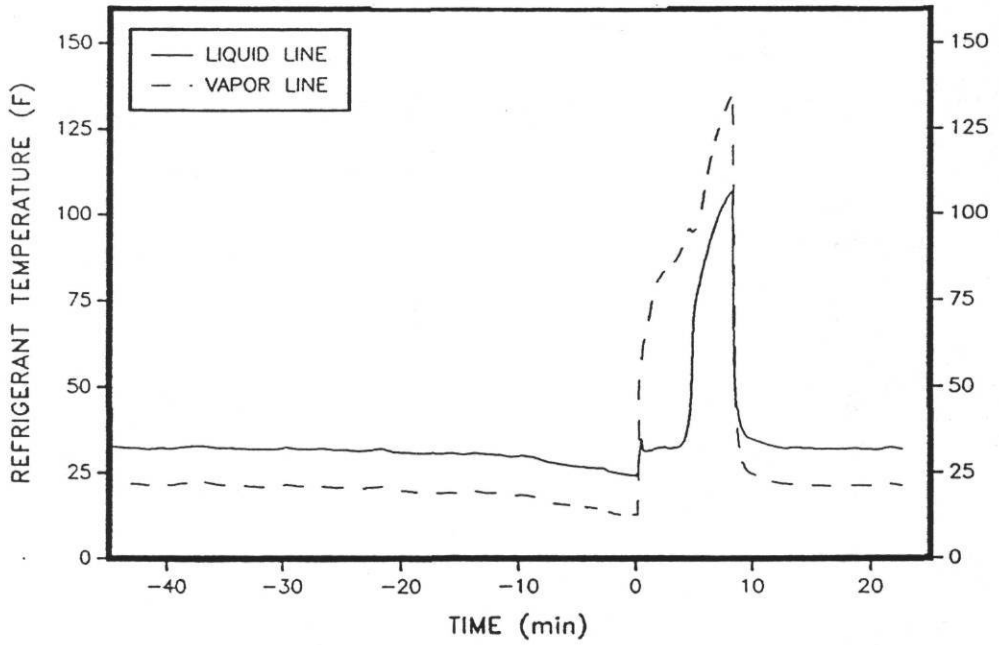

(b) Detail of Defrost

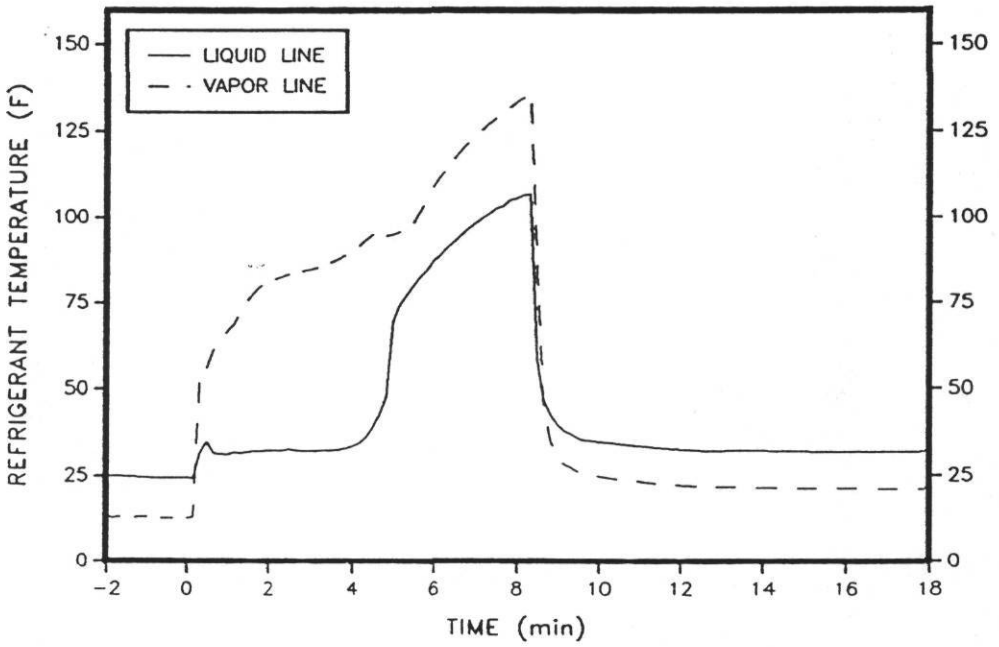

Figure 4.7. Refrigerant Temperatures Near Outdoor Coil. (Base Case).

With the fan motor unable to maintain torque under the high static pressure, there was a rapid drop in airflow from 1400 cfm to 1000 cfm through the outdoor coil(Figure 4.4a). With the rapid drop in airflow, the heat pump's capacity dropped from 2.4 tons to 2.2 tons over the same two minutes(Figure 4.2a).

As the frost accumulation increased, the outdoor coil temperature decreased (vapor line in Figure 4.7a). The reduction in outdoor coil temperature should encourage more frost growth which would increase the air pressure drop through the coil and decrease the heating capacity. The vapor line temperature, which was the suction line temperature during the heating mode, dropped from 23°F at -45 minutes to 15°F at -5 minutes as frost grew on the coil. With the reduction in heat transfer in the outdoor coil due to frost, the amount of vapor supplied to the compressor also decreased, which increased the density of the suction line vapor.

Defrost Initiation
(0.0 to 1.0 minutes)

As discussed in Chapter 3, the test criteria for defrost initiation was a 20% drop in system capacity from the maximum capacity(2.5 tons) reached after a defrost. Defrost was initiated when the capacity fell to 2.0 tons, at 0 minutes (Figure 4.2). The coil was fully covered with frost (Figure 4.8) and the accumulator was approximately 80% filled with liquid refrigerant before defrost initiation. This was equal to 48% of the system charge since the capacity of the accumulator and the system charge were approximately 110 ounces and 184 ounces, respectively. At defrost initiation, the reversing valve was energized and the outdoor fan was shut off, which dropped the outdoor airflow and pressure drop through the coil to zero. The reversing valve switched the direction of refrigerant flow from the heating mode, where the outdoor coil was the evaporator, to the cooling mode, making the outdoor coil the condenser.

As the reversing valve changed the direction of the refrigerant flow, an apparent equalization between the suction and discharge pressure lines occured(Figure 4.9). The discharge pressure dropped from 190 psia to 75 psia in 5 to 10 seconds, while the suction pressure surged upward from 50 psia to 90 psia. With the decrease in pressure rise through the compressor, the refrigerant flow rate fell to almost zero and the heat pump power dropped from 2.8 kW to 1.8 kW(Figure 4.10).

The sudden decrease in pressure in the indoor coil caused the liquid refrigerant located in the indoor coil before defrost to vaporize in the coil and flush toward the accumulator. Figure 4.11 shows the refrigerant superheat/subcooling conditions leaving and entering the indoor coil and the coil capacity. Temperature 24(T-24) was a probe located in the vapor line after the indoor coil and temperature 25(T-25) was a probe located between the defrost expansion device and the coil(see Figure 3.6). The pressures at T-24 and T-25,(P-40 and P-41, respectively) were used to calculate the saturation temperatures (Tsat-24 and Tsat 25) and the difference between T and Tsat was the amount of superheat or subcooling(SHSC) of the refrigerant. A positive value for SHSC-24 meant it was superheated and a negative value indicated subcooling. Also contained in Figure 4.11 is the capacity which was one indicator of the amount of refrigerant located in the indoor coil. When the coil contained no liquid or two phase refrigerant, the capacity should have been close to zero. As liquid refrigerant started filling the coil, the capacity should have risen and reached a maximum when SHSC-24 was zero.

At defrost initiation, the capacity in Figure 4.11 fell from 2.0 tons to 0.3 tons within 20 seconds. This sudden drop in capacity was principally caused by the boiling of refrigerant from the indoor coil. The flow of liquid refrigerant out of the coil can also be inferred from SHSC-24. As defrost was initiated, SHSC-24 rose from 15^{o}F to 30^{o}F and then dropped to 4^{o}F as the cool refrigerant vapor rushed out of the indoor coil (30 seconds). Since SHSC-24 did not drop to zero, as it would have if there had been liquid in the vapor line, all of the refrigerant in the outdoor coil apparently vaporized and no liquid went into the accumulator.

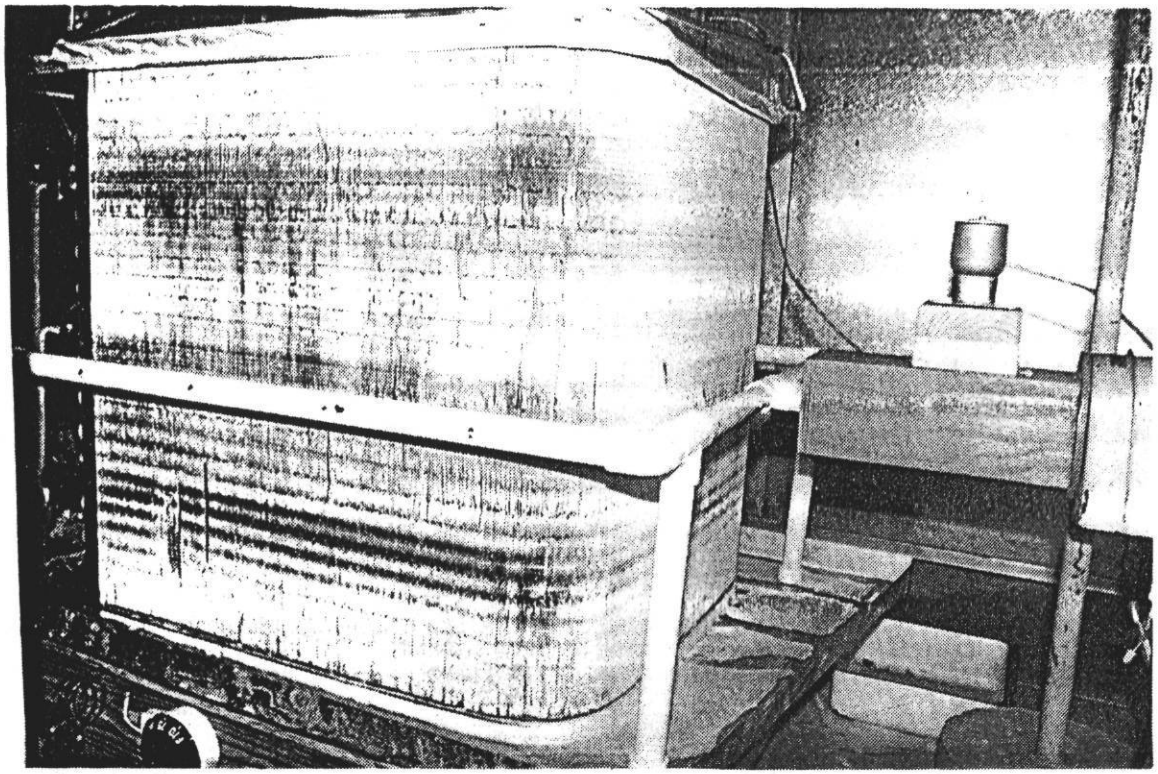

Figure 4.8. Outdoor Coil at Defrost Initiation.

(a) Complete Cycle

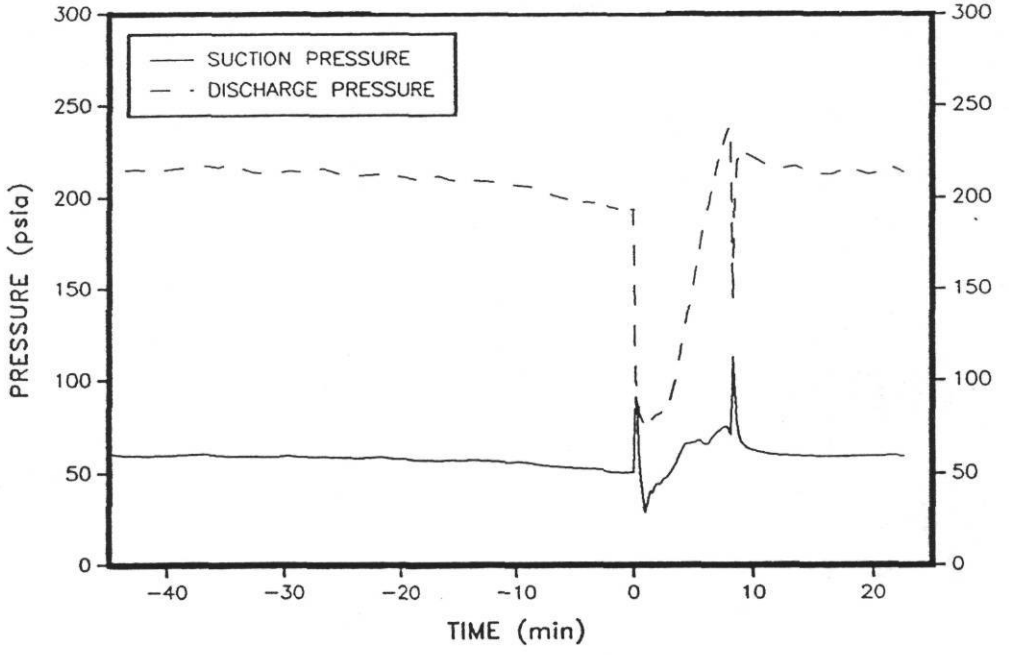

(b) Detail of Defrost

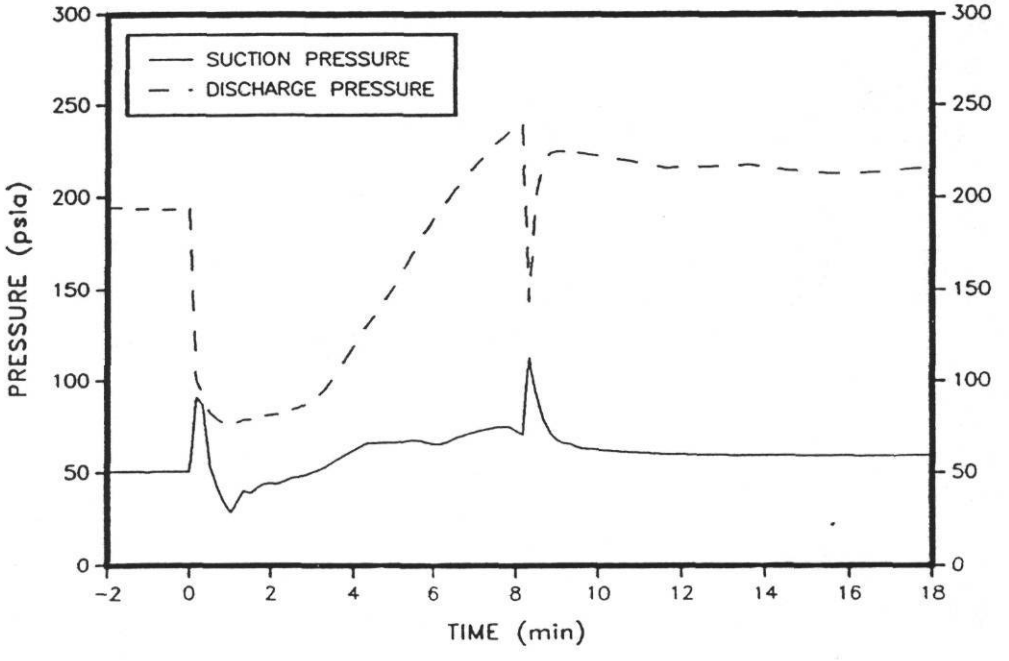

Figure 4.9. Compressor Suction and Discharge Pressures. (Base Case).

(a) Complete Cycle

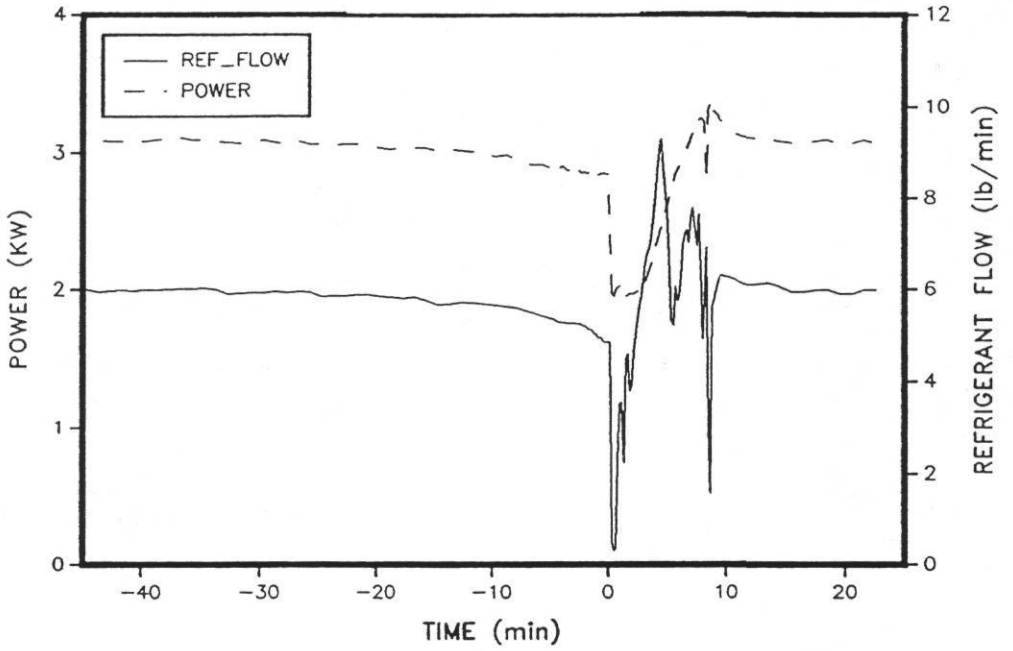

(b) Detail of Defrost

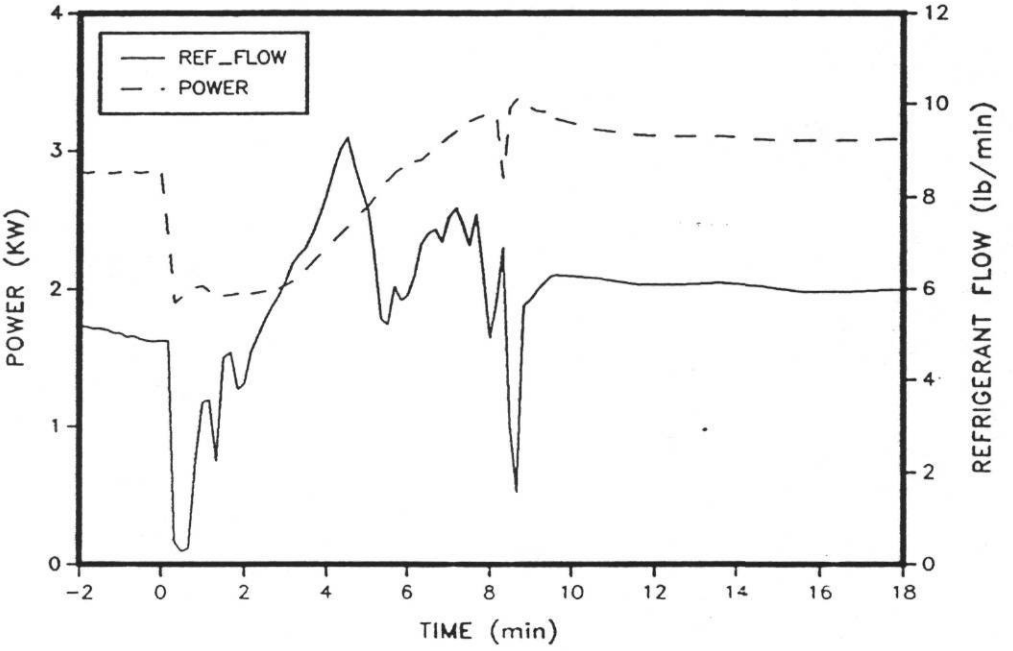

Figure 4.10. Refrigerant Flow Rate and Power Consumption. (Base Case).

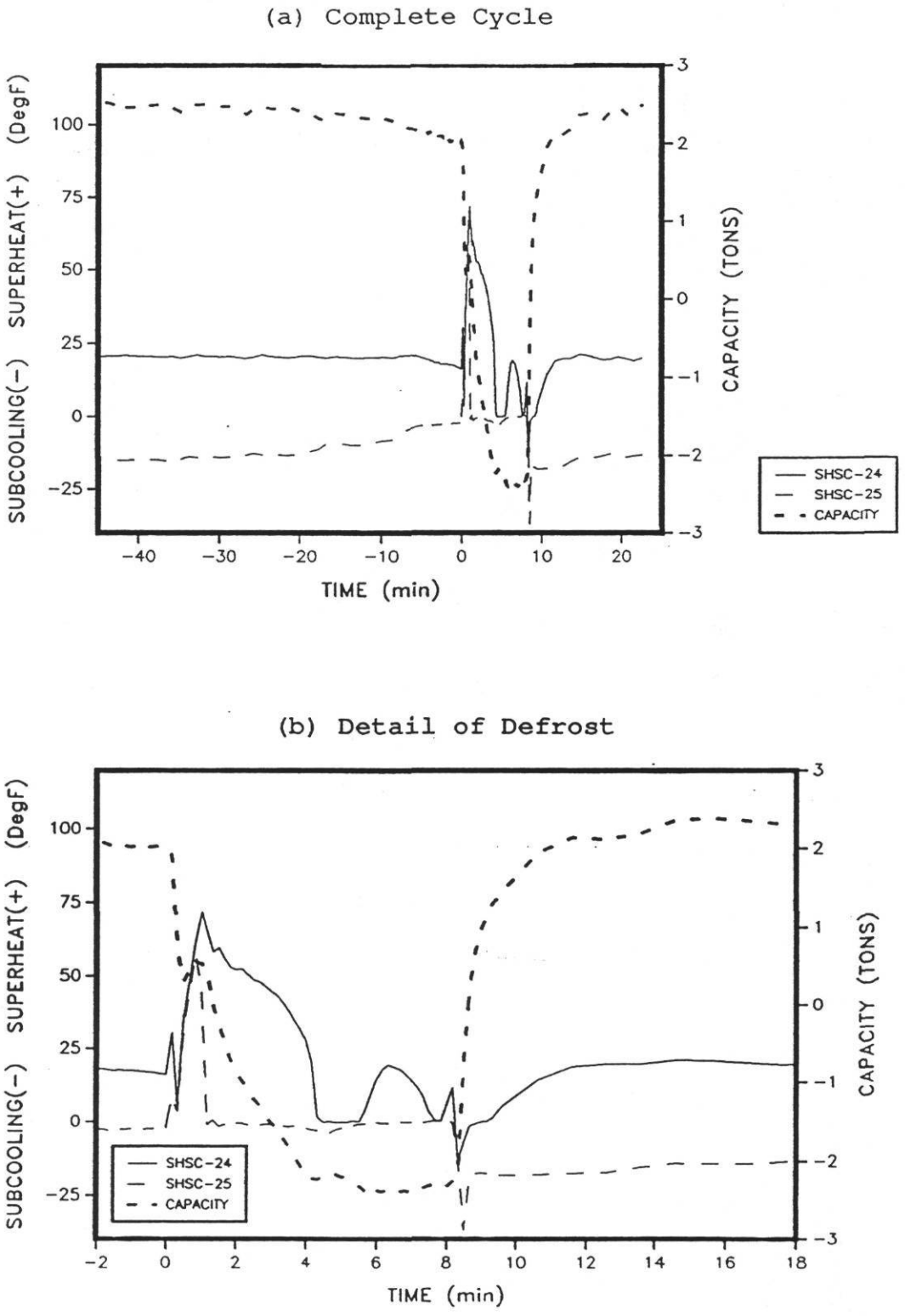

Figure 4.11. Superheat/Subcooling at T-24 and T-25 & Capacity (Base Case).

During this time, the refrigerant in the indoor coil, which was initially hot, boiled as the saturation pressure dropped. The accumulator was approximately 80% filled with the liquid refrigerant before defrost initiation and the level did not rise after initiation, indicating again that all of the refrigerant from the indoor coil vaporized before reaching the accumulator. With the indoor coil containing only low pressure vapor after defrost initiation, the compressor became temporarily "starved" of refrigerant and pulled the suction pressure down to 30 psia, approximately one minute after defrost initiation (Figure 4.9). As the suction pressure fell, the refrigerant in the accumulator started to boil and the accumulator temperature(T-accum) decreased to $0^{o}F$ (Figure 4.12). The saturation temperature of the suction line (Tsat-20) fell to $-10^{o}F$ at 1 minute. (Figure 4.12) The suction line temperature, (T-20) which was saturated during the first 40 seconds of the defrost cycle, became superheated for approximately 30 seconds. The superheat reached a maximum of $14^{o}F$ when the suction line pressure reached a minimum at 1 minute into the defrost.

The refrigerant that remained trapped in the accumulator was fed into the suction line of the compressor through the U-tube metering device at the bottom of the accumulator. The accumulator liquid level dropped from 80% full at the beginning of defrost to 25% full after 1 minute of defrost as the U-tube metering device fed the refrigerant into the compressor intake. Saturated refrigerant in the compressor intake was indicated by Figure 4.12b where T-20 was equal to Tsat-20. The heat from the compressor motor was used to boil any liquid refrigerant fed into the compressor from the accumulator. Since the indoor coil contained only low pressure vapor immediately after defrost initiation, the compressor was the only source of heat available to melt the frost from the outdoor coil during the first minute of the defrost cycle.

The liquid refrigerant was gone from the outdoor coil within 20 seconds from defrost initiation as indicated in Figure 4.11b with the superheated conditions at SHSC-24 and SHSC-25. With the liquid refrigerant gone from the outdoor coil, the capacity rose slightly to 0.5 tons because of some residual heat still in the coil, duct and flow straighteners. The capacity started dropping again at 1.0 minutes as refrigerant was fed into the coil through the defrost expansion device(TXV #57). The flow of refrigerant into the indoor coil was indicated in Figure 4.11b by the drop in superheat of SHSC-25 to zero. Data presented by Miller[13] showed the same small increase in capacity during the time immediately after the defrost initiation (Figure 2.5 in Chapter 2) that was observed in the base setup.

(a) Complete Cycle

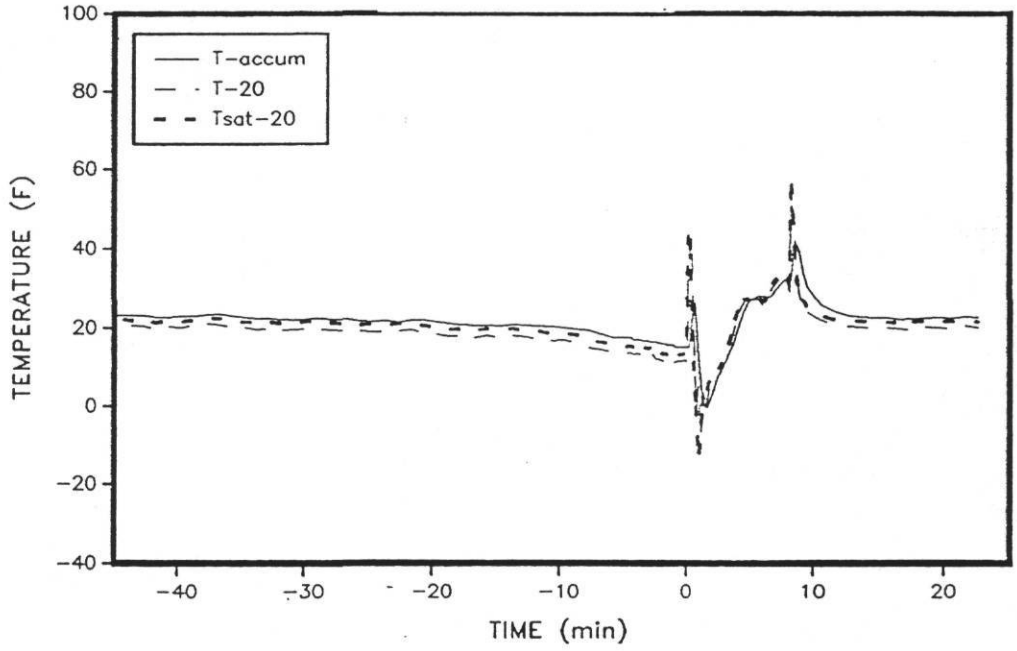

(b) Detail of Defrost

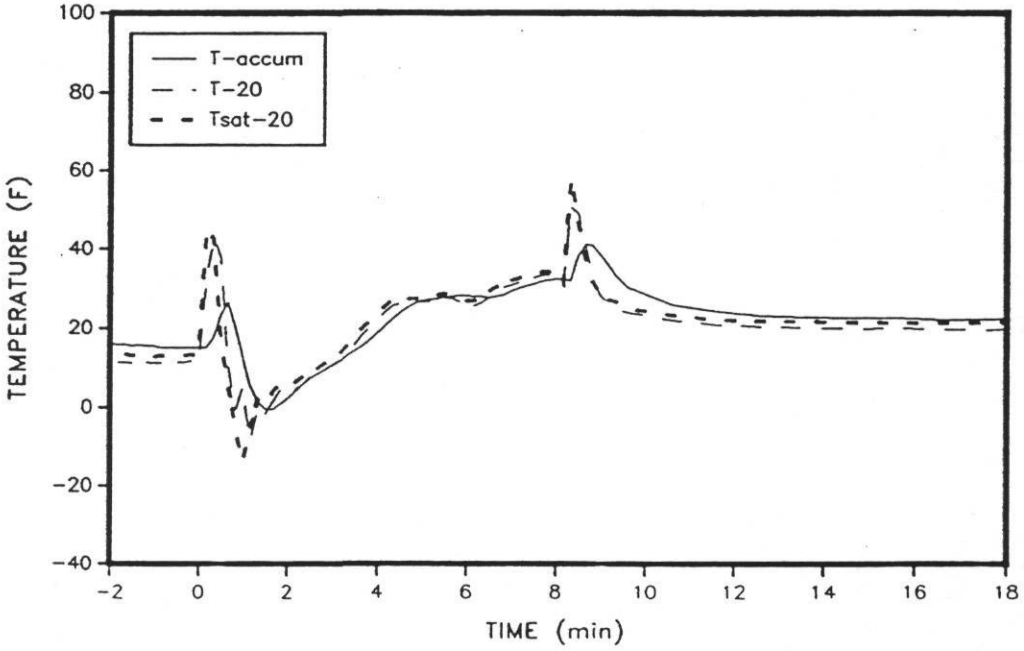

Figure 4.12. T-20, Tsat-20 and Bottom Temperature of Accumulator (Base Case).

Melting Frost
(1.0 to 4.2 minutes)

After one minute into the defrost cycle, there was evidence of the frost melting from the outdoor coil. Up to this point, the indoor coil had not supplied a significant amount of energy to the system, since the coil had contained only vapor. At 1.0 minute, the indoor coil capacity began to increase (Figure 4.11b) from 0.5 tons of heating capacity at 1 minute to 2.3 tons of cooling capacity at 4.2 minutes. This increase in cooling capacity was coincident with the rapid rise in refrigerant flow (Figure 4.10b) from approximately 2 lb/min at 1 minute to 9 lb/min at 4.2 minutes. As the indoor coil reached a maximum capacity of 2.3 tons, SHSC-24 fell to zero as liquid refrigerant overflowed the indoor coil into the accumulator. At 4.5 minutes, the accumulator level was approximately 25% full and started to rise as the suction line was filled with liquid refrigerant. The increasing saturation temperature from 1.0 minutes to 4.5 minutes was a result of the increasing flow of refrigerant vapor from the indoor coil to the compressor (Figure 4.10b) which increased the suction pressure from 30 psia to 70 psia(Figure 4.9b).

From 1.0 minute to 4.2 minutes into the cycle, frost was melted from the outdoor coil. Figures 4.13 and 4.14 show the defrosting coil at 2.0 minutes and 3.0 minutes, respectively. During this time, the temperature of the liquid refrigerant leaving the outdoor coil remained at 32°F as the phase change occured from frost to liquid water(Figure 4.7b). The subcooling of the liquid refrigerant leaving the outdoor coil (SHSC-26 in Figure 4.15) increased to 30°F during the same period as the compressor discharge pressure increased to 130 psia. These conditions greatly increased the capacity of the TXV and the refrigerant flow increased to 9.3 lbs/min(Figure 4.10b).

Draining Melted Frost
(4.2 to 8.1 minutes)

At 4.2 minutes, most of the frost had melted from the outdoor coil and the melting phase ended as the average leaving refrigerant temperature (T-17) rose above 32°F and continued to rise to 70°F in 30 seconds (Figure 4.7b). The end of the melting phase was determined when T-17 rose above 34°F. As T-17 rose to 70°F, the subcooling in the outdoor coil(SHSC-17) fell to approximately 4°F(Figure 4.15b). The subcooling upstream of the TXV (SHSC-26) did not fall as rapidly as T-17 and remained at approximately 10°F until 7 minutes.

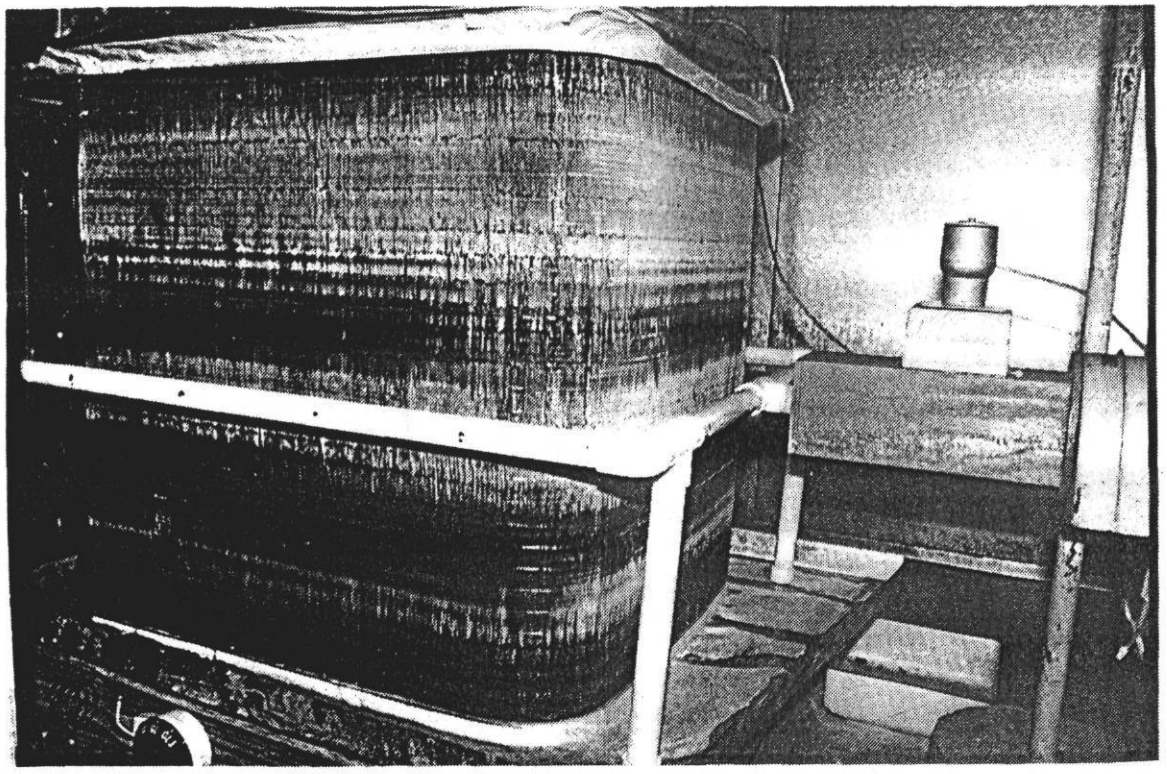

Figure 4.13. Outdoor Coil at 2 Minutes After Defrost.

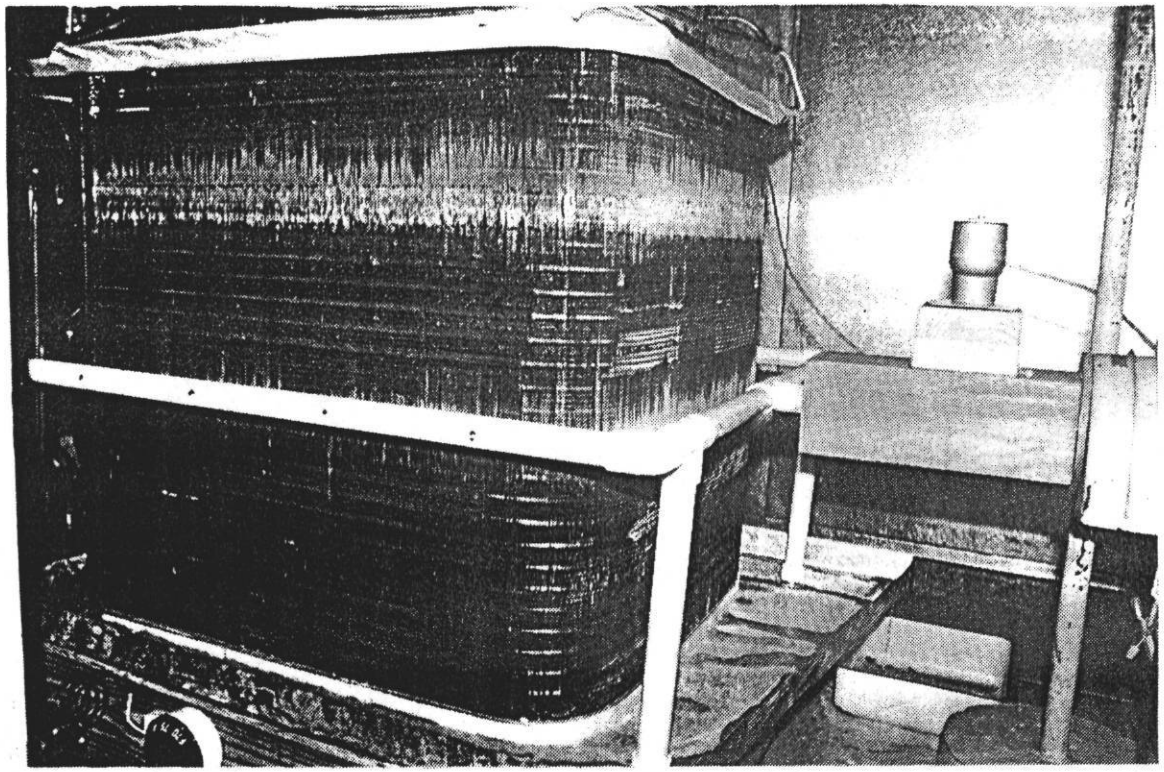

Figure 4.14. Outdoor Coil at 3 Minutes After Defrost.

While the internal movements of TXV #57 were not monitored during the defrost cycle, it is possible to infer its effects on the defrost cycle from the amount of superheat leaving the indoor coil(SHSC-24) and the refrigerant flow(Figure 4.11b). During the heating cycle, TXV #57 was bypassed, but its expansion bulb still sensed a superheated condition in the vapor line close to T-24. The TXV should have reacted to the superheated condition by opening its orifice to a maximum in an attempt to reduce the superheat. Thus, TXV #57 should have been wide open at defrost initiation and also during the melt phase. Refrigerant flow dropped to near zero at defrost initiation(0 minutes) as the reversing valve engaged. The flow rose steadily to over 9 lb/min at 4.5 minutes. The superheat at the outlet of the indoor coil(SHSC-24) remained over 30°F during this period, so TXV #57 should have remained wide open. At 4.4 minutes, the superheat dropped to zero as liquid refrigerant flooded the vapor line and TXV #57 closed down its opening and reduced the refrigerant flow from 9 lb/min at 4.5 minutes to 5.3 lb/min at 5.5 minutes.

When the refrigerant flow was reduced at 5.5 minutes, the indoor coil was able to increase the superheat as it rose to 20°F at 6.5 minutes. The TXV reacted to the increased superheat by opening larger and increasing the flow to 8 lb/min at 7.0 minutes. This reaction reduced the superheat to zero once more at 8.0 minutes. The TXV was unstable in its attempt to control the superheat(Figure 4.15) and the instability (or hunting) continued until the cycle was terminated. At this point, TXV #57 was again bypassed in the heating mode.

During the drain phase of the defrost, the leaving refrigerant temperature (T-17) in the outdoor coil rose from 32°F at 4 minutes to 105°F at defrost termination (Figure 4.7). As the frost melts the outdoor coil was exposed to the ambient temperature which caused a reduction of heat transfer from the refrigerant in the outdoor coil to the ambient. Consequently, this was an increase in the refrigerant temperature inside the outdoor coil. The increasing coil temperature resulted in an increase in compressor discharge pressure from 110 psia to 240 psia for the same period(Figure 4.9), which caused an increase in heat pump power from 2.2 kW to 3.2 kW (Figure 4.10).

(a) Complete Cycle

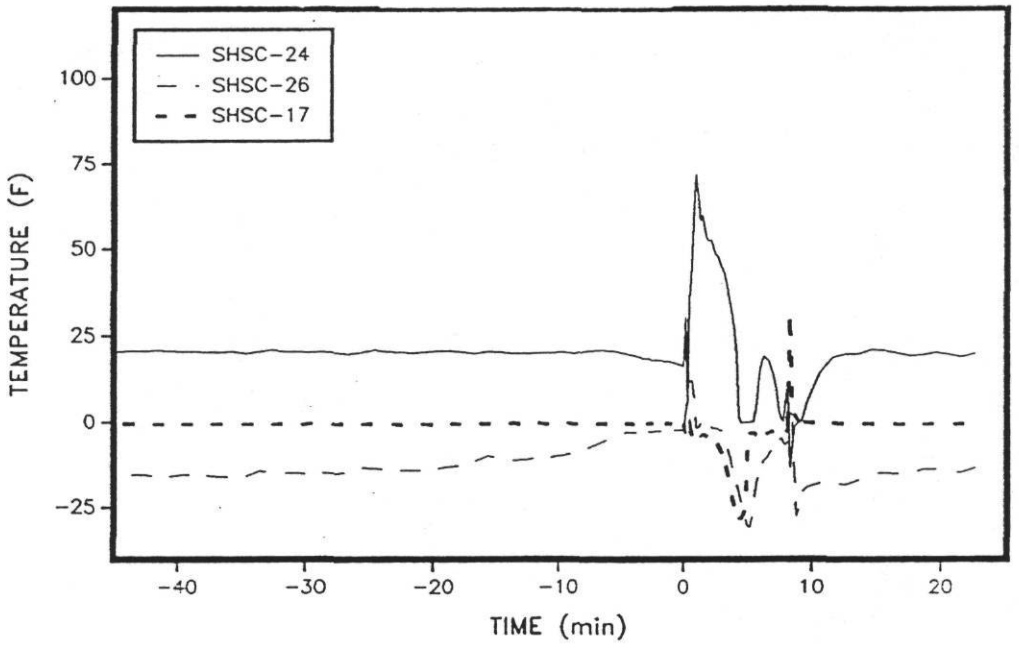

(b) Detail of Defrost

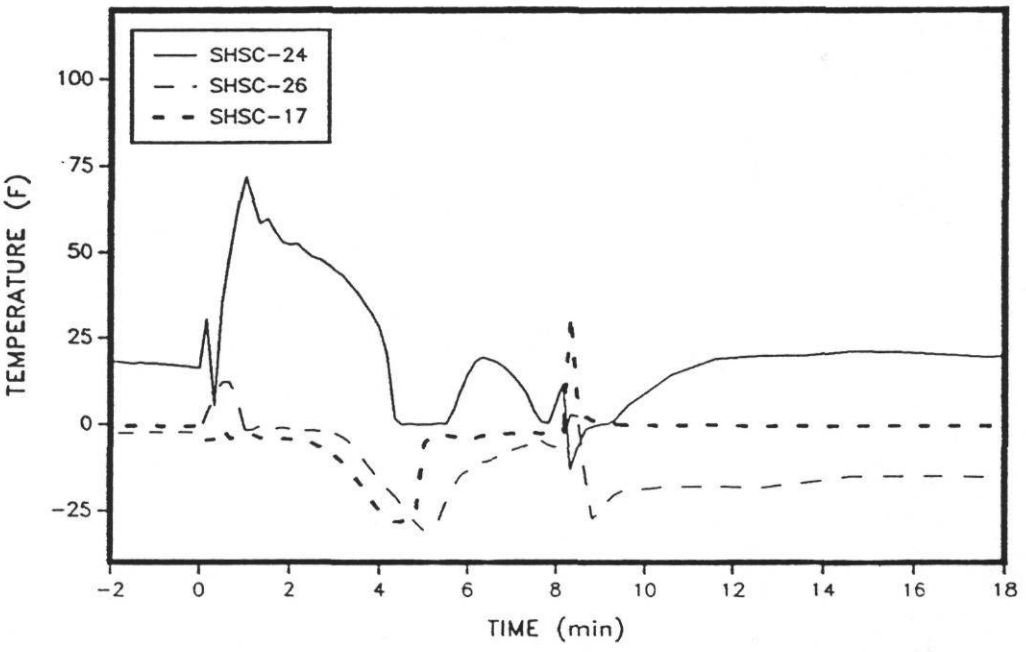

Figure 4.15. Superheat/Subcooling for T-17, T-25, and T-26. (Base Case).

Defrost Termination And Recovery

When the coil cleared of frost, the water produced by the melted frost was drained from the coil before terminating the defrost cycle. The outdoor coil had four parallel refrigerant circuits. The top circuit was designated as circuit 0. The middle circuits were 1 and 2. The bottom circuit was 3. In this test, termination was triggered when the temperature of the exiting bottom circuit(3) reached 65°F. This circuit and the termination scheme were chosen because they conformed to the manufacturers defrost termination scheme. The bottom circuit contained more liquid refrigerant during the defrost cycle and was also the coldest of the four circuits. Figure 4.16 shows a plot of the four circuit temperatures.

As the reversing valve was switched back to the heating mode, large pressure swings in both the liquid and vapor lines occured again (Figure 4.9). The pressure dropped 100 psi and then rose 80 psi in less than 20 seconds. The suction line received a similar shock of a 40 psi rise and drop in the same period. These pressure spikes were also reflected in Figure 4.9 as the power input to the compressor had a spike of -0.5 KW.

Unlike the beginning of the defrost cycle, where the indoor coil contained only low pressure vapor, the outdoor coil remained saturated after defrost termination, and the compressor was not starved for refrigerant. Figure 4.17 shows the refrigerant conditions in the vapor line(suction) at the outlet of the outdoor coil(T-18). After defrost termination, the vapor line remained saturated, providing sufficient refrigerant into the compressor. The refrigerant flow(Figure 4.15) also recovered within 30 seconds. The saturated condition contrasted with conditions after defrost initiation where there was a very high superheat(SHSC-24), in the suction line (Figure 4.11) and a large drop in suction pressure (Figure 4.9). The condenser was also at 70°F instead of 32°F so the discharge pressure of the compressor remained above 200 psia. These factors resulted in a relatively fast recovery compared to the defrost initiation and the heat pump returned to 80% capacity in two minutes, although it took the unit nearly 10 minutes to reach 100% capacity.

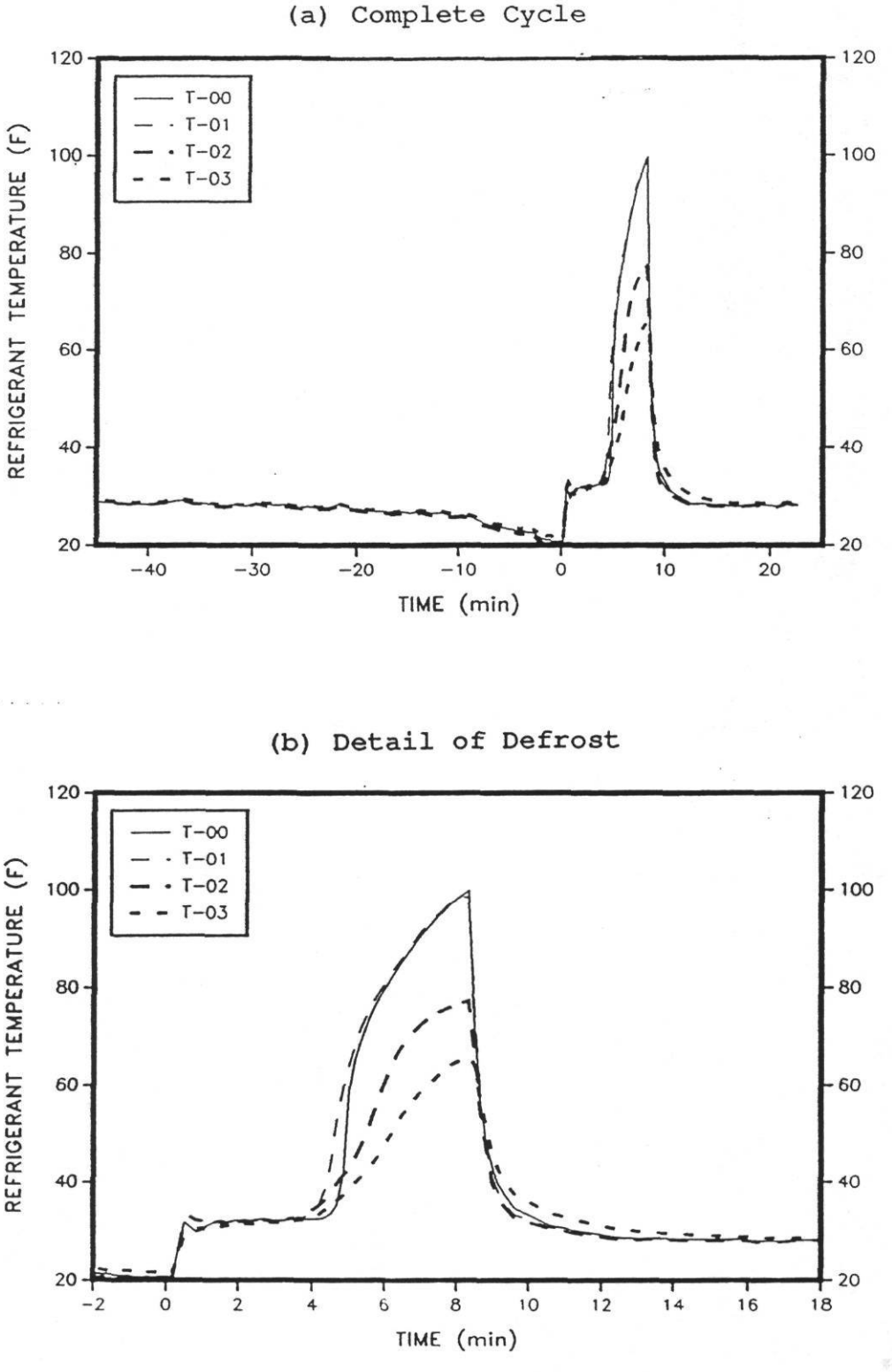

Figure 4.16. Outdoor Coil Circuit Temperatures at Defrost Termination (Base Case).

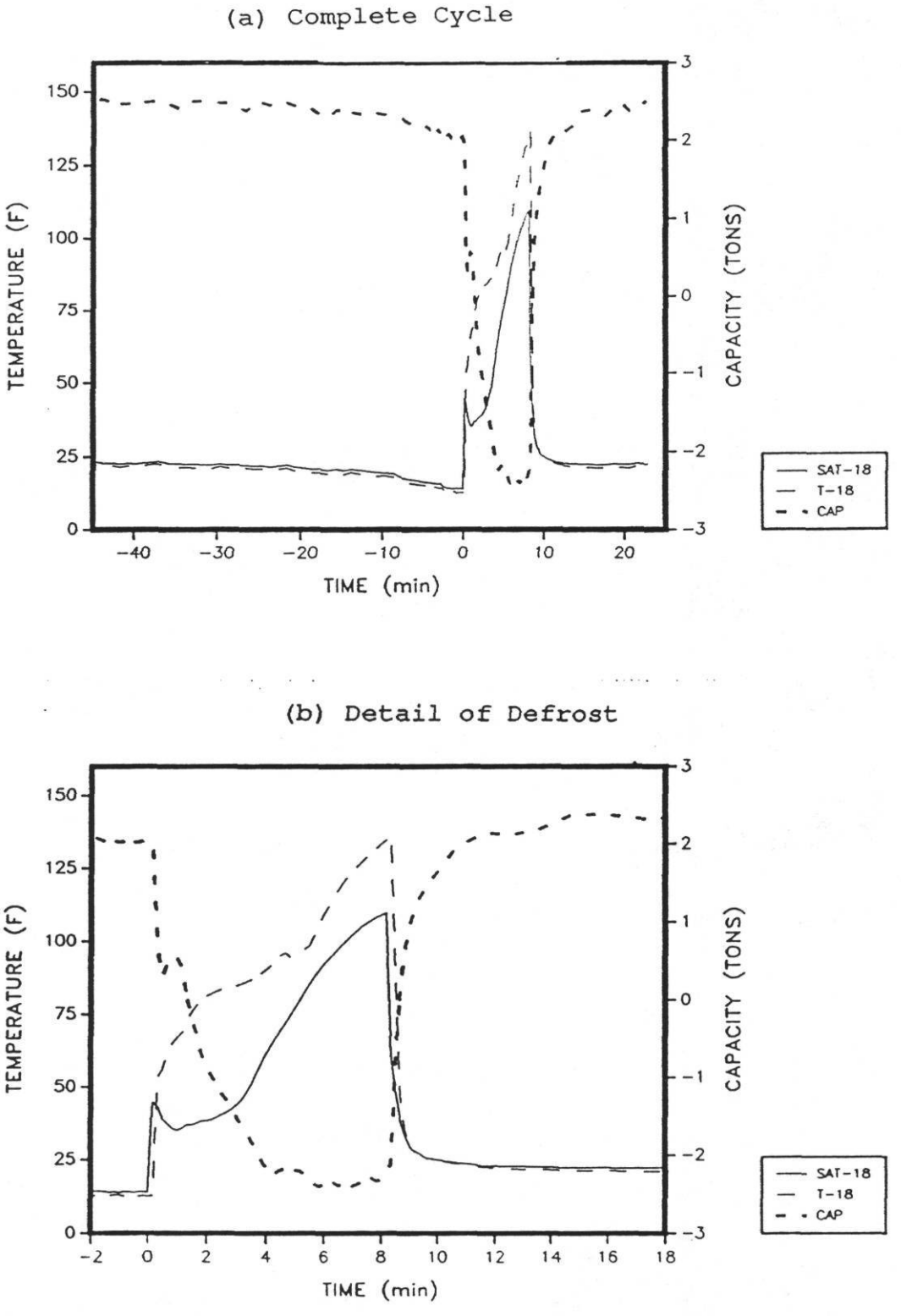

Figure 4.17. T-18, Tsat-18, and Capacity (Base Case).

Summary

To evaluate the effects of different expansion devices on a heat pump during the reverse cycle defrost, a base case unit and test had to be established as a point of comparison. The selected base expansion device was a thermal expansion valve labeled TXV #57 that was average in response time. Several defrosting runs were made with TXV #57 and the base case performance was established. A detailed analysis of the base case test was also made, which was used in the analysis of the comparison tests.

CHAPTER 5

COMPARISON OF TXVs WITH DIFFERENT RESPONSE TIMES

In addition to the base case thermal expansion valve (TXV), two other TXVs of the same model and capacity were installed in the heat pump to evaluate their effect on the defrost cycle performance. The only difference between the base expansion valve and the two others was in the response times to go from fully closed to fully open. These three TXVs were selected from a sample of nine TXVs provided by their manufacturer*. The three provided a sample of the slowest, fastest, and average response times. TXV #57, the base case TXV, was approximately the average of the group, while TXV #51 was the fastest and TXV #52 had the slowest response.

Figure 5.1 shows a plot of the response times of the three TXVs selected. The stroke range from fully closed to fully open was 0.024 inches. In a full open position, the equivalent port area for the 2 1/2-ton TXV was 0.0059 $in.^2$, which is equivalent to a 0.086 inch diameter orifice. The time constant for each TXV was the time it takes for the stroke to go from 0.0 to 63.2% of maximum stroke. All three of the TXVs had the same maximum stroke, so the time constant was the time it took the stroke to increase from 0.0 to 0.015 inches. Table 5.1 contains the TXV time constants.

Table 5.1. Time Constants for TXVs.

TXV #	TIME CONSTANT (seconds)
51	15
57	19
52	25

* Response tests were conducted by the TXV manufacturer at their test laboratories.

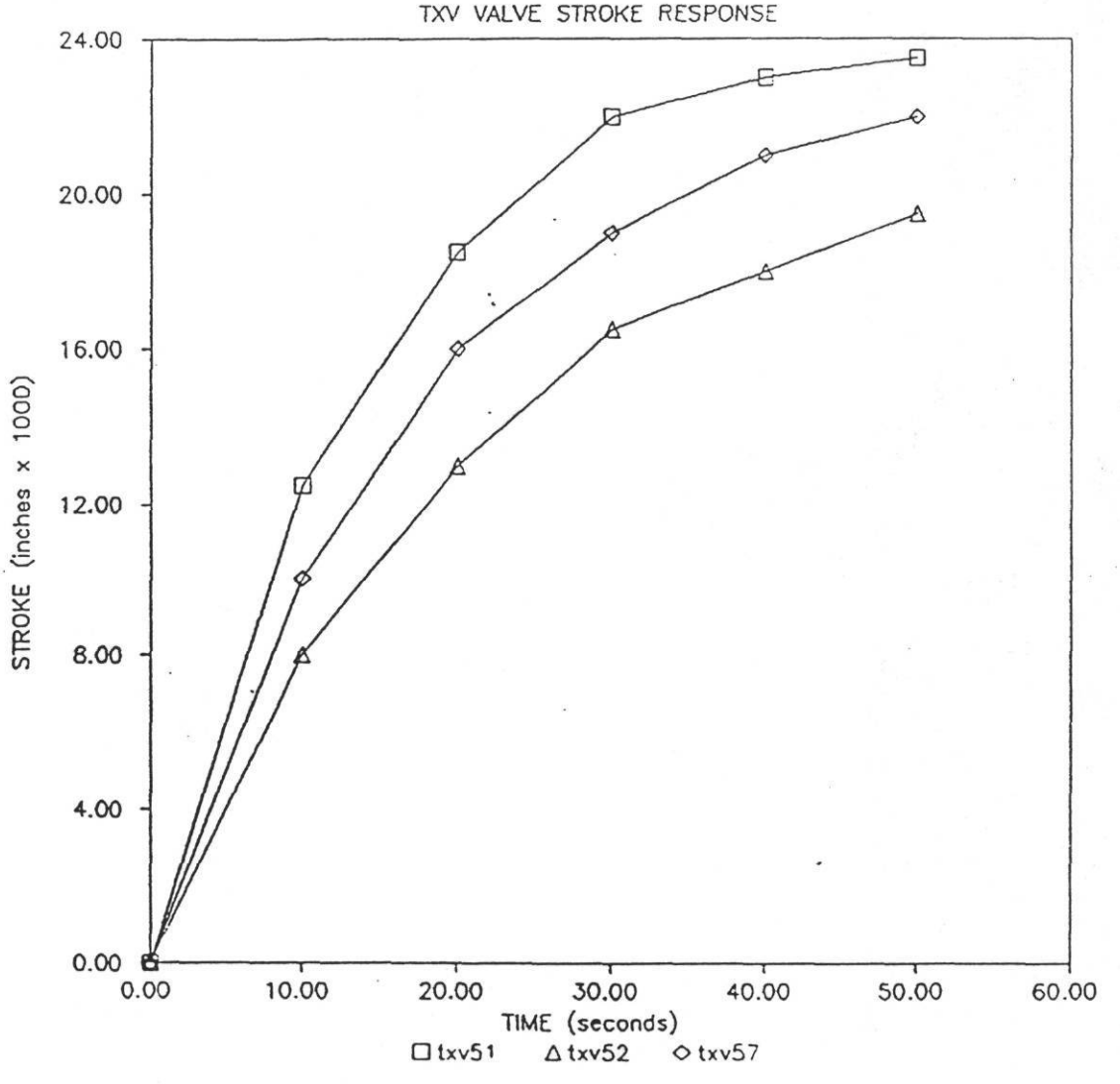

Figure 5.1. Response Times for Selected TXVs.

In comparing the impact of the TXVs on the heat pump system performance, four characteristics were considered: integrated COP, defrost time, melting time(the time required to melt the frost), and drain time(the period after the frost was melted and the water was draining from the coil). These values are presented in Table 5.2 for the three TXVs. The integrated COP was the ratio of the integrated heating output measured at the indoor coil over the integrated power consumption. The COP was measured over a complete frosting/defrost cycle which started at the termination of the previous defrost and ended at the termination of the present defrost.

The characteristics for each TXV were averages taken from three consecutive runs. The average deviations during the tests were +/- 1% for the COPs and defrost times and +/- 2% for the melt and drain times.

Table 5.2. Comparison of Defrost Characteristics* for Three Thermostatic Expansion Devices.

DEFROST EXPANSION DEVICE	INTEGRATED COP	DEFROST TIME (min)	MELT TIME (min)	DRAIN TIME (min)
TXV #57	2.26	8.06	4.22	3.83
TXV #51	2.22	8.33	4.39	3.94
TXV #52	2.16	8.28	4.00	4.28

* Characteristics are average values taken over three consecutive frosting/defrost cycles.

TXV #57(base case) had the best performance with a COP of 2.26 TXV #51(fast) was next with 2.22 and TXV #52(slow) had the lowest COP of 2.16. The difference between the COP for TXV #57 and TXV #51 was less than 1.8%, which was less than the combined experimental uncertainty. The COP for TXV #52 was 3.7% less than TXV #57. Though the variation was small, it was greater than the experimental uncertainty, and it indicated a small variation in defrost performance.

In analyzing the defrost times for #57 and #52, the times were broken into two parts: the melt time and drain time. The melt time for TXV #52 was 5.2% (13 seconds) shorter than TXV #57. However, the drain time was 11.7% (27 seconds) longer.

Figures 5.2 and 5.3 show the heating capacity and power consumption for TXV #57 and TXV #52, respectively. The power usage during the melt phase(approximately the first 4 minutes of defrost) stayed close to 2 kW because the constant temperature of 32^{o}F in the outdoor coil held the compressor discharge pressure below 100 psia for 1.5 minutes(Figures 5.4 and 5.5). The pressure rise through the compressor, and the power usage were also smaller during this period. The heating capacity fell to zero before 1.5 minutes into the defrost cycle. It then became negative and decreased to a negative 2.3 tons at the end of the melt phase.

After the melt phase, the rising power and negative capacity during the drain phase produced a larger penalty to the overall COP during the drain time than the during the melt time. Because the drain time for TXV #52 was 11.7% longer than the drain time for TXV #57, the integrated COP for TXV #52 was lower than TXV #57.

The reason for the shorter melt time and longer drain time of TXV #52 can be explained with the use of the refrigerant flow characteristics shown in Figures 5.6 and 5.7. The maximum refrigerant flow during the defrost cycle for both TXVs was 9.1 lb/min. TXV #52 reduced the refrigerant flow at approximately the same time in the defrost cycle as TXV #57, but only to 5.8 lb/min instead of 5.1 lb/min for TXV #57.

Figures 5.6 and 5.7 also show the superheat at the exit of the indoor coil(SHSC-24) for TXV #57 and TXV #52, respectively. For both TXVs, there was a larger rise in superheat at the exit of the outdoor coil during the first minute after defrost initiation caused by the evaporation of "hot" refrigerant left in the coil during the frosting

---

+ A negative capacity indicates cooling rather than heating.

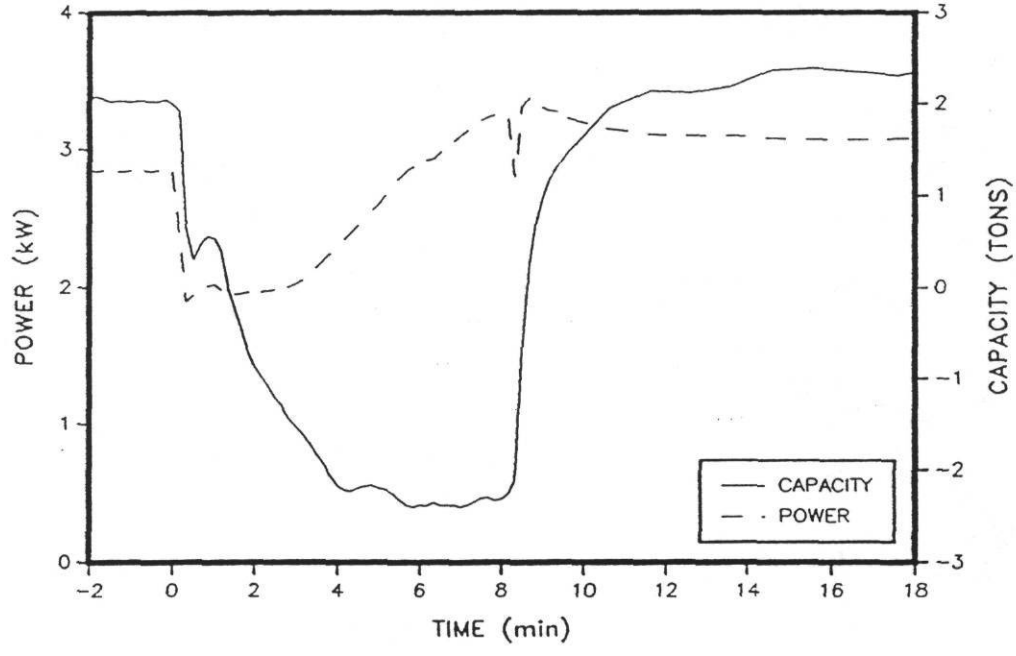

Figure 5.2. Power Usage and Heating Capacity for TXV #57 (Base Case).

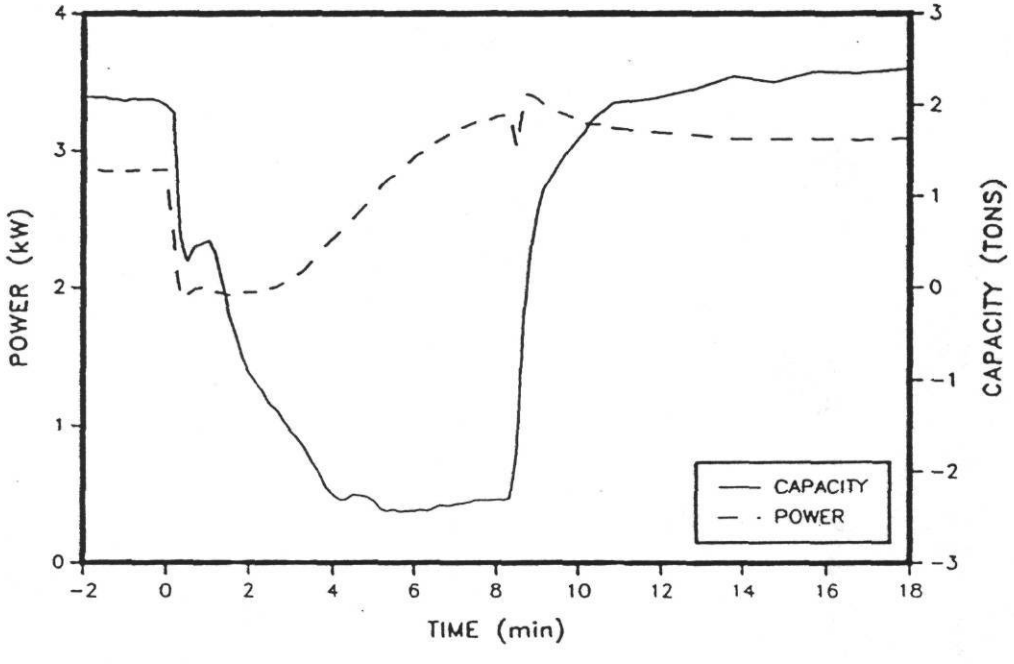

Figure 5.3. Power Usage and Heating Capacity for TXV #52.

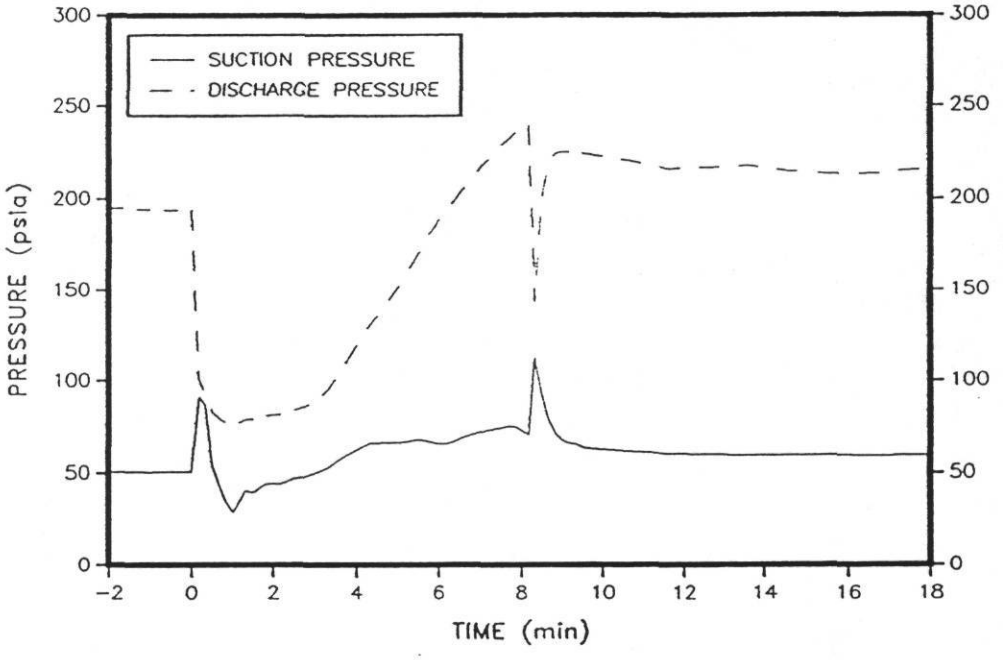

Figure 5.4. Compressor Suction and Discharge Pressures. for TXV #57 (Base Case).

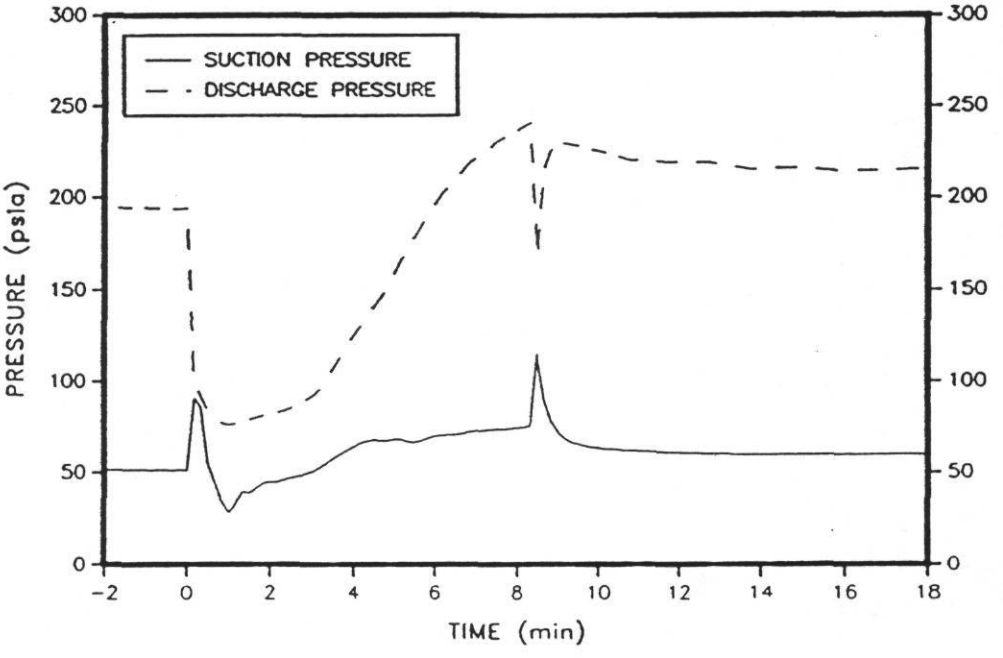

Figure 5.5. Compressor Suction and Discharge Pressures. for TXV #52.

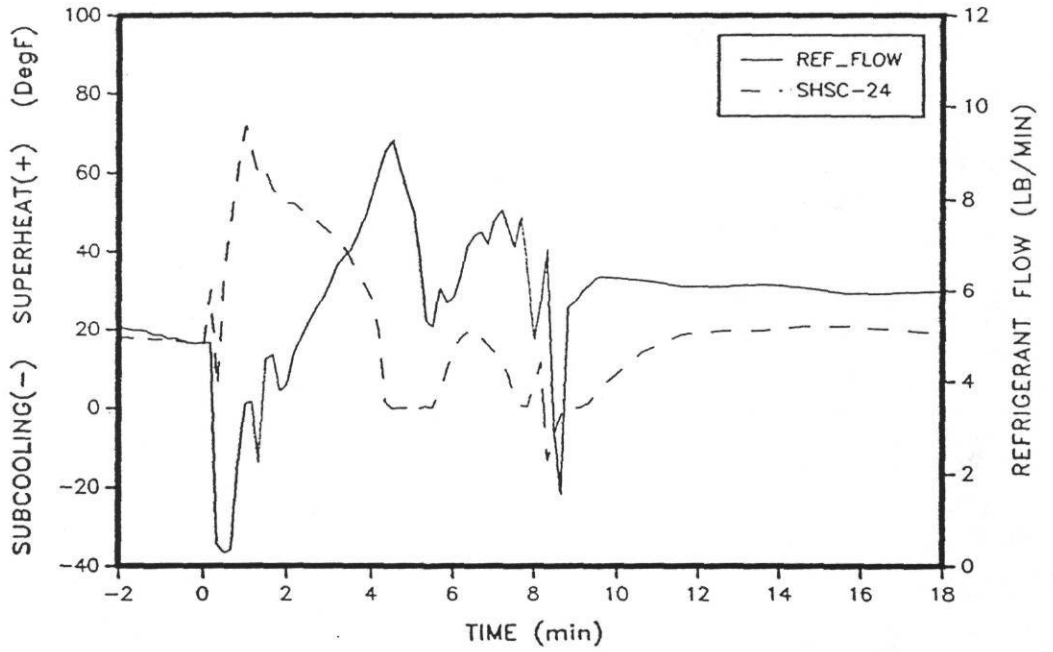

Figure 5.6. Superheat/Subcooling for T-24 & Refrigerant Flow for TXV #57 (Base Case).

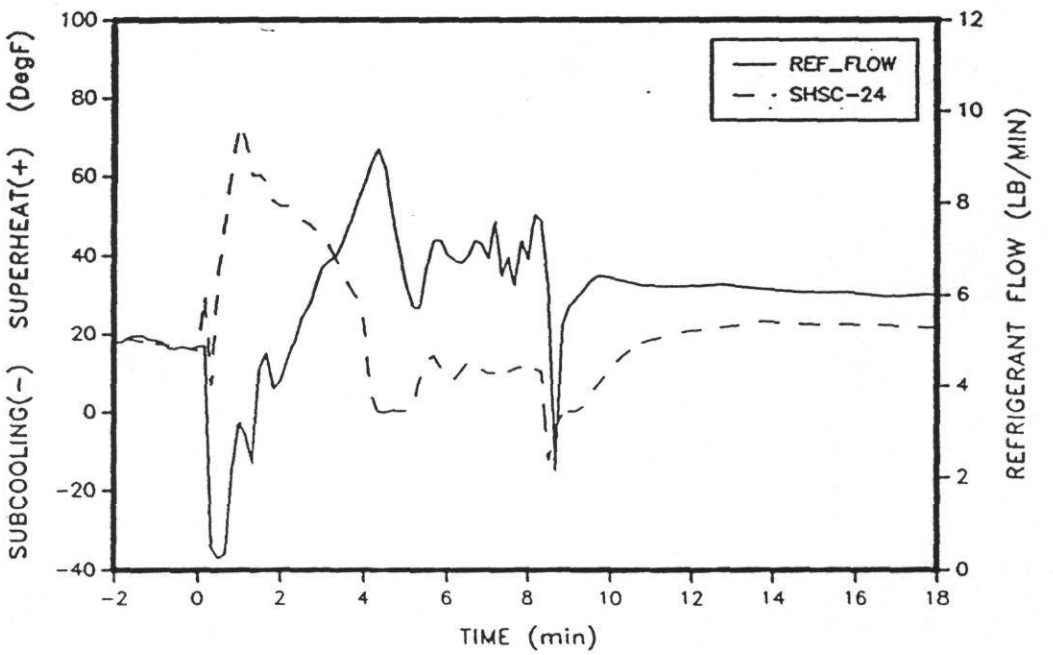

Figure 5.7. Superheat/Subcooling for T-24 & Refrigerant Flow for TXV #52.

period. The superheat peaked at approximately 70° F for both TXVs. Because the superheat was larger than the nominal 10°F rating of each value, they both responded by increasing the flow through the indoor coil. With the increase in flow, the superheat dropped. Both TXVs "overshot" the desired superheat and produced saturated conditions by 4.25 minutes into the defrost. The TXVs then both reduced flow in an attempt to produce the desired superheat.

After TXV #52 reduced the refrigerant flow, the flow out of the evaporator became superheated again at 5.2 minutes into the defrost compared to 5.5 minutes for TXV #57. The superheat for the slower TXV #52 from 5.5 minutes to the end of the defrost cycle appeared similar to a classical damped second order system. There were small, but damped oscillations in the superheat, with the average being approximately 10° F. The flow for TXV #52, during this time, rose up to 7 lb/min and experienced small oscillations between 6.2 and 7.2 lb/min. The superheat for the faster TXV #57 increased to a peak of 20° F, then reduced to 0° F at 7.7 minutes into the defrost. It then increased to 12° F at defrost termination. The refrigerant flow showed larger oscillations in flow during this time than did TXV #52. After dipping to 5.3 lbs/min, the TXV peaked at 7.8 lb/min (with small oscillations) at 7.1 minutes then dropped to 5.1 lb/min at 8 minutes. The flow then increased to 6.9 lb/min before defrost termination. After the slower TXV #52 reduced the refrigerant flow, the superheat began to increase at approximately 15°F at 5.5 minutes and then stabilized at 10°F at 8.0 minutes(Figure 5.7).

By stabilizing the flow, the slower TXV #52 had a lower average refrigerant flow during the drain period then the faster TXV #57. With the smaller refrigerant mass flow rate for TXV #52, less energy was transferred to the outdoor coil. Therefore, the outdoor coil did not heat up as fast as with TXV #57 which delayed the termination of the defrost cycle. The longer drain time penalized TXV #52 because it operated longer in the period where the cycle degradation was high, reducing the overall COP.

Figures 5.8 and 5.9 show the superheat and refrigerant flow characteristics for TXV #57 and TXV #51 respectively. The control characteristics of the TXVs were similar, but some variations were noticeable. At approximately one minute into the defrost, SHSC-24, (the superheat at the outlet of the indoor coil during the defrost cycle) rose to 75°F for TXV #51 which was approximately 5°F higher than TXV #57. After the drop in superheat near the end of the melt period, SHSC-24 for TXV #51 rose to 18°F at 6.5 minutes and remained at while SHSC-24 rose to 20°F. Even though the response time of TXV #51 was faster than either that of TXV #57 and TXV #52, it was not evident from the superheat data.

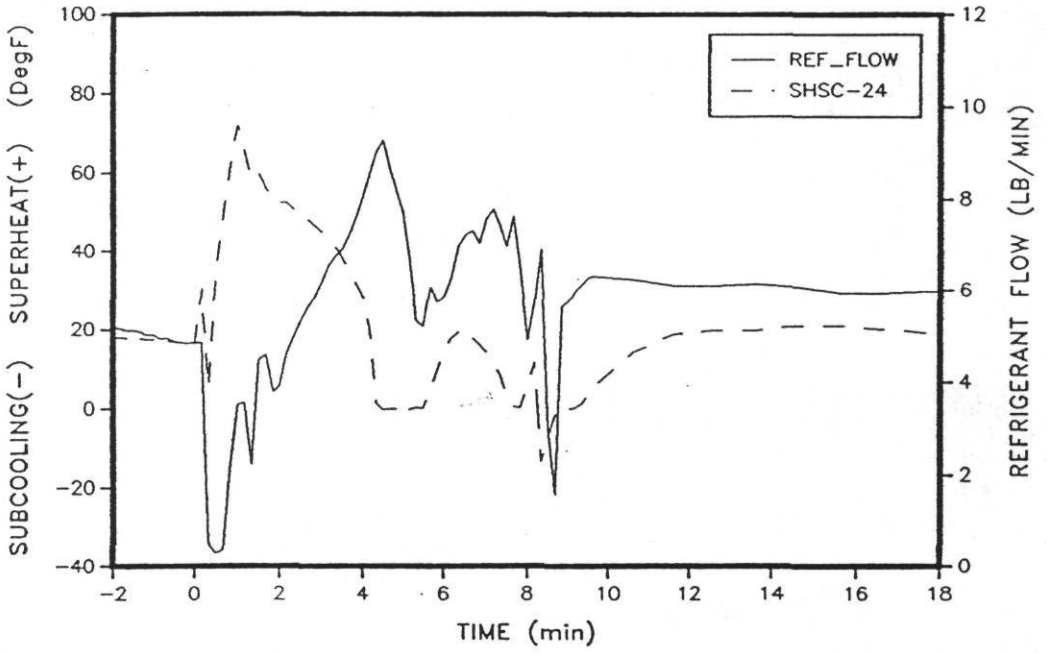

Figure 5.8. Superheat/Subcooling for T-24 & Refrigerant Flow for TXV #57 (Base Case).

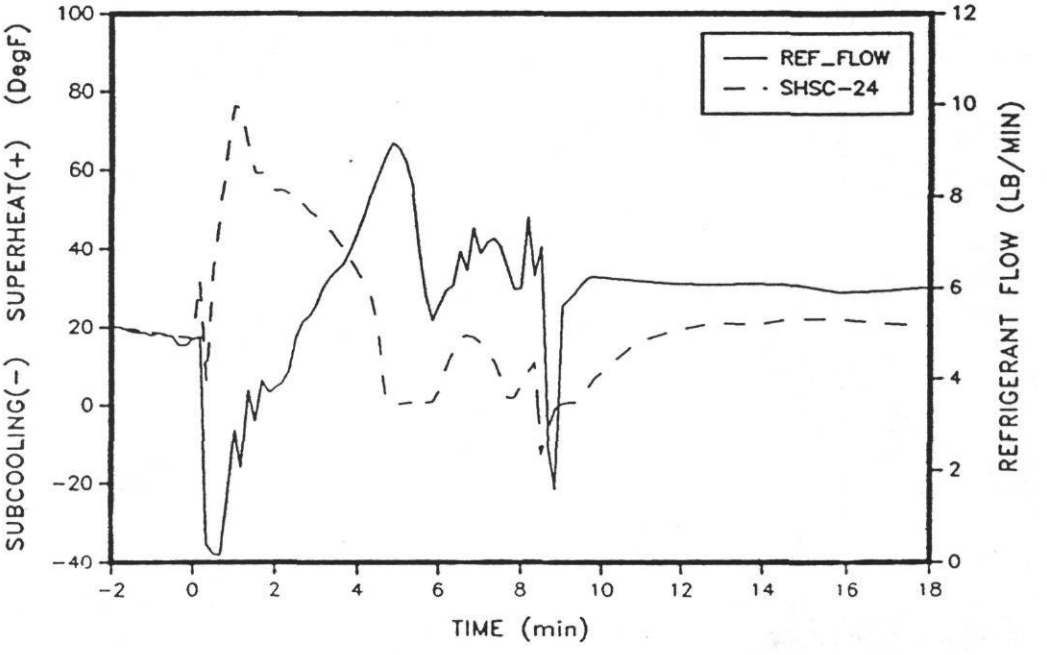

Figure 5.9. Superheat/Subcooling for T-24 & Refrigerant Flow for TXV #51.

The speed of the TXVs did not establish a discernible trend for the COP as was anticipated. TXV #57 had the highest COP but was average in response time. The expected trend was either fast response time to slow or the vice-versa.

Further tests using TXV #57 revealed different control characteristics from those shown during the initial comparison testing. Figures 5.10 and 5.11 show the refrigerant flow and superheat at T-24 for two tests run with TXV #57 at different dates. For these tests the test unit was disassembled and reassembled which means the TXV bulb was removed and then remounted to the suction line.

The differences between Figures 5.10 and 5.11 and the base case(Figure 5.8) were dramatic. The refrigerant flow for test 1 showed the largest variation from the base case as the refrigerant flow rose as high as 10 lb/min and only dropped to 7.5 lb/min before rising steadily to 8.5 lb/min at defrost termination. The superheat(SHSC-24) leaving the coil initially fell to zero like the base case but then rose to 20°F and remained there until termination. The refrigerant flow in Figure 5.11 was similar to the base case, but the similarities in this test using TXV #57 were not as close as the comparison between TXV #51 and TXV #57 in Figures 5.7 and 5.8.

The control variations in TXV #57 indicated the importance of the expansion bulb placement on the suction line. While the expansion bulb was mounted in the same position for every test, small variations in surface contact between the expansion bulb and the restraint line caused the control characteristics of TXV #57 to change drastically. It appears that the expansion bulb placement on the suction line was as important a factor in determining defrost response as was the internal response time of the TXVs.

SUMMARY

Three TXVs of different response times were tested, resulting in the highest COP for the base case TXV #57. The COP for TXV #51(fast response) was slightly less than TXV #57 and had similar control characteristic. TXV #52 (slow response) had the most stable control of refrigerant and superheat, but also had the lowest COP. Analysis showed that the stable control of TXV #52 allowed less refrigerant to flow to the outdoor coil which delayed the termination of the defrost, causing the reduction in COP.

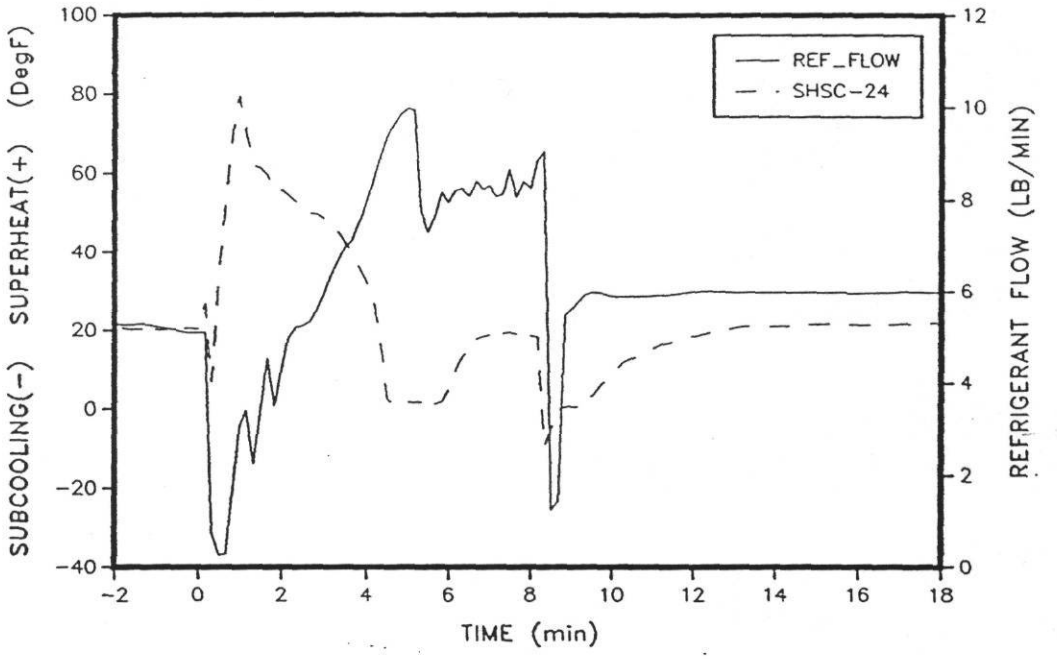

Figure 5.10. Superheat/Subcooling for T-24 & Refrigerant Flow for TXV #57 - Test #1.

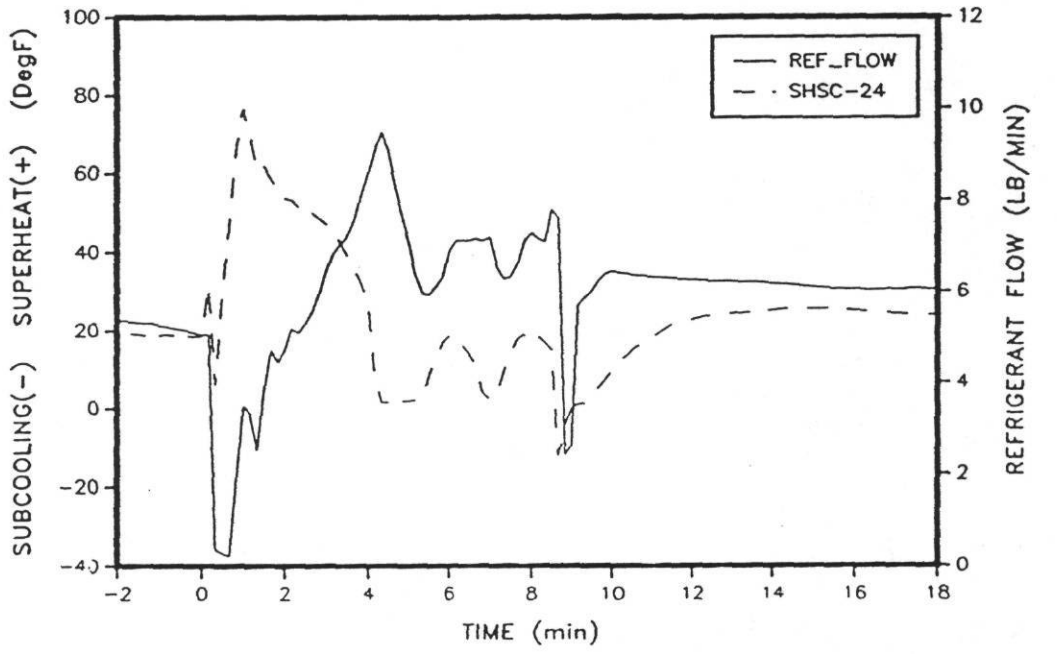

Figure 5.11. Superheat/Subcooling for T-24 & Refrigerant Flow for TXV #57 - Test #2.

Further testing with the base case revealed variations in refrigerant control characteristics using TXV #57. The variations were caused by expansion bulb remounting after the test setup was disassembled and reassembled between tests. The variations in the control characteristics for the three TXVs were not as great as that of TXV #57 with slight differences in bulb placement.

CHAPTER 6

COMPARISON OF DIFFERENT DIAMETER ORIFICES

The orifice analysis started with a comparison of the control characteristics of the base case TXV #57 and an orifice whose flow diameter was comparable to the maximum flow diameter for TXV #57. The orifice was labeled ORF 090. The ORF was an abbreviation for orifice and the number 090, referred to the diameter of the orifice in thousandths of an inch. Following the comparison of ORF 090 and TXV #57, the analysis continued with a comparison of the operation of six different sizes of orifices: ORF 059, ORF 070, ORF 076, ORF 090, ORF 101, and ORF OPEN. ORF OPEN was the orifice holder with the orifice removed, giving an approximate opening diameter of 0.300 inches, essentially no restriction.

Control Differences Between A TXV And An Orifice

As mentioned in Chapter 5, the base case expansion device(TXV #57) had an equivalent port area, when fully open, equal to a 0.087 inch diameter orifice. Since the diameter of ORF 090 was approximately equal to 0.087 inches, it was selected for comparison with TXV #57 during the reverse cycle defrost. Table 6.1 shows the effects of the two expansion devices on the defrost cycle.

Table 6.1. Comparison of Heat Pump System Characteristics Using TXV #57 and Orifice 090.

DEFROST EXPANSION DEVICE	INTEGR. CYCLIC COP	DEFROST TIME (minutes)	MELT TIME (minutes)	DRAIN TIME (minutes)
TXV #57	2.26	8.06	4.22	3.83
ORF #90	2.28	7.83	4.83	3.00

The overall performance of TXV #57 and ORF 090 were essentially equal as the COP varied by less than 1% and the defrost times by less than 3%. This similarity did not hold true for the melt and drain times. TXV #57 was able to melt the frost on the coil 12.6% (36 seconds) faster than ORF 090, but TXV #57 took 27.7% (49 seconds) longer to heat the coil and terminate the defrost during the drain time. The variations in melt time and drain time indicate differences in control characteristics even though the overall performances were similar.

The system refrigerant flow characteristics and the subcooling(SHSC-26) at the inlet of TXV #57 and ORF 090 are shown in Figures 6.1 and 6.2, respectively. For the first 2 minutes into defrost, the refrigerant flow for both expansion devices followed similar trends. After defrost initiation, the refrigerant flow dropped close to zero and then rose into a period of unstable flow. This unstable flow was caused by the saturated condition at the inlet to the expansion device(T-26) as shown in Figures 6.1 and 6.2. T-26 was superheated during the first minute of defrost and at 1 minute became saturated as liquid started flowing through the expansion device into the indoor coil. At 2 minutes, characteristics between the two expansion devices started changing as the subcooling for TXV #57(T-26) started increasing and reached -16^{o}F at 4 minutes(Figure 6.1). During the same period in Figure 6.1, the refrigerant flow stabilized and rose from 4 lb/min to 8 lb/min. In Figure 6.2, T-26 did not become subcooled for ORF 090 until after 3 minutes. This delayed the rise in refrigerant flow for ORF 090 as it reached 6.5 lb/min at 4 minutes. Since the flow for ORF 090 was lower than that for TXV #57 during the melt phase , less hot refrigerant was pumped into the outdoor coil and the melt time was longer for ORF 090 than TXV #57.

Shortly after 4 minutes, the refrigerant flow for TXV #57 rose to 9.3 lb/min and then fell to 5.3 lb/min at 5.5 minutes. The flow for ORF 090 surpassed TXV #57 during this phase and rose to 10.6 lb/min at 5.5 minutes. During the remainder of the defrost, the refrigerant flow for ORF 090 averaged approximately 8.5 lb/min, while the flow for TXV #57 averaged 6.5 lb/min. ORF 090 allowed 30% more hot vapor into the coil during the drain phase than did TXV #57. This shortened the drain time by 50 seconds from that of TXV #57.

In Chapter 4, the control of refrigerant flow by TXV #57 was discussed in detail. The drop in refrigerant flow from 9.3 lb/min to 5.3 lb/min(Figure 6.1) at 4.5 minutes was probably caused by the closing down of the TXV port after

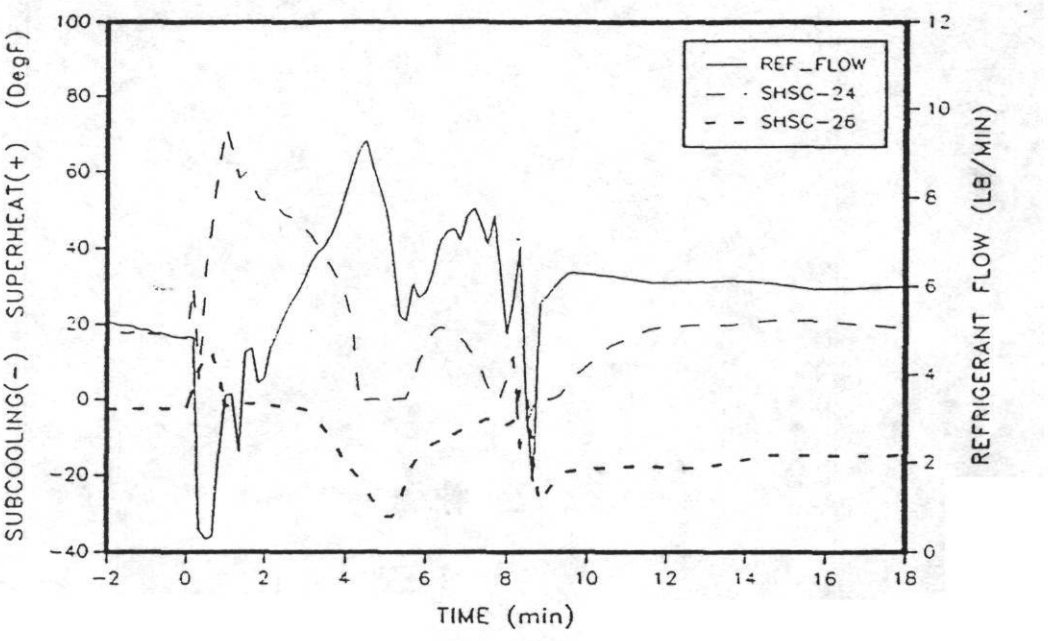

Figure 6.1. Superheat/Subcooling for T-24, T-26 & Refrigerant Flow for TXV #57 (Base Case)

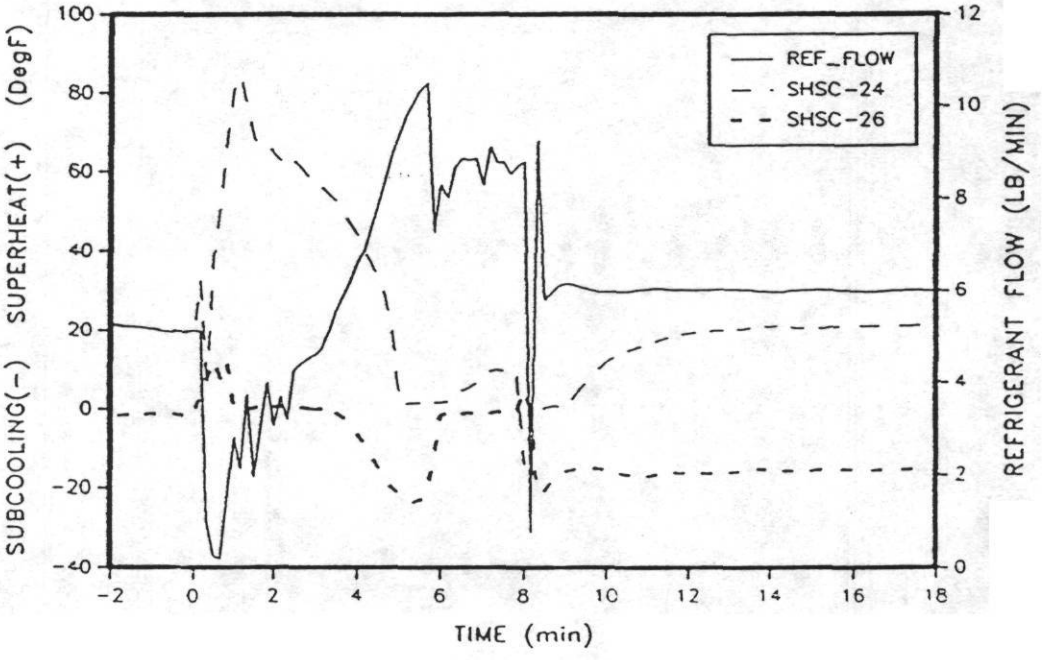

Figure 6.2. Superheat/Subcooling for T-24, T-26 & Refrigerant Flow for ORF 090.

the superheat at T-24 fell to zero at 4.4 minutes (Figure 6.1). ORF 090 had a similar reduction in its flow as it fell from 10.5 lb/min to 7 lb/min at 5.5 minutes in Figure 6.2. Since the orifice was stationary, the flow control must be caused by the refrigerant conditions at the inlet to the orifice. Figure 6.2 shows the subcooling (T-26) of the refrigerant entering the orifice. The start of the refrigerant drop at 5.7 minutes coincided with the drop in subcooling from -25°F at 5.5 minutes to -5°F at 6 minutes. The TXV #57 and ORF 090 inlet pressure(Figures 6.3 and 6.4, respectively) at 5.5 minutes were both approximately 150 psia.

Assuming the flow characteristics for an orifice were similar to a capillary tube, as stated by Krakow and Lin[22], the percentage reduction in flow through the orifice could be estimated from the Basic Rating Curves for capillary tubes in the ASHRAE 1983 Equipment Handbook[23]. From Figure 38 in chapter 19 of the Equipment Handbook, the mass flow rate for 25°F subcooling and 150 psia inlet pressure results in a normalized mass flow rate of 100 lb/hr.+ The reduced normalized flow rate with 5°F subcooling and the same inlet pressure was found to be 68 lb/hr, a 32% reduction. Applying the same percentage reduction to the 10.5 lb/min, flow rate in Figure 6.2 at 5.5 minutes yielded a reduction to 7.1 lb/min. The flow actually dropped to 7.0 lb/min, a 33% reduction. Thus, it would appear that the change in flow conditions at the inlet to the capillary tube were responsible for the large drop in flow for the orifice.

Comparison Of Different Diameter Orifices

This section focuses on the defrost cycle effects of using different diameter orifices for the defrost expansion device. The orifice diameters ranged from 0.059 inch to approximately 0.300 inch (no restriction). As was done in previous sections, the effect of the orifice on the system performance is discussed first, followed by an analysis of the refrigerant dynamics.

Table 6.2 shows the COP and defrost times for the different orifices. The COP increased with the size of orifice from a low of 2.03 for ORF 059 to a high of 2.30 for

---

+ These results are for an 80 inch long and 0.064 inch ID capillary tube

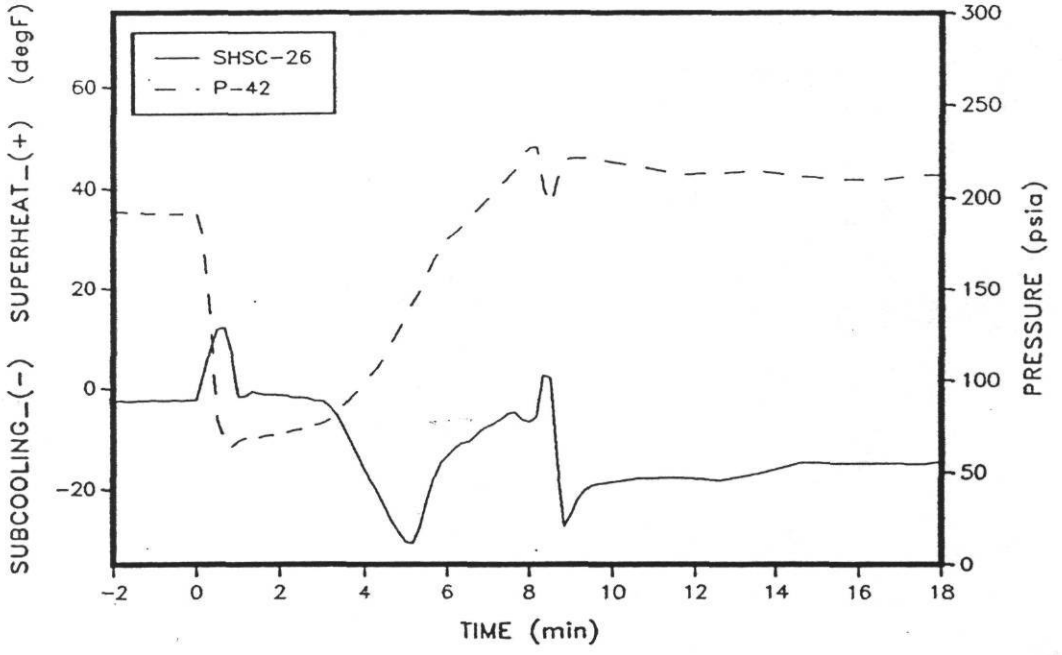

Figure 6.3. TXV #57 Inlet Pressure and Subcooling (Base Case).

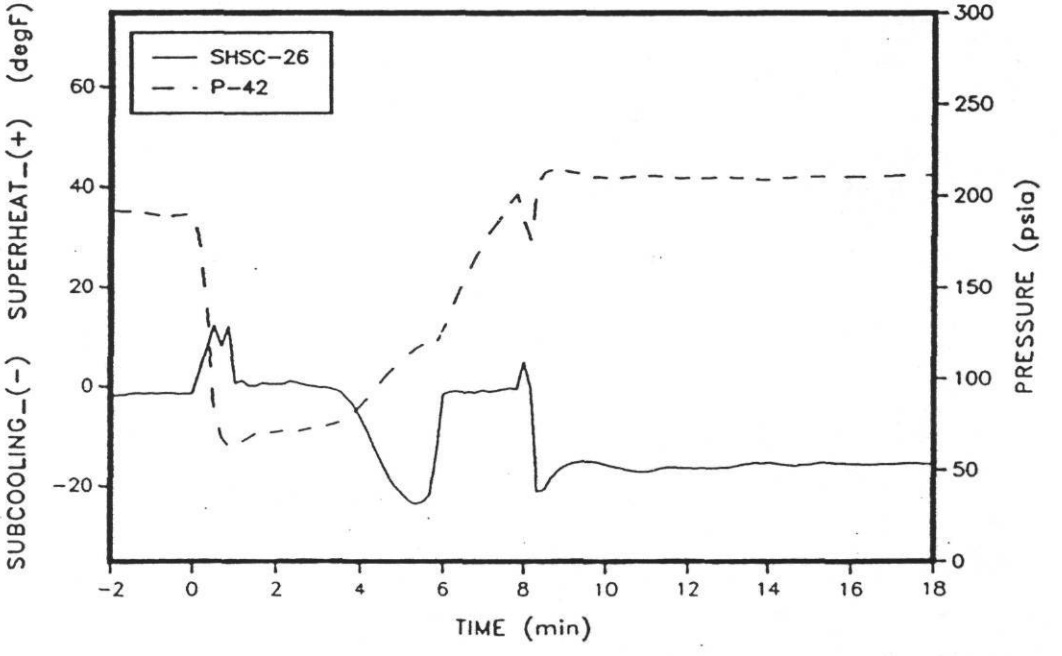

Figure 6.4. ORF 090 Inlet Pressure and Subcooling.

ORF OPEN. Directly responsible for the variation in COP was the trend of decreasing defrost times with increasing orifice size, which agreed with Young's study[12]. The defrost times are plotted in Figure 6.5 along with the melt and drain times. The relationship between orifice size and defrost time is nearly linear except for ORF 059. Breaking the total defrost time into the melt and drain times, yielded some explanation why ORF 059 had such a longer defrost cycle. The melt times showed essentially a linear trend from the 0.059 to the 0.101 inch orifice. While a similar trend was evident for the melt times from the 0.070 with orifice up to the 0.101 inch orifice, 0.059 inch orifice had a drain time that was approximately twice as long as would be expected if the trends from 0.020 to 0.10 inches were extrapolated the 0.059 inch. Thus, the drain time is primarily responsible for the longer defrost times of the 0.059 inch orifice. ORF 059 is consistent with the melt times of the other orifices, but during the drain time, ORF 059 takes over twice as long as the other orifices to terminate the defrost.

Table 6.2. Comparison of Heat Pump System Characteristics Using Various Diameter Orifices.

DEFROST EXPANSION DEVICE	INTEG. CYCLIC COP	DEFROST TIME (minutes)	MELT TIME (minutes)	DRAIN TIME (minutes)
ORF #59	2.03	14.53	6.72	7.61
ORF #70	2.21	9.71	6.00	3.71
ORF #76	2.22	9.33	5.44	3.90
ORF #90	2.28	7.83	4.83	3.00
ORF #101	2.30	7.33	4.44	2.94
ORF OPEN	2.30	6.61	3.72	2.89

Some of the operating conditions of the orifices are listed in Table 6.3. The minimum suction pressure and the

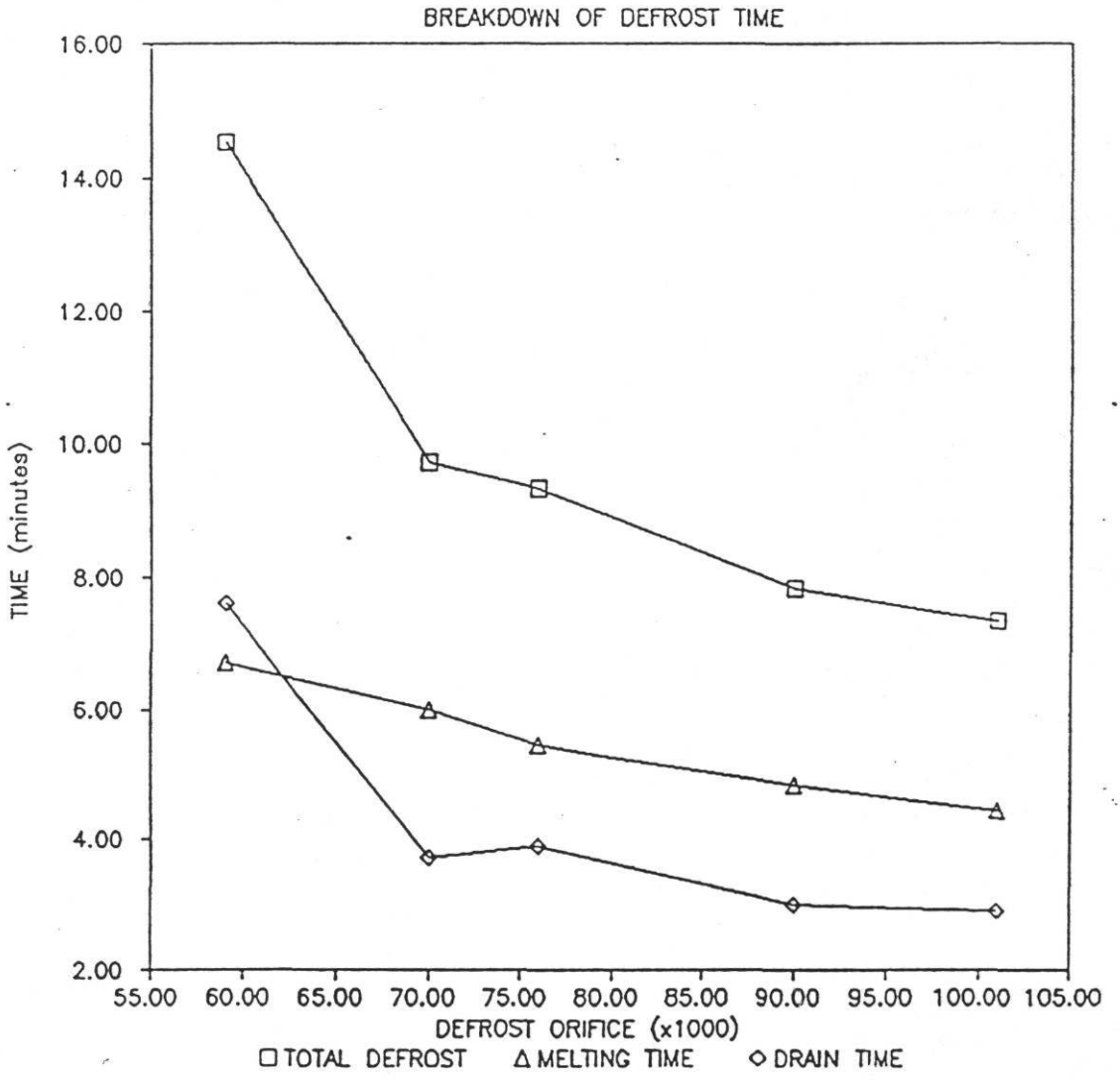

Figure 6.5. Graph of Defrost Times in Relation to Orifice Size.

maximum superheat are related to each other and are directly related to the restriction of refrigerant flow by the defrost orifice. At the initiation of defrost, the orifice meters refrigerant into the indoor coil and eventually into the compressor intake. A small orifice provided less refrigerant to the compressor which caused the suction pressure to drop as indicated in Table 6.3. Note, that with the small orifice, ORF 059, the suction pressure went below atmospheric pressure.

Because the indoor coil contained only low pressure vapor shortly after defrost initiation (Chapter 4), the reduced suction pressure lowered the saturation temperature which raises the superheat at T-24. The maximum superheat

Table 6.3. Operating Conditions for Different Diameter Defrost Orifices During the Reverse Cycle Defrost.

DEFROST EXPANSION DEVICE	MINIMUM SUCTION PRESSURE (psia)	MAXIMUM DISCHARGE PRESSURE (psia)	MAXIMUM SUPERHEAT @ T-24 (F)	MAXIMUM REFRIG. FLOW (LB/MIN)
ORF #59	13	283	112	6.8
ORF #70	16	244	100	8.8
ORF #76	18	245	96	9.5
ORF #90	23	230	84	10.5
ORF #101	27	220	75	11.2
ORF NONE	35	220	59	11.4

was the highest for ORF 059 with 112°F and decreased with increasing orifice size to 59°F with ORF OPEN.

In general, the larger the orifice size used during the reverse cycle defrost, the larger the refrigerant flow into the outdoor coil. The large orifice allowed more refrigerant to flow into the outdoor coil which melted the frost quicker and heated the coil up faster than with a smaller orifice. This shortened the defrost time and increased COP for the complete cycle.

The refrigerant flow for ORF OPEN is shown in Figure 6.6. After defrost initiation, the refrigerant flow dropped to zero and then immediately rose to 5 lb/min at 1 minute. From 1 minute to 2 minutes, the flow was unstable similar to ORF 090 but at a higher flow rate. The refrigerant flow increased rapidly from 2 minutes until 4 minutes where it reached a maximum flow rate of 11.4 lb/min. Figure 6.6 also shows the subcooling at the entrance to the orifice(SHSC-26). As the subcooling at 4.2 minutes dropped from -10°F to -2°F, the refrigerant flow dropped from 11.4 to 6 lb/min. Figure 6.2 displays the same characteristics for ORF 090, but the flow was only 10.5 lb/min and the subcooling was at -24°F before it fell to 2°F.

The control characteristics of ORF OPEN and ORF 090 were similar to the other orifices tested except for ORF 059. Figure 6.7 shows the refrigerant flow for the system using ORF 059 as the defrost orifice. The flow dropped to zero at 1 minute and stayed under 3 lb/min until 5 minutes. ORF 059 reached a peak flow of 6.8 lb/min at 9 minutes and stayed at 6.5 lb/min until defrost was terminated. There was no drop in refrigerant flow and the subcooling remains at -20°F for the remainder of the defrost cycle.

While the larger orifices provided faster defrosts, they also appeared to create potential problems with liquid in the compressor. Figures 6.8 and 6.9 show the potential problem of compressor slugging caused by the high refrigerant flow for the ORF 090 and ORF 101, respectively. In Figure 6.8, the refrigerant condition at the compressor discharge (T-19) is shown for ORF 090. At 6 minutes, T-19 dropped toward Tsat-19 but rose immediately to maintain a superheated condition at the compressor discharge. If T-19 dropped down to Tsat-19, the outlet of the compressor would be saturated and the compressor would be pumping some liquid refrigerant. Figure 6.9 shows saturated vapor in the compressor discharge for ORF 101. At 6 minutes, T-19 dropped down to Tsat-19 where the flow was saturated for a short period. The saturated condition indicated some liquid had passed through the compressor. For ORF 090, and smaller orifices, the compressor discharge remained superheated. ORF 101 and ORF OPEN both experienced short periods of saturated conditions at the compressor outlet.

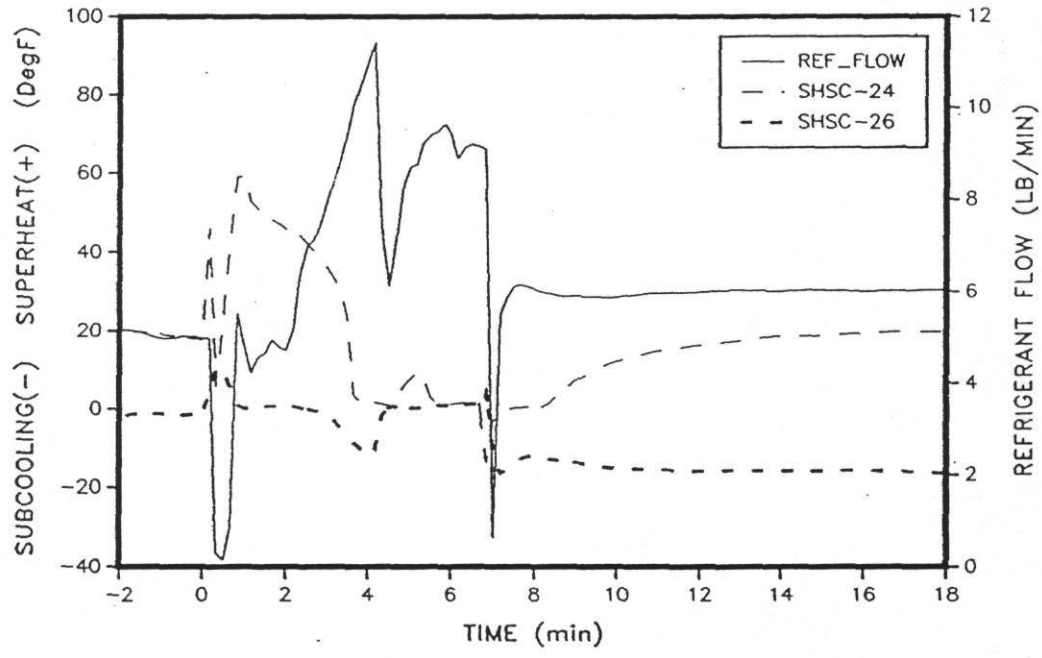

Figure 6.6. Superheat/Subcooling for T-24,T-26 & Refrigerant Flow for ORF OPEN.

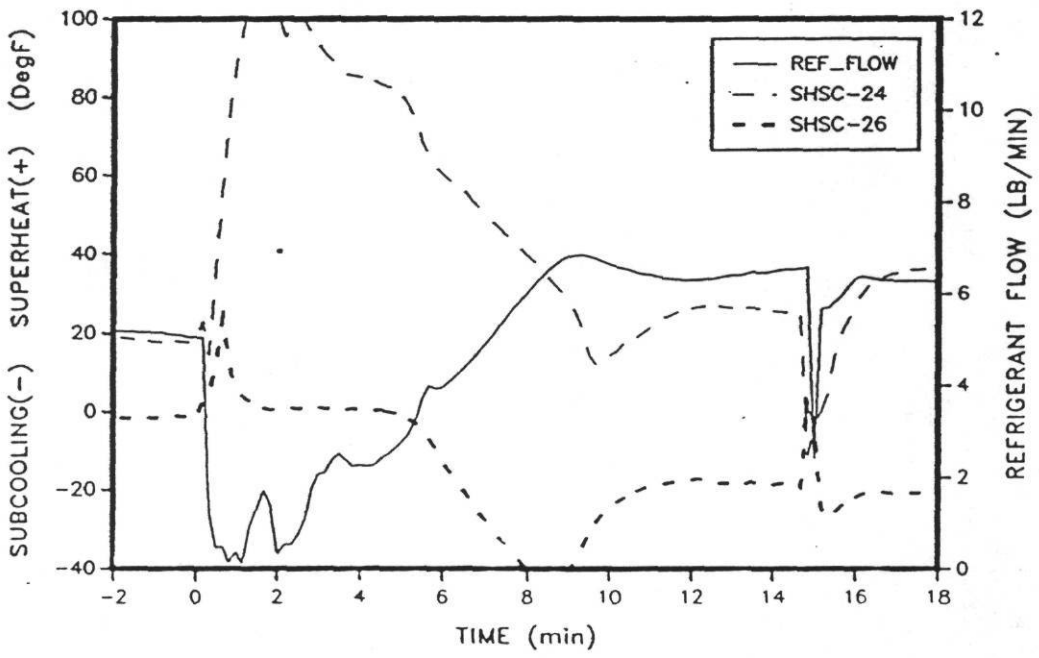

Figure 6.7. Superheat/Subcooling for T-24,T-26 & Refrigerant Flow for ORF 059.

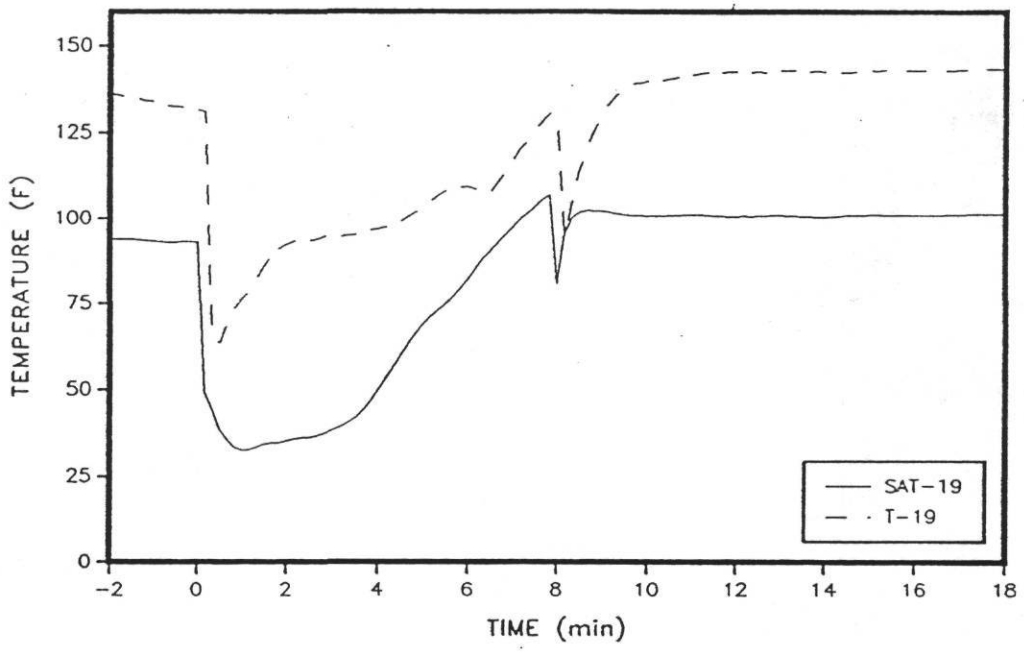

Figure 6.8. Refrigerant Conditions at Compressor Discharge for ORF 090.

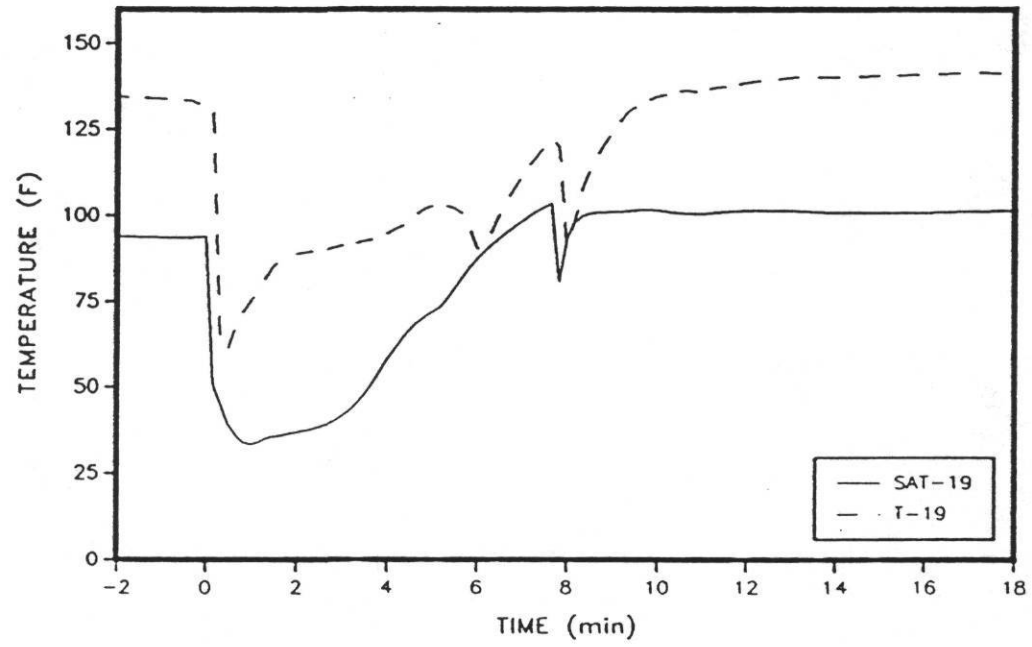

Figure 6.9. Refrigerant Conditions at Compressor Discharge for ORF 101.

SUMMARY

The refrigerant flow characteristics of an orifice and a TXV were compared. Though the TXV melted the frost off the coil faster than an equivalent diameter orifice, the TXV reduced the flow of refrigerant during the drain period of the defrost and took longer to complete the defrost cycle.

Five different size orifices were also compared for their effect on the reverse cycle defrost. In general, the larger the orifice, the more refrigerant is supplied to the outdoor coil during the defrost and the quicker the defrost. The larger orifices reduced the maximum discharge pressure, the minimum suction pressure, and the maximum superheat leaving the indoor coil during the defrost cycle.

CHAPTER 7

ALTERNATE DEFROST STRATEGIES

Tests involving alternate system operation schemes on system components other than those used in the base-case test configuration are discussed in this section. These tests included: (1) fan pre-start tests, where the outdoor coil fan was started at set times prior to termination of the defrost period; (2) fan delay tests, where the outdoor coil fan was not energized following the defrost period until after a certain delay time had elapsed; (3) two-stage defrost, where the compressor was turned off during the later part of the defrost period to allow defrost water to drain prior to resumption of heating-mode operation; (4) an indoor fan shut-off test, in which air flow across the indoor coil during defrost was stopped; and (5) a test series in which the base-case 3-ton compressor was replaced by a 2.5-ton compressor. Each test series typically included at a minimum of three complete frost/defrost cycles during which all performance parameters were monitored and during which a cyclic ''steady state'' was achieved based on repeatable defrost times and defrost water collection levels.

Table 7.1 lists the integrated cyclic coefficients of performance (COPs), cycle times, defrost times, and defrost water collection levels for each of the test series included in this study except the indoor fan off test. Results from the the indoor fan off test were not included because a complete cycle using this scheme was not run for reasons discussed later. Tests using two-stage defrost strategy showed an increase of 6.6% cyclic COP compared to test results of the base-case defrost strategy. The cyclic COP of the 20 second fan pre-start tests was comparable (0.4% higher) than the base case results. The 40 and 60 second fan pre-start tests yielded slightly lower cyclic COPs compared to that of the base test series (as much as 3% lower for the 60 second pre-start). While the 20 second fan pre-start tests showed a 0.2 minute decrease in defrost time, the 40 and 60 second pre-start tests had higher defrost times compared to the base tests.

The 2.5-ton compressor tests had longer cycle times (73.8 minutes compared to 67.5 minutes) with longer defrost times (8.2 minutes compared to 7.5 minutes). Although longer operation time was definitely a benefit, the integrated cyclic COP of the 2.5-ton compressor tests was within 0.4% of that of the base configuration. Apparently, the energy penalty of the 0.7 extra minutes of defrost balanced the benefits of the longer heating period between defrosts seen in the 2.5-ton compressor tests.

Table 7.1 - Performance Characteristics for Frost/Defrost Tests

AVERAGE PERFORMANCE CHARACTERISTICS*				
TEST CASE	INTEGRATED COP	CYCLE TIME (min)	DEFROST TIME (min)	WATER COLLECTED (ml)
Base	2.27	67.5	7.53	1870.
2.5 Ton	2.26	73.8	8.22	1820.
Pre-20	2.28	66.7	7.33	1750.
Pre-40	2.26	68.0	7.72	1850
Pre-60	2.21	65.2	8.17	1760
Del-45	2.20	70.3	8.56	1580.
2-Stage	2.43	69.4	7.79	1800.

* Based on a minimum of three tests for each case

Fan delay tests showed a 3% decrease in cyclic COP from the base-case. As shown later in this section, this decrease could be attributed to higher discharge pressures following the defrost and an associated increase in power consumption beyond normal post-defrost levels. Each test series is discussed more in the following sections.

Fan Pre-Start Tests

Fan pre-start tests were performed with the intention of observing how starting the outdoor coil fan just prior to defrost cycle termination would affect the capacity recovery period following a defrost interval. Because the data acquisition equipment only allowed scans at approximately ten second intervals, it was decided to choose fan pre-start times that were multiples of ten seconds. Fan pre-start times of 20, 40, and 60 seconds satisfied our criteria. The maximum pre-start time was restricted to 60 seconds because it was felt that a longer time could possibly interfere with the normal reverse-cycle defrost process. Furthermore, any benefits gained by fan pre-start would have to be weighed against energy consumption by the fan during the additional on time.

To start the outdoor fan at a specific time before defrost cycle termination, it was necessary to anticipate when the cycle would be terminated. For the base-case, defrost termination occured when the refrigerant temperature exiting the lowest of the four refrigerant circuits on the outdoor coil reached 65^{o}F. Averages of data from approximately 26 base-case frost test periods showed that the coil exiting temperature was 59.5, 61.5, and 63.4 F at 60, 40, and 20 seconds respectively before defrost cycle termination (Figure 7.1). Thus, these temperatures were used as a basis for starting the outdoor coil fan prior to defrost termination for a given fan pre-start test. For example, during the defrost for the 60-second pre-start test, when the outdoor fan was energized the temperature of refrigerant leaving the bottom circuit of the outdoor coil rose above 59.5^{o}F. The defrost cycle was terminated 60 seconds later.

The primary benefit of pre-starting the outdoor fan appeared to be in favorable pressure characteristics seen at defrost termination. Figure 7.2 shows compressor suction and discharge pressures during a sample base-case defrost. Defrost termination at 7.5 minutes was accompanied by a suction pressure rise of 50 psi followed by a rapid drop of 60 psi. The discharge pressure dropped 115 psi and then rapidly rose 100 psi. These pressure spikes were a result of the sudden exposure of the high pressures in the outdoor coil to the suction line and the low pressures in the indoor coil to the discharge line of the compressor when the

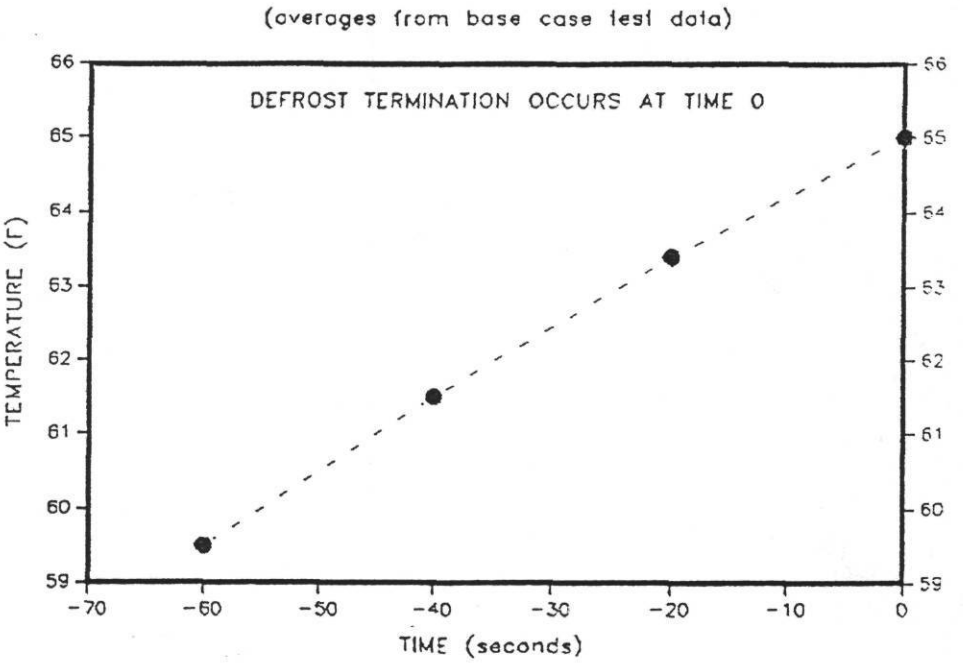

Fig. 7.1 Refrigerant Exit Temperature from Bottom Circuit of Outdoor Coil Prior to Defrost Termination (base case)

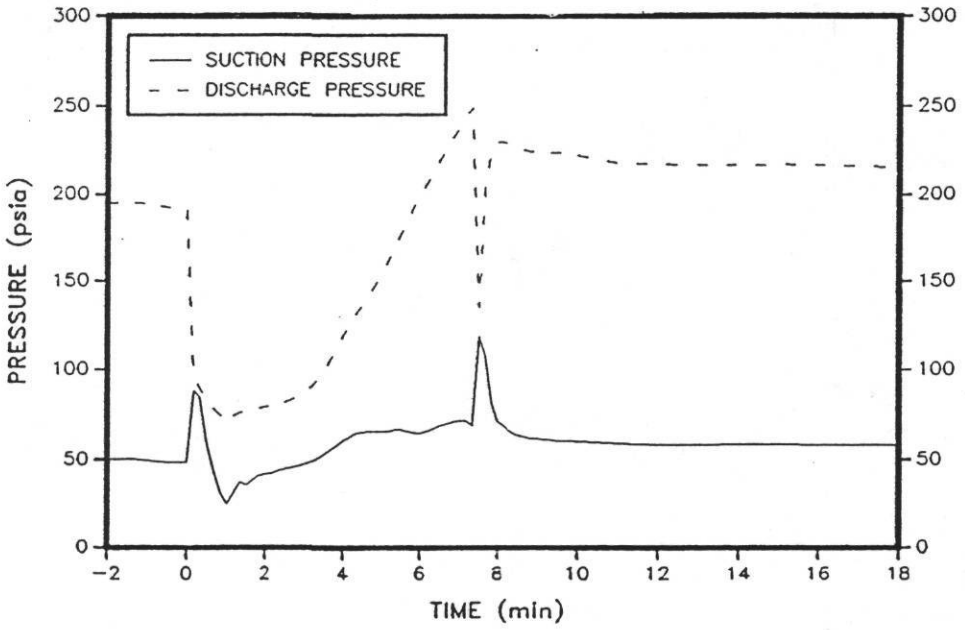

Fig. 7.2 Compressor Suction and Discharge Pressures during Defrost Base Case

reversing valve was de-energized at the end of the defrost.

Figure 7.3 is a plot of the suction and discharge pressures for a sample 20-second fan pre-start test. As seen for the 20-second pre-start test in Figure 7.3, the suction pressure actually dropped 15 psi initially, then rose 20 psi, and then fell 15 psi as the defrost was terminated. Discharge pressure experienced a less sudden drop of 100 psi, then rose 70 psi, and then gradually rose another 15 psi as normal heating mode operation was resumed. The 100 psi pressure drop occurred during the fan pre-start period. The fan pre-start cooled the outdoor coil, reducing the condensing temperature in the outdoor coil.

Figure 7.4 details vapor line refrigerant temperatures for the defrost period of the 20-second fan pre-start test. SAT18 is the saturation temperature of refrigerant at the entrance outdoor coil (or the condensing temperature). The saturation temperature was obtained from calculations which used refrigerant pressure data taken at a point 13 inches from the coil in the vapor line. SAT18 started dropping at seven minutes into the defrost. The temperature dropped from 105^{o}F to 65^{o}F in the 20 seconds before defrost termination which occurred at 7.3 minutes. The lower condensing temperature in the outdoor coil was reflected by a lower discharge pressure of the compressor.

Although this pressure drop was comparable in magnitude to that seen when the reversing valve was switched for the base case (100 psi compared with 115 psi), the drop associated with the fan pre-start was at a controlled rate. The lower condensing pressure caused the reduction in pressure changes seen when the reversing valve switched suction and discharge lines to the compressor at defrost termination. The reduction in severity of the pressure spikes experienced during termination of the defrost period should cause less mechanical stress on the compressor during this transient period. A reduced rate of pressure change is equivalent to a reduced shock on system refrigerant lines. Reduced shock should correspond to reduced line vibration and noise for the fan pre-start tests.

Of the fan pre-start tests, the 20 second fan pre-start method presented the most favorable performance characteristics compared to the base-case operation scheme. Spikes in discharge and suction pressures at defrost termination were reduced, and the average of integrated cyclic COP values for the 20-second fan pre- start tests of 2.28 was slightly better than that of the base case (2.27 %). On the other hand, a decrease in the average of integrated cyclic COPs of the 40 and 60-second fan pre-start tests below that of the base case was seen (0.4 % and 3 % decreases respectively). However, suction and discharge pressure transients of the 40 and 60-second fan pre-start

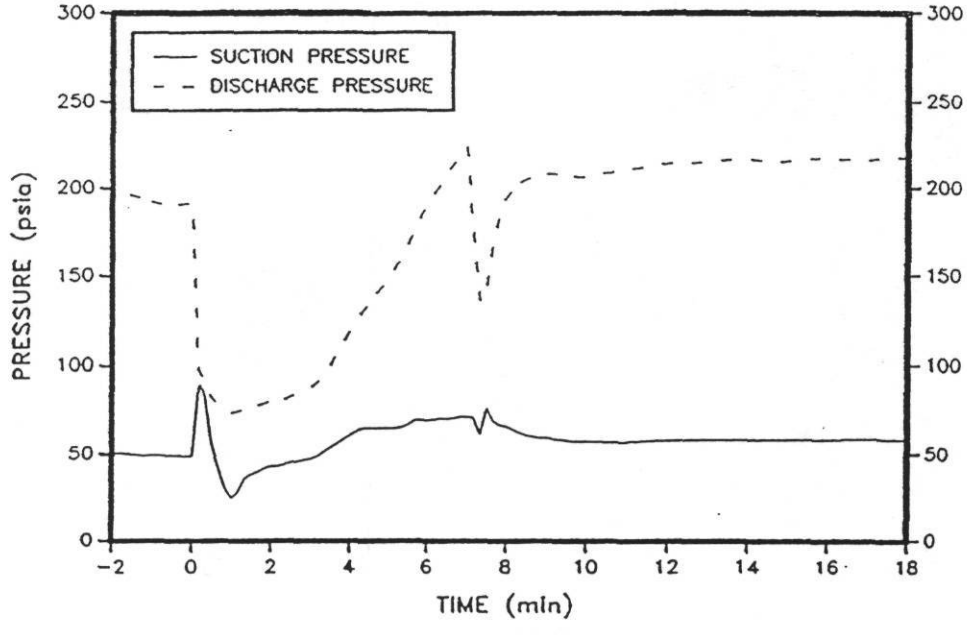

Fig. 7.3 Compressor Suction and Discharge Pressures during Defrost
20-Second Pre-Start

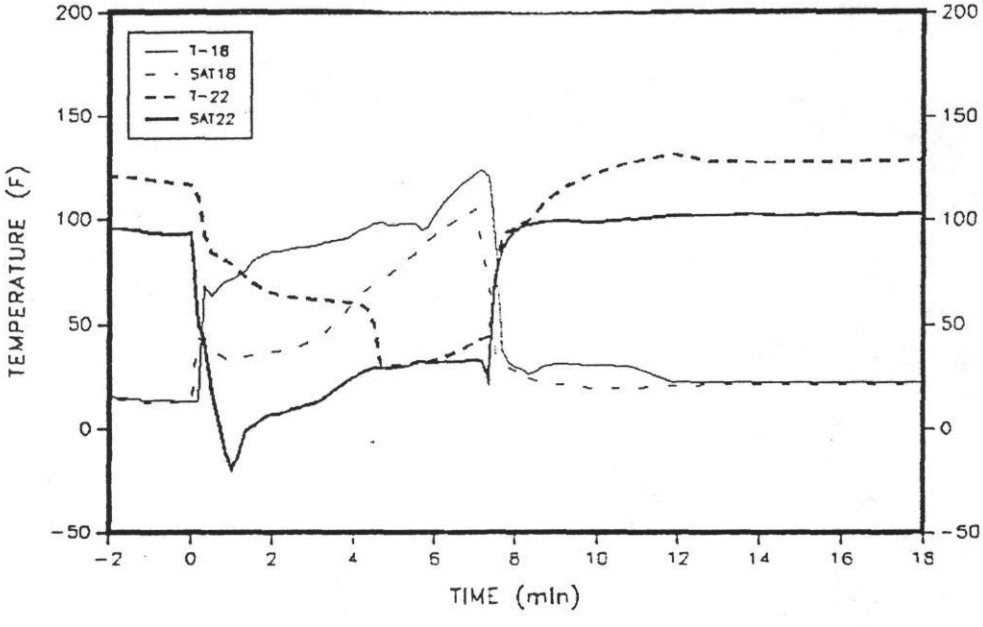

Fig. 7.4 T-18 and SAT18 Entering Outdoor Coil
20-Second Pre-Start Defrost

tests were even less severe than those of the 20-second fan pre-start tests.

Figure 7.5 compares defrost termination discharge pressure transients for sample tests selected from each of the base-case and fan pre-start test series. Likewise, Figure 7.6 compares suction pressure transients at defrost termination for these tests. These figures reflect the favorable pressure effects described for the 20-second fan pre-start tests. However, both the 40-second pre-start method and the 60-second pre-start method introduced an average discharge pressure drop of 120 psi in the moments before defrost termination. This effect is seen in Figure 7.5. The base-case defrost strategy tests showed an average 109 psi pressure drop after defrost termination while the 20-second fan pre-start method tests dropped the discharge pressure only 92 psi before defrost termination. Although the 40 and 60-second pre-start tests increased the discharge pressure drop, the drop spanned a longer time period than did that of the base-case test (45 seconds compared with 10 seconds). As seen in Figure 7.5, the 20-second fan pre-start method brought the discharge pressure to 135 psia at termination. This level was equivalent to the minimum reached during the base-case test. The level for the 20-second fan pre-start test was reached at a controlled rate of 20 seconds duration while the drop for the base-case test occurred as the reversing valve was switched. The 40 and 60-second pre-start methods undershot the termination pressure. However, in all of the fan pre-start tests, the increase in discharge pressure following the initial drop at defrost termination was not as rapid as the increase seen for the base-case tests.

As seen in the suction pressure transients shown in Figure 7.6, fan pre-start removed the suction pressure spike seen at defrost termination in the base-case test. For a base-case test, switching of the reversing valve at defrost termination re- circuited the outdoor coil from the discharge line of the compressor to the suction line. The high pressure in the outdoor coil then caused a spike in suction pressure. When the outdoor coil fan was started prior to defrost termination during a fan pre-start test, outdoor coil pressure fell as described previously. The 20-second pre-start appeared to drop the pressure to a level which minimized changes in suction pressure at defrost termination. The 40 and 60-second pre-starts over-compensated and caused an average 40 psi drop in suction pressure as illustrated in Figure 7.6.

Variations in integrated cyclic COPs for the fan pre-start tests can be attributed to slowed capacity recovery following the defrost for the pre-start tests (Figure 7.7), as well as to increased defrost times (Table 7.1). An increased energy consumption over that of the base-case

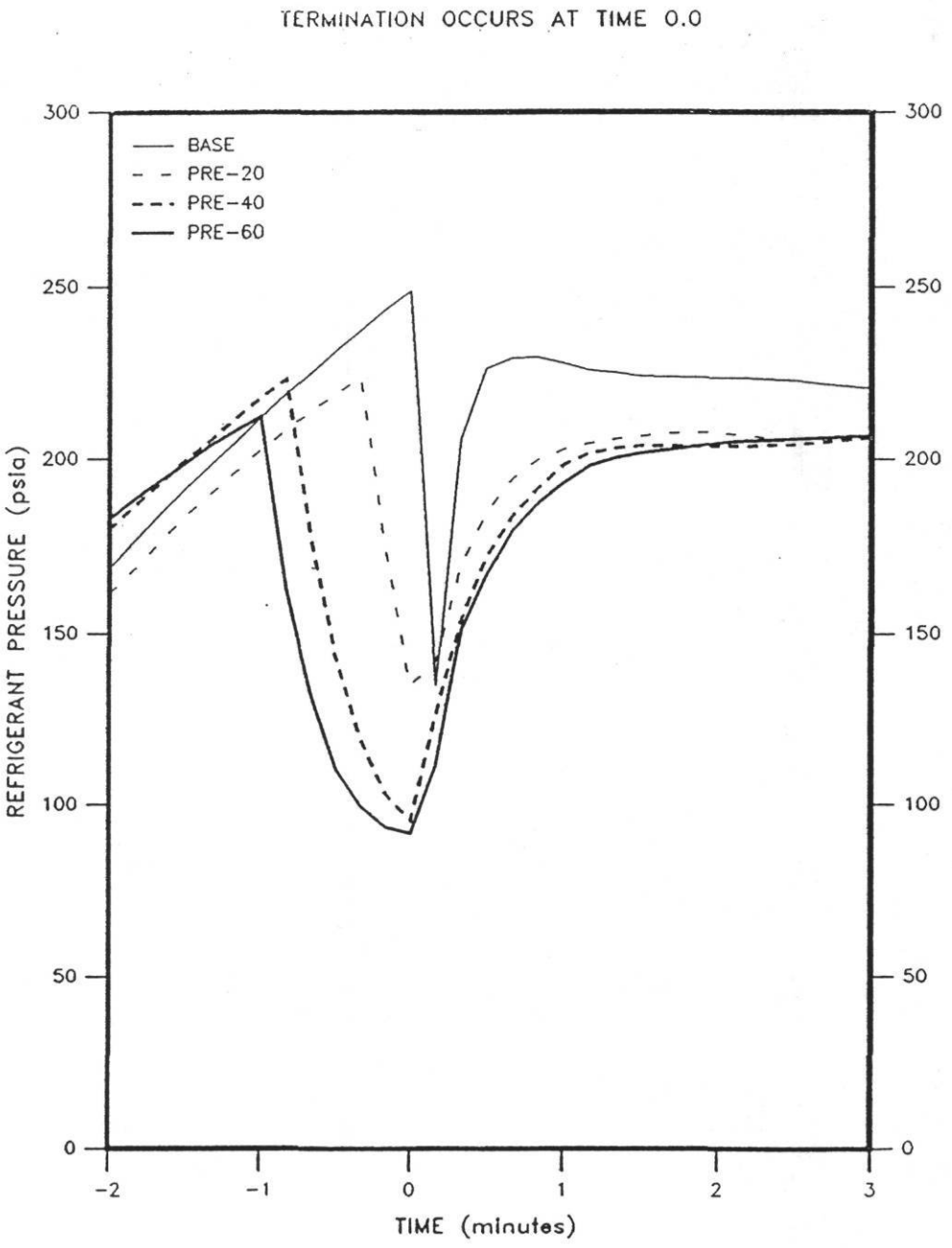

Fig. 7.5 Discharge Pressure Transients at Defrost Termination
Fan Pre-Start and Base-Case Tests

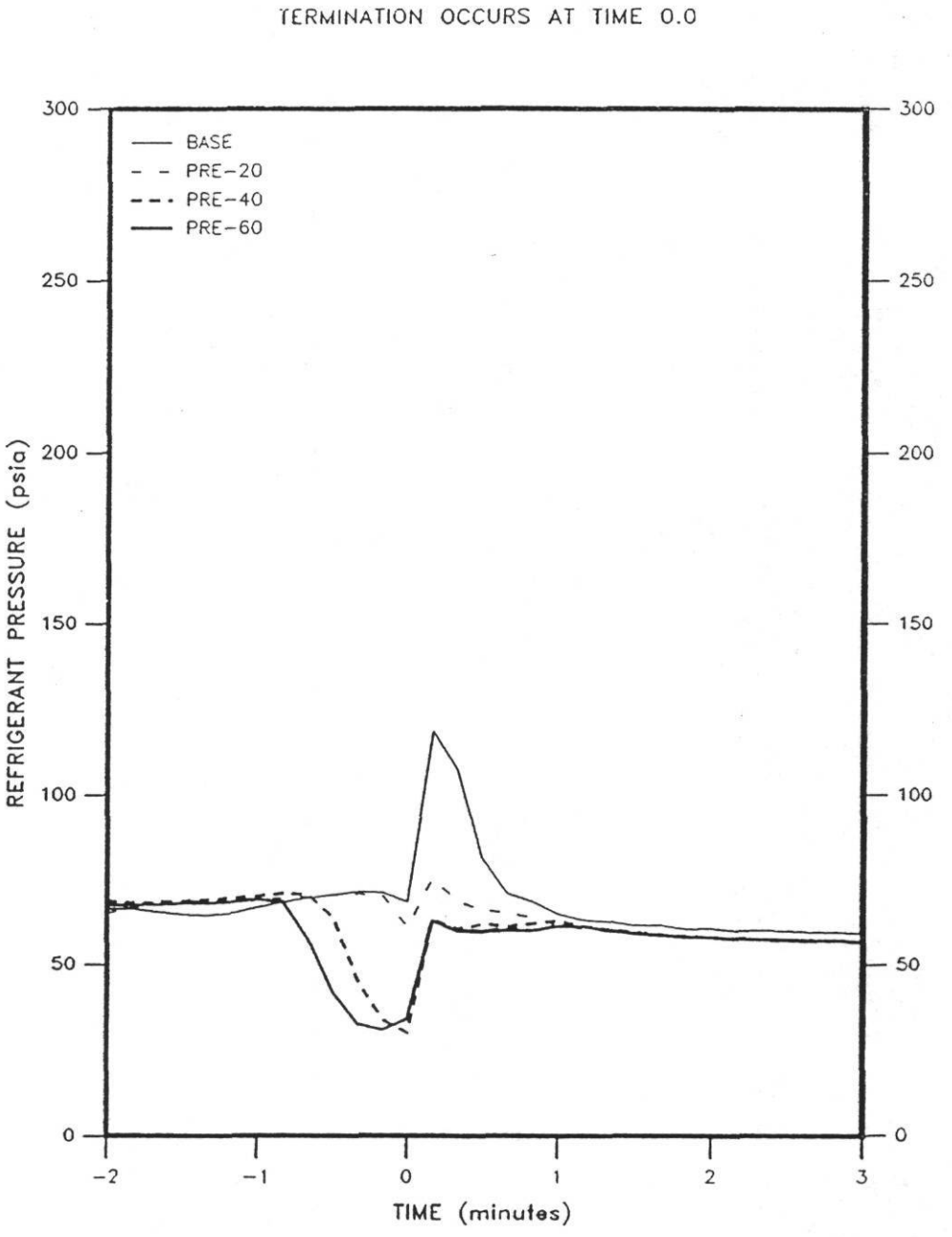

Fig. 7.6 Suction Pressure Transients at Defrost Termination
Fan Pre-Start and Base-Case Tests

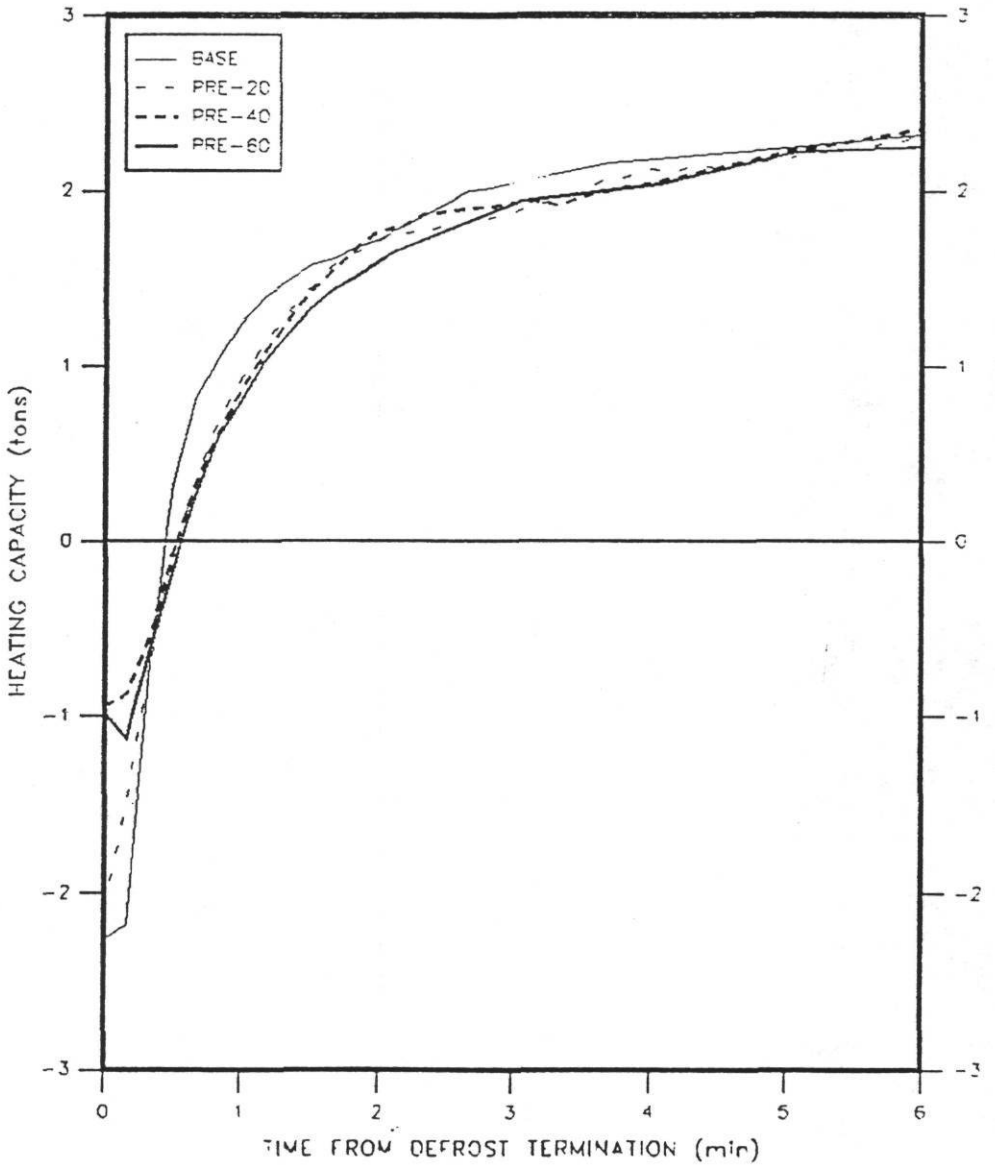

Fig. 7.7 Post-Defrost Heating Capacity Recovery
Fan Pre-Start and Base-Case Tests

defrost strategy was expected to result from additional fan on-time for the fan pre- start tests but did not occur. Figure 7.8 shows the variation in power and heating capacity for a frost/defrost test of the base case. Figure 7.9 shows the variation in power usage and heating capacity for a test run of the 20-second fan pre-start scheme. The power draw of the 20-second pre-start test actually dropped when the fan was started at seven minutes into the defrost (Figure 7.9). The power dropped 0.6 KW for almost one minute. Power for the base case dropped a comparable amount, but returned to its previous level within 10 seconds after the defrost termination (Figure 7.8). An increase in power consumption for the 20-second fan pre-start was not seen because reduced discharge pressure reduced the load on the compressor, reducing power consumption. Similar decreases in power were observed for the 40 and 60-second fan pre-start tests. However, effects observed during the drain period of the 40 and 60 second fan pre-start tests contributed to limiting the overall system performance. Table 7.2 compares drain period time, energy consumption, and indoor coil cooling effect for the base-case and fan pre-start test schemes. Drain times increased for the 40 and 60-second fan pre-start tests as did the cooling effect. Both of these factors (slower capacity recovery and longer defrost time) degraded integrated cyclic COP values.

Table 7.2 - Comparison of Drain Period Effects

DRAIN PERIOD SUMMARY FOR FAN PRE-START TESTS			
TEST	DRAIN ENERGY (WH)	DRAIN TIME (minutes)	COOLING EFFECT (BTU)
Base	129	3.14	1496
PRE-20	126	3.17	1471
PRE-40	132	3.39	1542
PRE-60	144	3.83	1660

Fan Delay

The fan delay was selected for this study because it was felt that a delay in blowing air over the outdoor coil as the heat pump returned to normal heating operation would allow harvesting of residual heat near the outdoor coil that

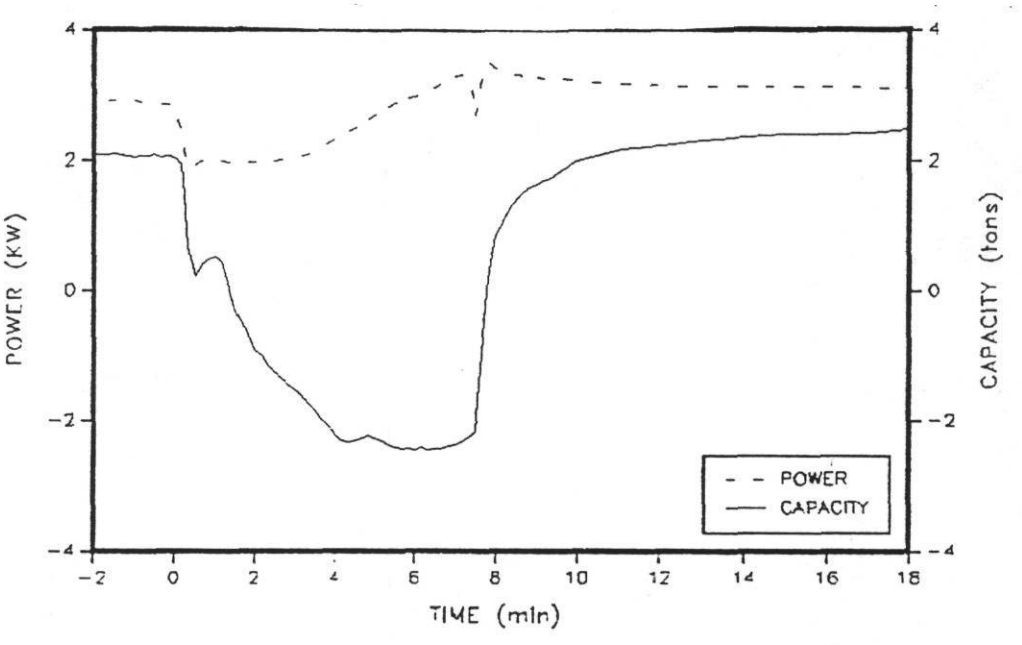

Fig. 7.8 Power Draw and Heating Capacity Variations during Base-Case Defrost

was left over from reverse-cycle defrosting of the coil. There was an improvement in capacity recovery following the defrost period. (Figure 7.9) With the fan delay, the capacity increased to 1.56 tons at 1 minute past defrost termination. By comparison, the heating capacity only reduced 1.24 tons at 1 minute for the base test. It takes the capacity in the base test approximately 3 minutes to equal that with the fan delay.

A plot of compressor suction and discharge pressures for a sample test of this scheme shows that discharge pressure following the defrost reached a peak of 275 psia (Figure 7.11). This pressure was 25 psi more than the peak seen in the base configuration (Figure 7.2). Compressor suction pressure peaked near 125 psi, representing a 5 psi increase over the peak seen for the sample base-case test. These changes are reflected in Figures 7.12 and 7.13 which respectively, compare discharge and suction pressure changes of a sample fan delay test with changes for a sample test utilizing the base-case defrost strategy. The increase in peak discharge pressure following the defrost period for the fan delay test was reflected in a peak compressor power of 3.5 kw for almost one minute (Figure 7.14). After this peak, the power quickly reduced to 2.5 kw. In contrast, there was a momentary 3.4 kw peak for the base-case which rapidly settled to a steady 2.85 kw (Figure 7.8). This difference in power usage counteracted the capacity recovery improvement of the fan-delay method over the base-case method as indicated by the 3% drop in cyclic COP (Table 7.1).

The increase in peak discharge pressure following the defrost period for the fan delay test was reflected in a peak compressor power of 3.5 KW for almost one minute (Figure 7.11). After this peak, the power quickly reduced to 2.5 KW. In contrast, there was a momentary 3.4 KW peak for the base-case which rapidly settled to a steady 2.85 KW (Figure 7.7). This difference in power usage counteracted the capacity recovery improvement of the fan-delay method over the base-case method as indicated by the 3% drop in cyclic COP (Table 7.1).

Indoor Fan Off

The reverse cycle defrost of air source heat pumps is characterized by a cooling of the indoor duct air that provides heat for defrosting the outdoor coil. The indoor fan off test was conducted to evaluate if the energy contained in the refrigerant in the indoor coil and in the coil mass itself would supply enough heat to defrost the outdoor coil.

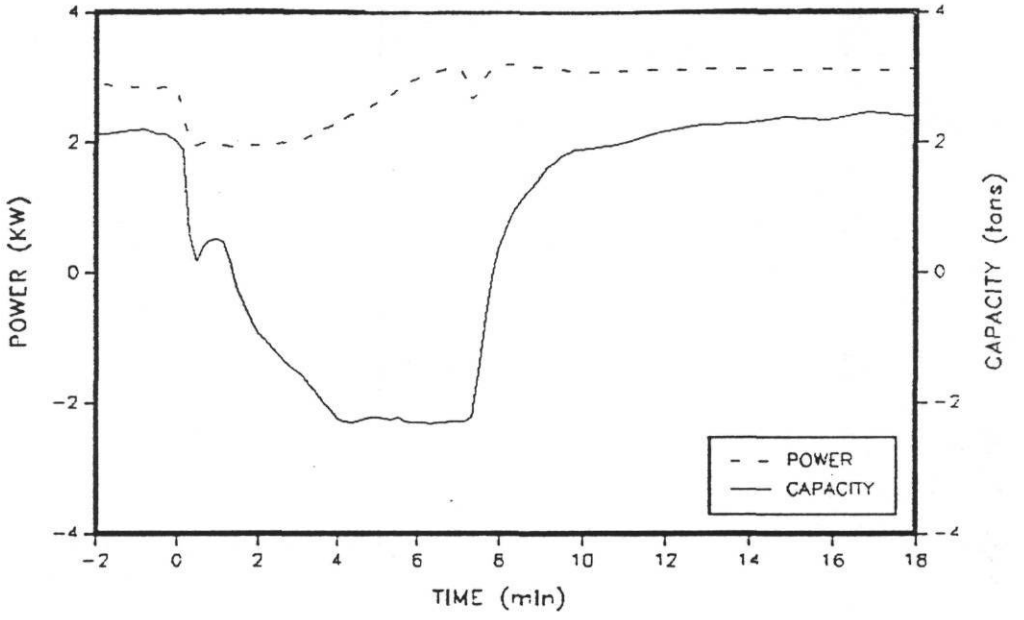

Fig. 7.9 Power Draw and Heating Capacity Variations during 20-Second Fan Pre-Start Defrost

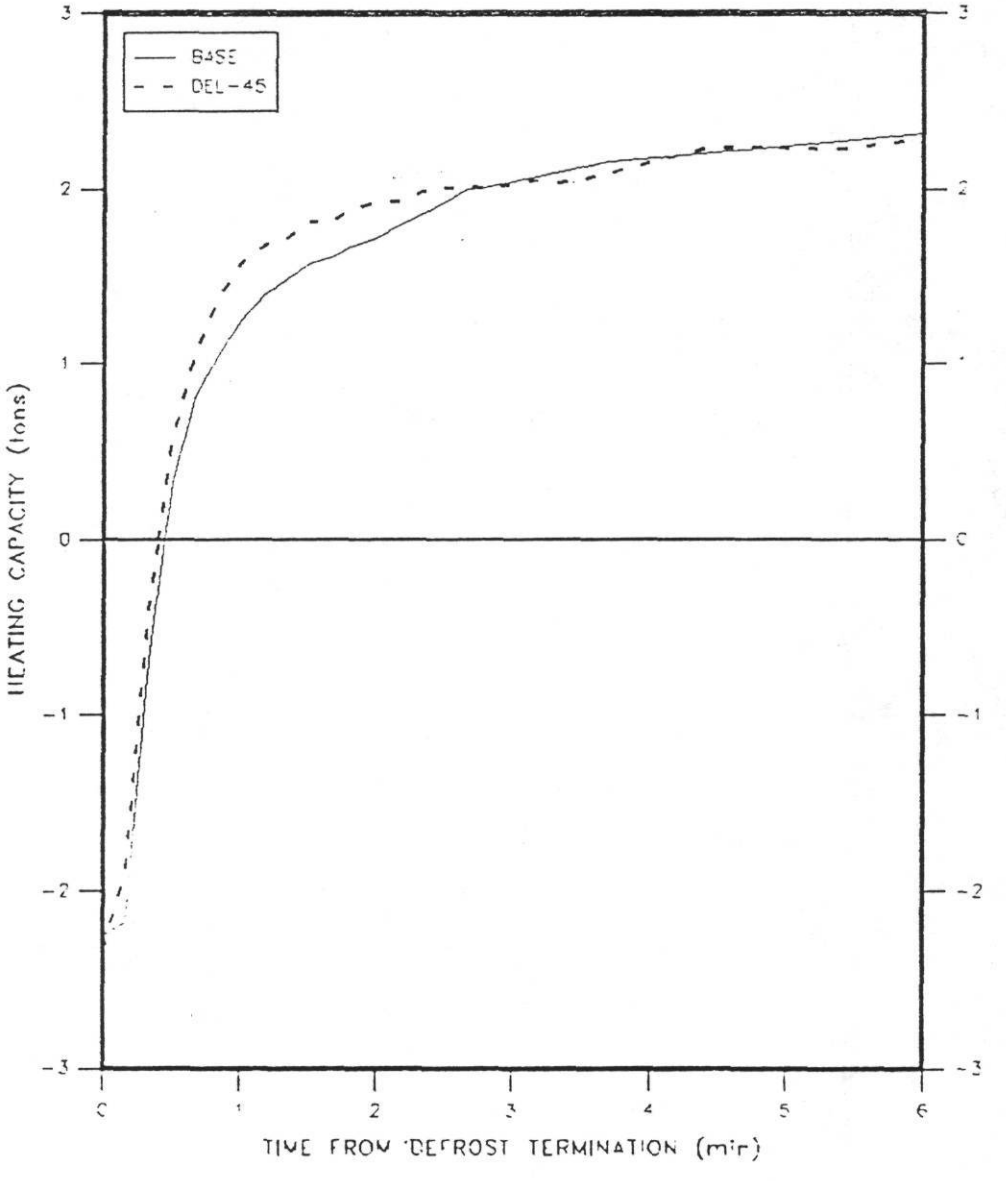

Fig. 7.10 Post-Defrost Capacity Recovery of Base-Case and Fan Delay Tests

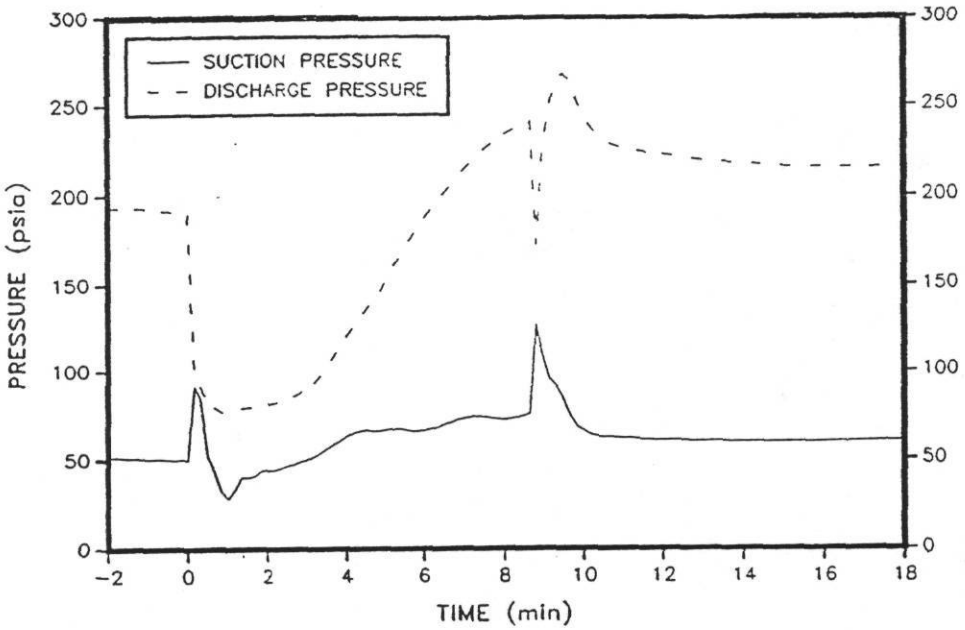

Fig. 7.11 Compressor Suction and Discharge Pressures during Fan Delay Defrost

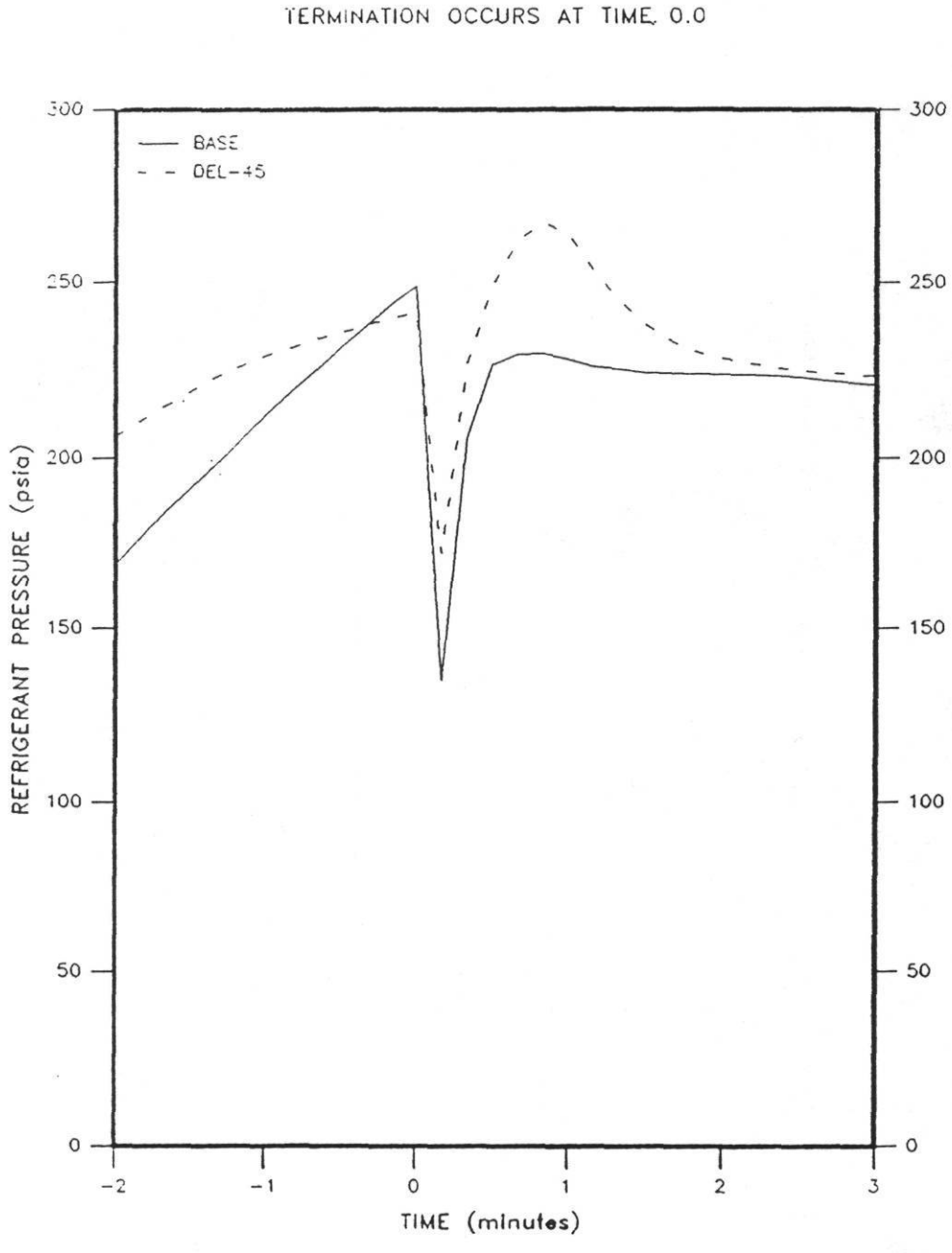

Fig. 7.12 Compressor Discharge Pressure Transients At Defrost Termination Fan Delay and Base-Case Defrosts

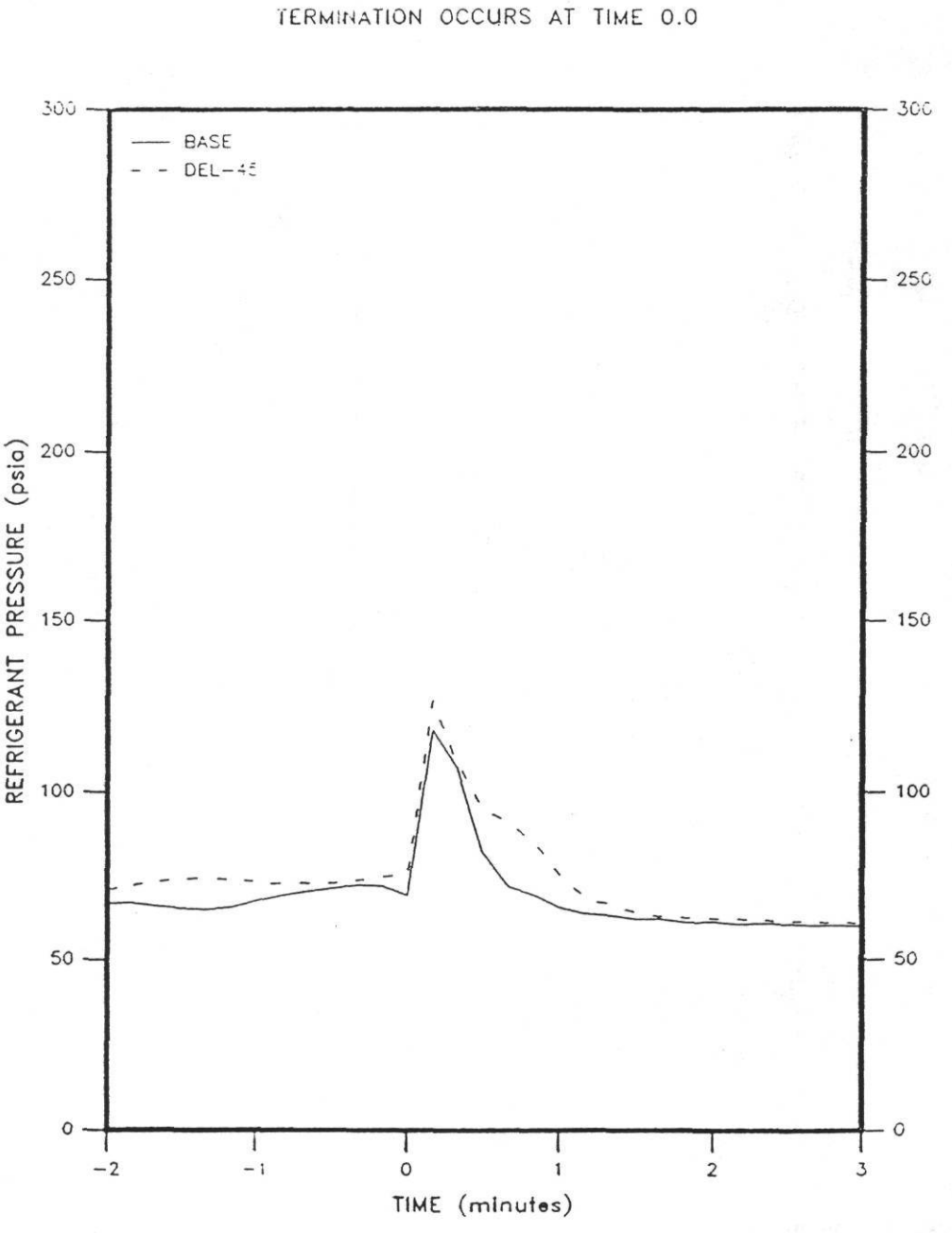

Fig. 7.13 Compressor Suction Pressure Transients at Defrost Termination Fan Delay and Base-Case Defrosts

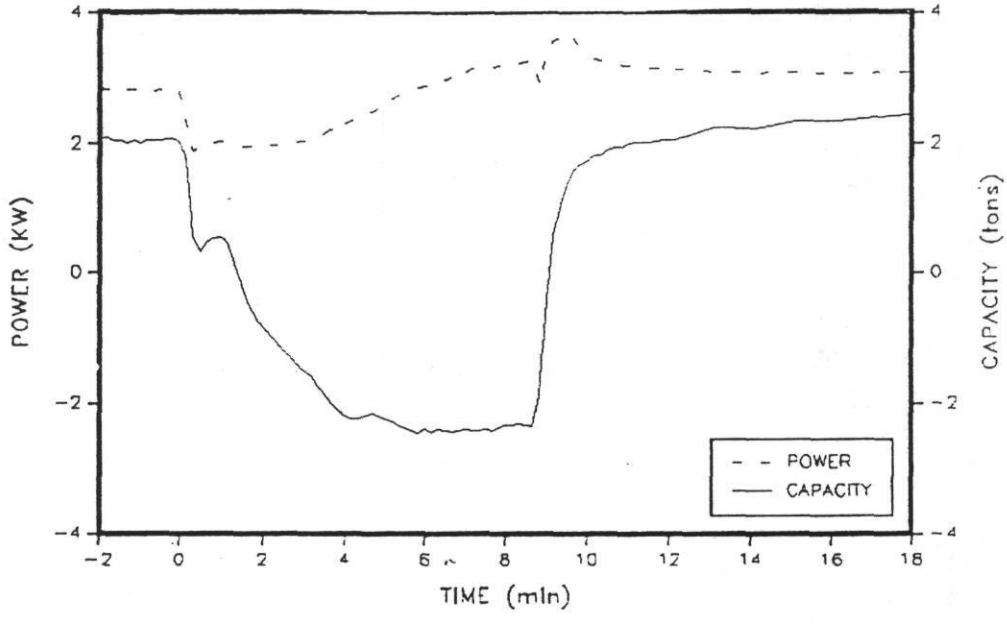

Fig. 7.14 Power Draw and Heating Capacity Variations during Fan-Delay Defrost

Figure 7.15 shows the temperature of refrigerant leaving the bottom of the four outdoor coil refrigerant circuits (T-3) during a sample frost test period for the indoor fan off operation scheme. During a defrost period, T-3 represented the temperature of refrigerant leaving the bottom circuit of the four refrigerant circuits in the outdoor coil. For the base-case, this temperature was monitored during the defrost period, and when it reached 65°F, the defrost was terminated. T-3 never reached 65°F with the indoor fan off (Figure 7.15). The defrost cycle was allowed to continued for over 20 minutes, during which time the temperature of refrigerant leaving the bottom circuit of the outdoor coil had stabilized near 60°F and the refrigerant flow rate had stabilized near 2 pounds per minute (Figure 7.15). Because the outdoor coil lower circuit exiting temperature failed to reach the temperature established as the defrost cycle termination point, the test was terminated after 24 minutes of defrosting. Although T-3 failed to reach the 65°F defrost termination point,

T-3 increased above the freezing point at six minutes into the defrost. This increase in exiting temperature was associated with the complete melting of frost on the coil, suggesting that the termination point could be lowered to a suitable value that would allow melting of the frost and enough drain time to let the coil clear of water.

A comparison of Figures 7.16 and 7.17 reveals a major limitation to this defrost method. Figure 7.16 depicts the normal discharge temperature (T-19) for the compressor during a sample defrost test using the base-case defrost method. SAT-19 is the saturation temperature for the discharge temperature. Saturation temperature was computed from refrigerant pressure data taken at the point where the temperature was measured. T-19 was measured 13 inches from the outdoor coil by a probe in the vapor line. The discharge refrigerant remained superheated throughout the defrost period.

In Figure 7.17, discharge temperature (T-19) for the indoor fan-off test was plotted along with the saturation temperature (SAT-19). After six minutes of defrosting, the temperature of refrigerant leaving the compressor coincided with the saturation temperature for the discharge pressure, suggesting a probable flow of two-phase refrigerant through the compressor. Liquid slugging in the compressor would have a definite impact on lifetime and reliability of a compressor operating after 6 minutes with the indoor fan off during the defrost period.

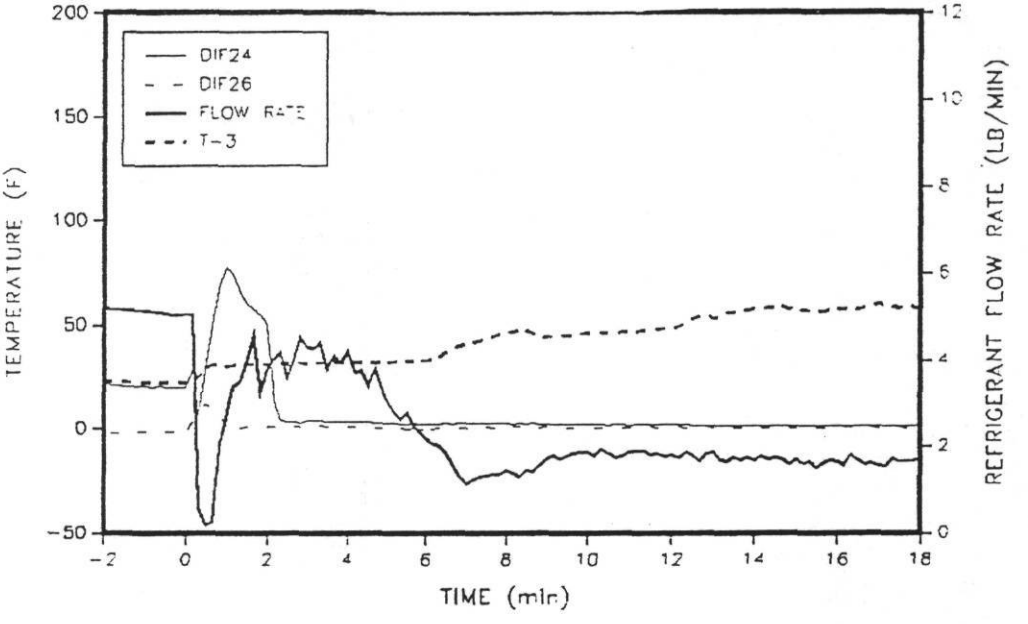

Fig. 7.15 Refrigerant Flow Rate and Exit Temperature from Outdoor Coil Bottom Circuit Indoor Fan Off

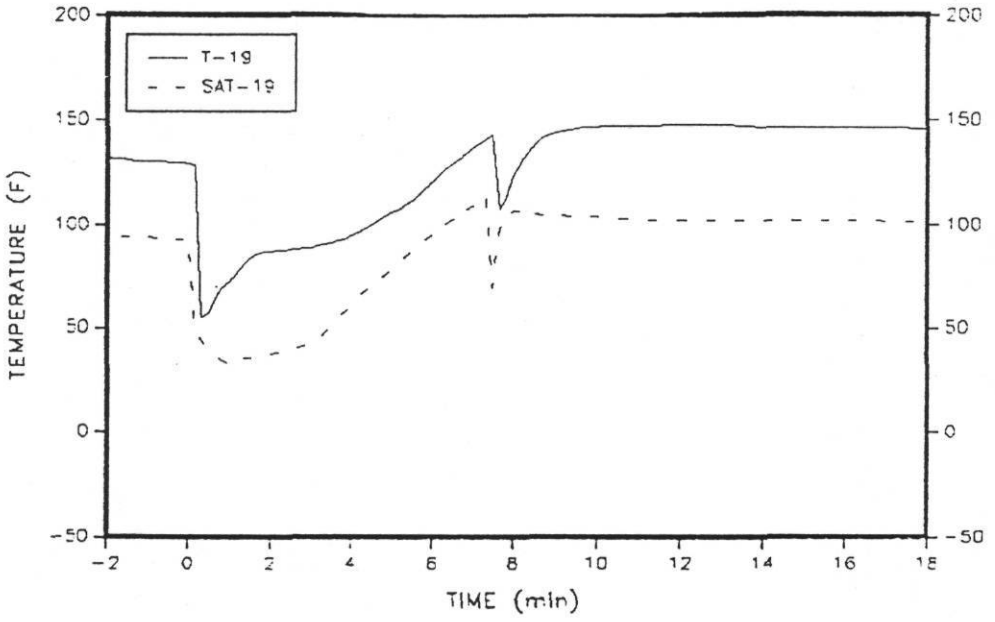

Fig. 7.16 Compressor Discharge Temperature and Saturation Temperature Base Case

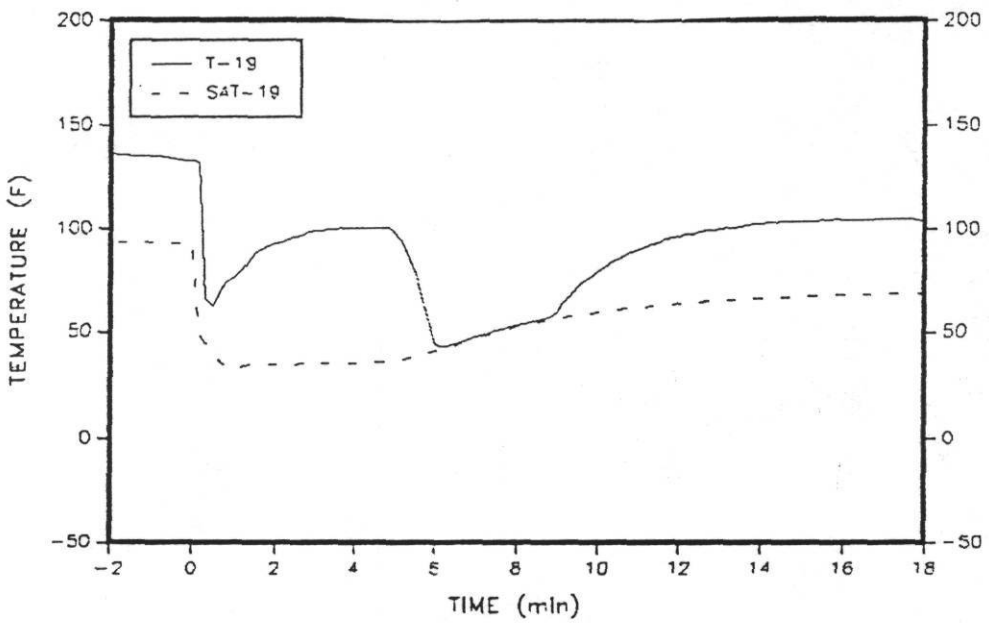

Fig. 7.17 Compressor Discharge Temperature and Saturation Temperature Indoor Fan Off

Compressor Size

The 3-ton capacity compressor of the base case heat pump configuration was replaced with a 2.5-ton capacity compressor to study the effect of compressor size on frost/defrost period operation characteristics. All other base-case configuration components were retained. By reducing the capacity of the compressor, a high efficiency unit with over-sized coil surfaces was simulated. As shown earlier in Table 7.1, the average system cycle time for the 2.5-ton compressor tests was 9% longer than that of the average for the base-case tests (An increase from 67.5 minutes to 73.8 minutes). This 6.3 minute increase included a 0.7 minute increase in average defrost time, the and 5.6 minutes increase in heating operation. The longer overall cycle should result in a decrease in the frequency of defrosts in field operations. The average cyclic COP of 2.26 (Table 7.1) for the 2.5-ton compressor tests was less than 1% from that of the base-case.

Two-Stage Defrost

The two-stage defrost scheme was developed after reviewing test results from a number of base-case frost test periods. During the base defrost, it was noted that after the frost had melted from the outdoor coil (signified by an average refrigerant exiting temperature rise above 32^{o}F), approximately 3.2 additional minutes were required to raise temperature of refrigerant leaving the bottom circuit of the outdoor coil to 65^{o}F (the defrost cycle termination point). During the last several minutes of the defrost period of the tests, the frost on the outdoor coil had been melted and was presumably draining. After the frost had melted from the outdoor coil, the cooling capacity of the heat pump was at its maximum (-2.3 tons heating, Figure 7.9). In addition, the compressor power increased during this drain period. Thus, the drain period was the time with the largest energy penalty.

Stoecker, et al.[24] observed a similar effect during hot-gas defrosting of industrial refrigerant coils and suggested a two-stage defrost where refrigerant gas flow to the coil being defrosted could be stopped when frost had melted. Then, a sufficient amount of time would be allowed for the coil to drain, and after that time, the coil would be returned to normal evaporating operation. To accomplish a two-stage defrost for the test heat pump, the average temperature of refrigerant exiting the outdoor coil was monitored during the defrost test period. When this temperature exceeds 34^{o}F it implies that frost on the coil was melted. At that time, the compressor was stopped while the outdoor coil was allowed to drain for 3.17 minutes (the typical drain time during a normal coil defrost). Then, the

heat pump was returned to the heating mode with a clean coil.

From Table 7.1, cyclic COP for this scheme showed a 6.6% improvement over the base-case COP. Figure 7.18 shows power draw and heating capacity values for a sample two-stage defrost test. Power draw dropped from 2.5 KW to 0.5 KW during the compressor shut down period. The reduction in power draw increased cyclic COP, as discussed previously. The large negative capacity at 46 minutes (-2.3 tons) started to diminish after compressor shut-down and continued to diminish until defrost termination at which time cooling of the indoor air had completely stopped. During the last three minutes of this test, a constant cooling capacity of 2.3 tons was seen. (Figure 7.8)

The two-stage defrost improved overall performance as well as the transient response at defrost termination. Figure 7.19 shows the suction and discharge pressures for the two-stage test. These pressures experienced step changes at defrost termination, and the pressure spikes seen during the base-case tests were not seen (Figure 7.2).

Figures 7.20 and 7.21 depict system refrigerant pressures and temperatures, respectively, during the 2-stage defrost. Refrigerant pressures throughout the system equalized at 100 psia, at approximately 5 minutes into the cycle and then fell to 90 psia by defrost termination. Temperature response was varied. T-24, T-25, and T-26 measured near the indoor coil stayed near the saturation temperature (48^{o}F). Vapor line temperatures, T-18, T-19, T-20, T-21, and T-22 dropped toward the saturation temperature. Temperatures T-16 and T-17 in the liquid line near the outdoor coil remained subcooled. This subcooled liquid remained available for evaporation use in the outdoor coil at the start of normal heating operation. This availability was possibly reflected in a comparison of capacity recovery between the base-case and two-stage defrost schemes (Figure 7.22). Capacity recovery for the two-stage defrost strategy tests led that of the base-case defrost strategy tests.

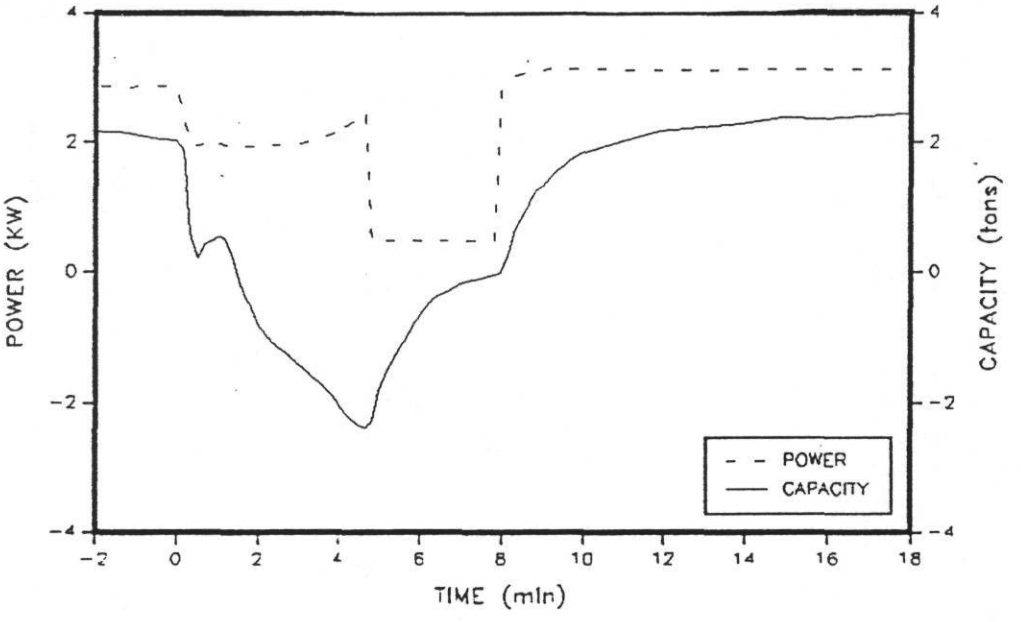

Fig. 7.18 Power Draw and Heating Capacity during Defrost Period
Two-Stage Defrost

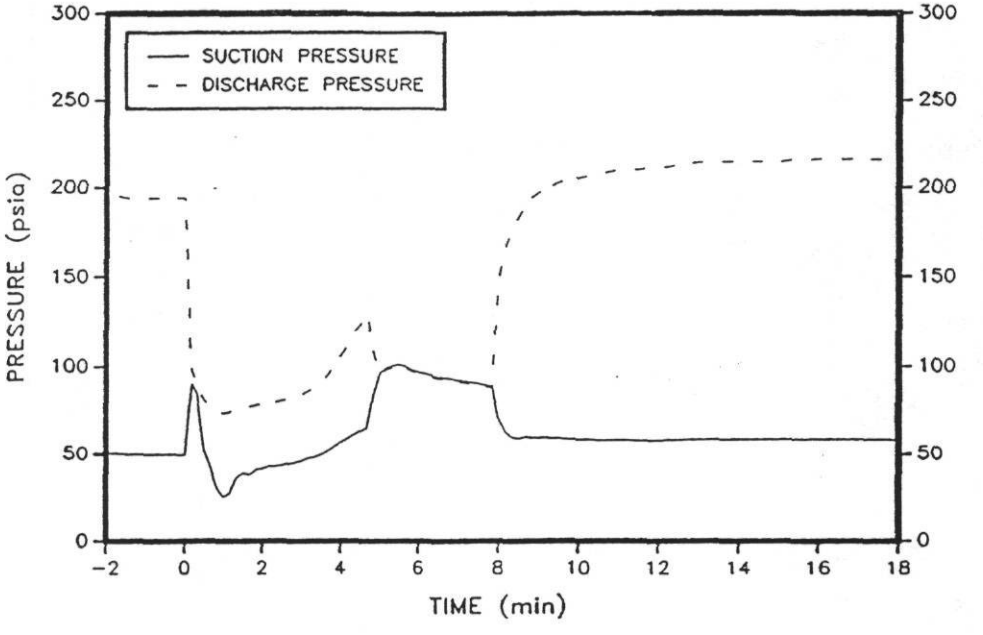

Fig. 7.19 Compressor Suction and Discharge Pressures during Two-Stage Defrost

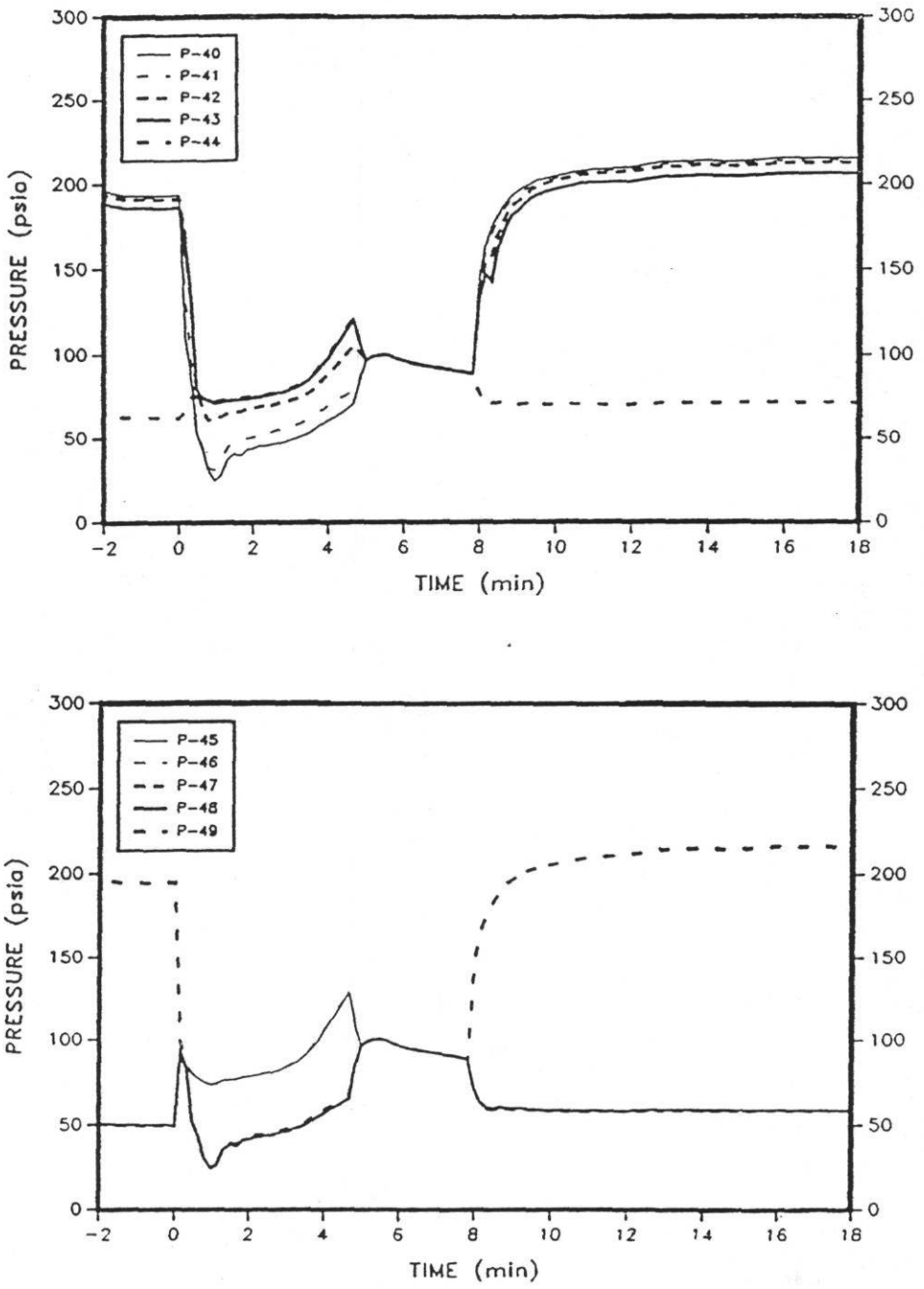

Fig. 7.20 System Refrigerant Pressures during Two-Stage Defrost

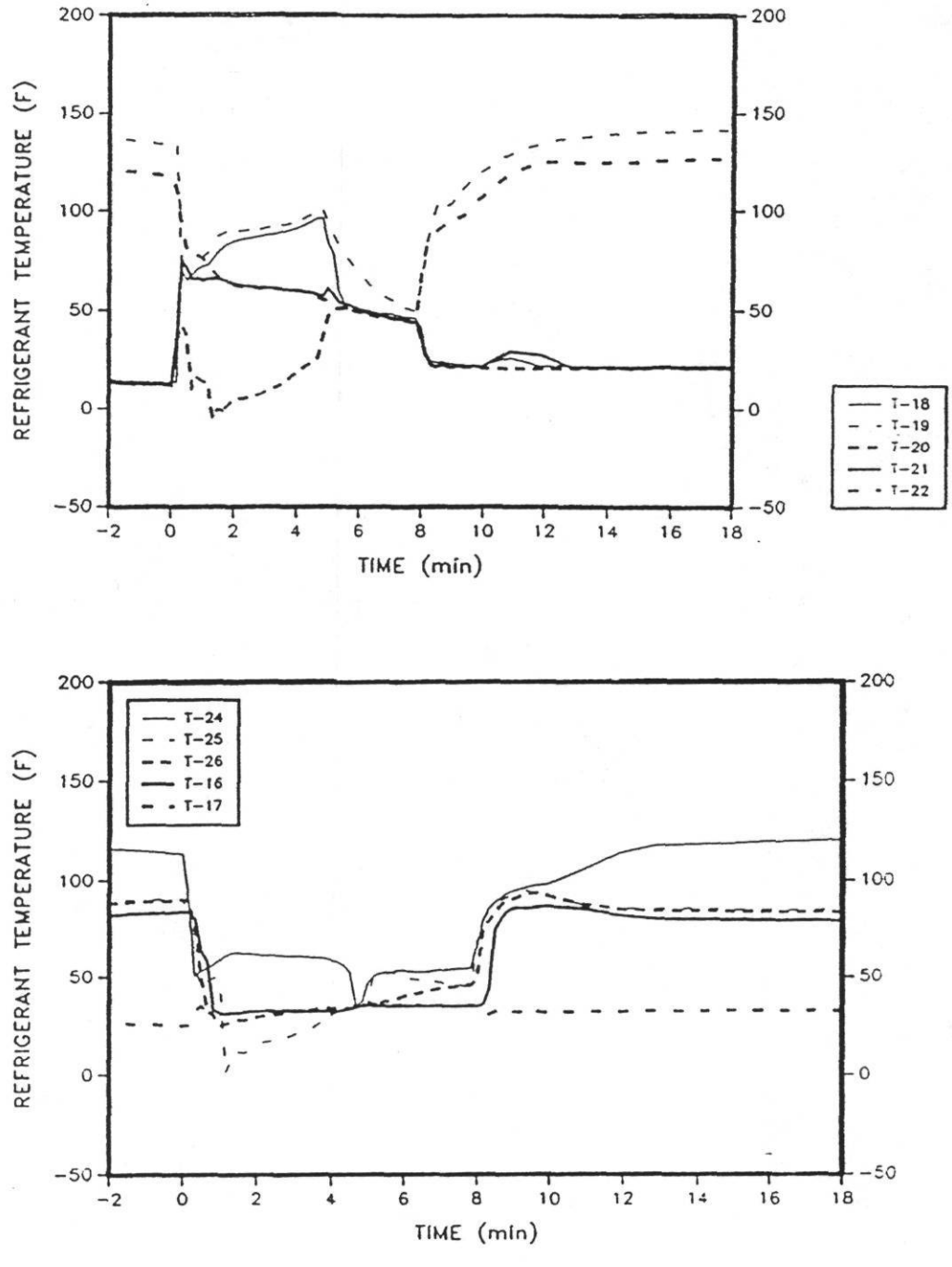

Fig. 7.21 System Refrigerant Temperatures during Two-Stage Defrost

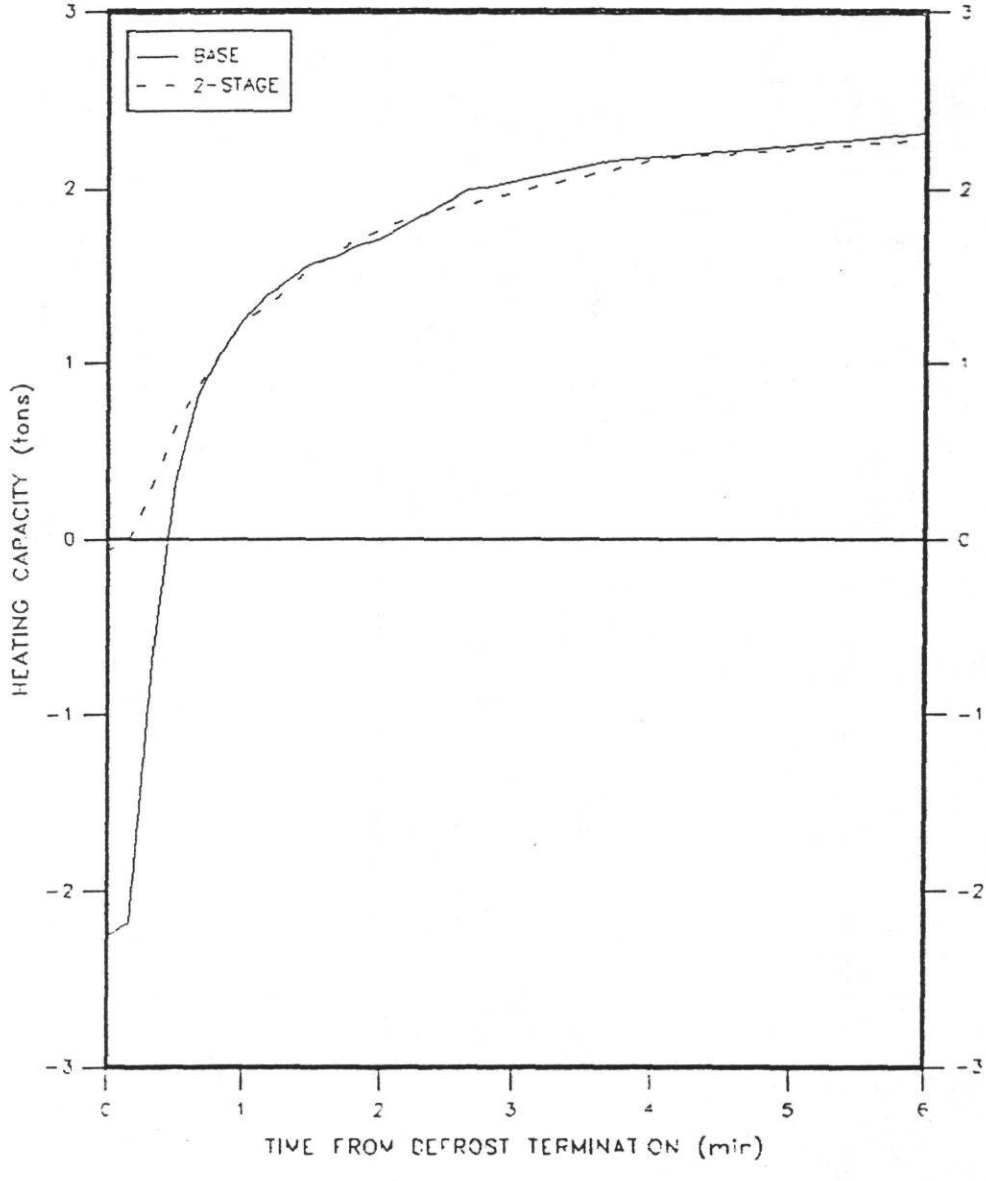

Fig. 7.22 Capacity Recovery following Base-Case and Two-Stage Defrosts

SUMMARY

Tests of alternative defrost strategies to the base case were discussed in this chapter. These tests included 20, 40, 60 second fan prestart tests, 45-second fan delay tests an indoor fan off test, and two-stage defrost tests. In addition, tests involving replacement of the 3.0 ton capacity base-case compressor with a 2.5 ton compressor were done.

The two-stage defrost strategy tests had a cyclic average COP that was 7% higher than that of the base-case tests. The fan pre-start defrsot strategy tests showed a reduction in the rate of pressure transients at defrost termination. It was felt that the indoor fan off strategy to be not a viable option.

CHAPTER 8

CONCLUSIONS AND RECOMMENDATIONS

The focus of this investigation was on the transient performance of an air-to-air heat pump during the defrost cycle. The relevant literature was first surveyed to evaluate what work had been done in analyzing the defrost cycle and help provide information on possible avenues of investigation. A research plan was developed, an experimental apparatus was then constructed, and data collected. The experiments were performed on a 3 ton air-to-air heat pump which was instrumented and installed in the two psychrometric rooms at the Energy Systems Laboratory at Texas A & M University. A base configuration was designated for the defrost expansion device, compressor size and defrost strategy. Alternate expansion devices, one alternate compressor, and several alternate defrost strategies were tested to evaluate their effect on the performance of the unit during the defrost cycle. Major conclusions and recommendations from this study are listed below.

Conclusions

Any conclusions from this study must be tempered by the fact that the experimental work was done using one heat pump. This heat pump was manufactured by a company to have a specific performance. While many of the characteristics observed and measured may be similar to that of other units, their magnitudes may differ substantially. Unfortunately, this limitation is generic to any study in which only one piece of equipment is studied.

The thermal expansion valves appear to be well suited as defrost expansion devices because of their ability to vary orifice size in respond to changing conditions in the system. During the early minutes of the defrost cycle, the high superheat at the outlet of the indoor coil kept the TXVs in a wide open position during much of the melt phase of the defrost cycle. Maintaining a wide open position provided for larger refrigerant flows, which speeded the defrost. As the outdoor coil cleared of frost, the TXV responded by dropping the flow rate.

The speed of the thermal expansion devices had little impact in the overall performance of the heat pump during the defrost cycle. While the slowest responding TXV provided more stable control of the refrigerant flow during defrost, it had a slightly longer defrost cycle and lower COP than the fastest responding TXV.

The response of the TXV in the system appeared to be as much a function of minor changes in how the bulb was attached to the refrigerant tubing as it was on the internal response time of the TXV. Our tests indicated that even though a technician may place the same bulb in the same location on a refrigerant tube using the same attachment procedure, the bulb can respond differently each time. There were apparently enough differences in contact surface area, tightness of the bulb to the tubing, etc., that exact repeatability from run to run may not be possible. The major differences among different runs with the same TXV were the refrigerant dynamics. System performance did not vary significantly with bulb attachment.

Orifice size was a major factor in influencing the defrost time and the integrated COP of the frosting/defrost cycle. The orifices showed a trend of faster defrost times as the orifice diameter was increased. The faster times were the result of increased refrigerant flow with the larger orifices.

It appeared that orifices must be sized carefully for use during the defrost cycle. The smallest orifice (0.059 inch diameter) in this study restricted refrigerant flow so severely during the first minutes of the defrost cycle that the compressor pulled a partial vacuum on the suction line. In addition, the smallest orifice had defrost times that were significantly longer than the 0.070 inch diameter orifice. On the opposite end, the larger orifices appeared to produce liquid "slugging" in the compressor for a short interval at the end of the melt period because of the large mass flows they had established in the system.

Pre-starting the fan before defrost termination provided substantial benefits in reducing the pressure spikes in the discharge and suction pressures when the reversing valve was engaged. The 20 second pre-start provided the best combination of pressure reduction and coefficient in performance.

While a fan delay had better capacity recovery after defrost termination than the base case, it had major drawbacks that would make it a less desirable alternative to the base case. First, the COP was lower for the fan delay than for the base. Second, both the discharge and suction pressure spikes at defrost termination increased over the base case.

Shutting off the indoor fan during the defrost cycle would require selecting a different defrost termination criteria than used in this study. With no airflow over the indoor coil, the unit was not able to produce enough capacity for the exiting refrigerant temperature of the

outdoor coil to reach 65 F. In addition, this mode of operation produced flooding in the compressor for several minutes in defrost cycle.

The two-stage defrost cycle produced the largest increase in COP of the defrost strategies or hardware studied. In addition, the two-stage defrost eliminated the pressure spikes at defrost termination experienced in the base case.

Recommendations

If the characteristics of heat pumps undergoing the reverse cycle defrost are going to be adequately characterized, it would seem important that more than one system be studied. Testing other systems could show "generic" characteristics of the defrost cycle as opposed to those that may be specific to a particular system. It is recommended that one or two other systems be instrumented and examined in as much detail as the one in this study.

While performing the testing, several ideas for improving the test setup were developed to better track refrigerant migration during the defrost. The accumulator should have some type of level indicator to allow precise measurement of liquid level in the accumulator. The accumulator used in this study had sight glasses in it. These did not allow for precise measurement of liquid level. Another change would be the installation of another refrigerant flow meter between the compressor and the accumulator. Refrigerant flow was monitoredat the outlet of the outdoor coil. During the defrost transient, refrigerant flow varies in different parts of the system. Multiple metering would provide better information on the unsteady flow distribution in the system.

The two-stage defrost appears to be a defrost strategy that should be further investigated. It improved the COP and the pressures in the discharge and suction lines at defrost termination. There is probably an optimal time for initiation of the second stage and for the unit to be shutdown after melting the frost from the outdoor coil. These times are probably dependant on factors such as the ambient air temperature, humidity, wind velocity, etc. Further study of this method might yield results that are even better than those demonstrated here.

It is recommended that fan pre-start be incorporated in heat pump defrost termination schemes. The reduction in pressure spikes at defrost termination should reduce noise in the refrigerant lines as well as reliability of discharge and suction valves in the compressor.

This study did not consider the use of an electronic expansion valve (EEV) for use in the defrost cycle. Because EEVs can be driven by a "smart" algorithm, it may be possible to have an EEV vary its opening and closing to optimize performance during the defrost cycle.

APPENDICES

REFERENCES

1. American Society of Heating, Refrigeration and Air-Conditioning Engineers, ASHRAE Handbook: 1985 Fundamentals, pp. 1.4. 1985.

2. "Standard for Unitary Heat Pump Equipment", Standard No 240-76, The Air-Conditioning and Refrigeration Institute, Arlington, VA.

3. Didion, David A.; and Kelly George E., "New Testing and Rating Procedures for Seasonal Performance of Heat Pumps," ASHRAE Journal, Vol. 21, No. 9: pp. 40-44, September, 1979.

4. Baxter, V.D.; Abbatiello, L.A.; and Minturn, R.E., "Comparison of Field Performance to Steady State Performance for Two Dealer-Installed Air-to-Air Heat Pumps," ASHRAE Transactions, Vol. 88, Part 2:941-953, 1982.

5. Wildin, M. W.; Fong, A.; Wilson, C.; and Nakos, J., "Analysis of the Effects of Cycling on Energy Use of Installed Air-to-Air Heat Pumps in Albuquerque, New Mexico." Third Annual Heat Pump Technology Conference, Oklahoma State University, April 1978.

6. Goldschmidt, V.W.; and Hart, G.H., "Heat Pump System Performance: Experimental and Theoretical Results", ASHRAE Transactions, Vol. 88, Part 1: pp. 479-488, 1982.

7. Bittle, B.B.; and Goldschmidt, V.W., "Effect of Cycling and Frost Formation on Heat Pump Performance", ASHRAE Transactions, Vol. 89, Part 2: pp. 743-754, 1983.

8. Baxter, V.D.; and Moyers, J.G., "Air-Source Heat Pump: Field Measurement of Cycling, Frosting and Defrosting Losses", ORNL/CON - 150, 1981-83.

9. Tanaka, N.; Yamanaka, G.; and Ikeuchi M., "Experimental Study on the Dynamic Characteristics of a Heat Pump:, ASHRAE Transactions, Vol. 88, Part. 2, 1982.

10. Miller, W.A., "Laboratory Examination and Seasonal Analysis of Frosting and Defrosting for an Air to Air Heat Pump", ASHRAE Transactions, Vol. 93, Part. 1, 1987.

11. Mulroy, W.J., "The Effect of Short Cycling and Fan Delay on the Efficiency of a Modified Residential Heat Pump", ASHRAE Transactions, Vol. 92, Part 2: pp. 813-826, 1986.

12. Young, David J., "Development of a Northern Climate Residential Air-Source Heat Pump", ASHRAE Transactions, Vol. 86, Part 1: pp. 671-686, 1980.

13. Miller, W.A., "Frosting Experiments for a Heat Pump Having a One-Row Spine-Fin Outdoor Coil", ASHRAE Transactions, Vol. 90, Part 1: pp. 1009-1025, 1984.

14. Trask, Allen, "The Heat Pump Defrost Problem", Fifth Annual Heat Pump Technology Conference, Oklahoma State University, April, 1980.

15. West, James E., "Defrosting Air to Air heat Pumps Present and Future", Fourth Annual Heat Pump Technology Conference, Oklahoma State University, April, 1979.

16. Department of Energy (DOE) - Test Procedures for Central Air Conditioners, Including Heat Pumps (1979)

17. "Laboratory Methods of Testing Fans for Rating", ANSI/ASHRAE Standard 51-1985 (ANSI/AMCA 210-85).

18. "Methods of Testing for Seasonal Efficiency of Unitary Air-Conditioners and Heat Pumps", ANSI/ASHRAE Standard 116-1983.

19. American Society of Heating, Refrigeration and Air-Conditioning Engineers, ASHRAE Handbook: 1985 Fundamentals, pp. 5.4-5. 1985.

20. Kartsounes, G.T.; and Erth R.A., "Computer Calculation of the Thermodynamic Properties of Refrigerants 12, 22, and 502," ASHRAE Transactions, pp. 88-103, 1971.

21. American Society of Heating, Refrigeration and Air-Conditioning Engineers, ASHRAE Handbook: 1988 Equipment, pp. 3.2-3.3, 1988.

22. Krakow, K.I.; and Lin S., "Refrigerant Flow Through Orifices", ASHRAE Transactions, Vol. 94, Part. 1, 1988.

23. American Society of Heating, Refrigeration and Air-Conditioning Engineers, ASHRAE Handbook: 1988 Equipment, pp. 19.26, 1988.

24. W.F. Stoecker, J.J. Lox, Jr., R.J. Kooy, "Energy Considerations in Hot-Gas Defrosting of Industrial Refrigeration Coils", ASHRAE Transactions, Vol. 89, Part 2A, 1983.

APPENDIX A

Refrigerant and Moist Air Property Calculations

Experimental data used in the calculation of moist air thermodynamic properties included dry bulb and wet bulb temperatures of the indoor air and dry bulb and dew point temperatures of the outdoor air as well as the ambient barometric pressure. Data used in the calculation of refrigerant 22 thermodynamic properties at a given location in the refrigerant circuit included pressure and temperature of the refrigerant at that location. Properties which were calculated were enthalpy and density of the moist air for capacity and flow rate calculations, and saturation temperature and enthalpy of the refrigerant for state determination and capacity calculations as well. Procedure used in these property calculations are discussed in this appendix.

Moist air thermodynamic properties were calculated with computer subroutines developed from perfect gas relations presented in the ASHRAE Fundamentals, 1985 [1]. Capabilities provided by the routines included computation of specific volume of the moist air and enthalpy of the air when given dry bulb and wet bulb or dew point temperatures.

Refrigerant thermodynamic properties were computed using computer routines written by Kartsonnes and Erth [20]. These routines permitted a state evaluation to determine if the refrigerant was subcooled, saturated, or superheated. For example, for a given refrigerant pressure the saturation refrigerant temperature was computed and compared with the measured refrigerant temperature to determine the state. Routines were available to provide superheated refrigerant enthalpy as well as saturated vapor and liquid enthalpies.

APPENDIX B

Uncertainty Analysis

Capacity of the test heat pump was calculated during frosting/defrosting test periods using the enthalpy change of air flowing across the indoor coil and the flow rate of that air. An uncertainty analysis for a representative capacity calculation is given in the paragraphs which follow. The uncertainty analysis provides a measure of the maximum uncertainty expected in the calculated value of capacity. Data used in the analysis was taken from scan data collected during a base configuration heat pump test. Data from the specific scan selected for the analysis was recorded 41 minutes before defrost initiation of the test run. Run-time values used in the calculation of instantaneous heating capacity were:

entering air temperature - 70.0°F
exiting air temperature - 91.6°F
Flow chamber pressure drop - 1.3 in wg
Ambient wet bulb temperature - 49.5°F
Ambient barometric pressure - 30.19 in Hg

These data were used as inputs to a psychrometric property and nozzle flow rate program to obtain the following calculated values.

Air flow rate - 1249.5cfm
entering air enthalpy - 19.923 Btu/lbma
exiting air enthalpy - 25.135 Btu/lbma
specific volume of air - 13.838 ft^3/lbma

Air side capacity is calculated from the following equation:

$$ASCAP = \frac{60 * Q * (H_{out} - H_{in})}{(12000 * V_{out})} \qquad (B.1)$$

where:

ASCAP = air side capacity (tons)
Q = air flow rate (cfm)
h_{in} = entering air enthalpy (Btu/lbma)
H_{out} = exiting air enthalpy (Btu/lbma)
V_{out} = specific volume of air (ft^3/lbm)

The air-side capacity for the sample data was 2.353 tons.

Data taken from a given scan during heat pump testing constituted a single sample measure. Thus, the method of Kline and McClintock [B1] may be used to arrive at the uncertainty in a value calculated for a single sample

experiment such as air-side capacity data. According to the method, the uncertainty in the calculated value of a quantity, R, which is a function of n independent variables, $X_1, X_2, \ldots\ldots X_n$, is given by:

$$W_R = \left[\left(\frac{\partial R}{\partial X1} W_{X1} \right)^2 + \left(\frac{\partial R}{\partial X2} W_{X2} \right)^2 + \ldots + \left(\frac{\partial R}{\partial Xn} W_{Xn} \right)^2 \right]^{1/2} \qquad \text{(B.2)}$$

where:

W_R = uncertainty in the calculated value of R

W_{X1} = uncertainty in the value of X_1

W_{Xn} = uncertainty in the calculated value of X_n

Therefore, if the uncertainty in the variables, $X_1 \ldots X_n$, is known, then the uncertainty in the calculated value of R can be obtained. Equation B.2 can be used with Equation B.1 to write an expression for per unit uncertainty in air-side capacity. The resulting equation is of the form:

$$\frac{W_{ASCAP}}{ASCAP} = \left[\left(\frac{W_Q}{Q} \right)^2 + \left(\frac{W_{h-in}}{h_{out} - h_{in}} \right)^2 + \left(\frac{W_{h-out}}{h_{out} - h_{in}} \right)^2 \left(\frac{W_{v-out}}{v_{out}} \right)^2 \right]^{1/2}$$

where:

WASCAP = Uncertainty in calculated capacity

W_Q = Uncertainty in air flow rate

W_{h-in} = Uncertainty in entering air enthalpy

W_{h-out} = Uncertainty in exiting air enthalpy

W_{v-out} = Uncertainty in specific volume of air

Now, the problem is reduced to one of finding uncertainties in Q, h_{in}, h_{out}, and v_{out}. Air flow rate, Q, is measured in a nozzle flow chamber which meets ANSI/ASHRAE 51-1985 (ANSI/AMCA 210-85) specifications. Following recommendations in this standard, the uncertainty in air flow rate is found to be 1.4% of the calculated flow rate value.

As previously stated, the values of enthalpy and air specific volume were obtained from a computer program which utilized curve fits of psychrometric data and the ideal gas laws in a series of data reduction steps. The required input data included dry bulb temperature, wet bulb

temperature, and barometric pressure. The functional dependence of enthalpy and specific volume on the input data is complicated, making calculation of the partial derivations required in the Kline and McClintock equation difficult. If these partial derivatives could be found, then, for example, uncertainty in the calculated value of entering air enthalpy could be found from the following equation:

$$W_{h\text{-}in} = \left[\left(\frac{\partial h_{in}}{\partial \text{Bar Pr}} W_{\text{Bar Pr}} \right)^2 + \left(\frac{\partial h}{\partial \text{TDB}} W_{\text{TDB}} \right)^2 + \left(\frac{\partial h_{in}}{\partial \text{TWB}} W_{\text{TWB}} \right)^2 \right]^{1/2}$$

where:

Bar pr = ambient barometric pressure
TDB = dry bulb temperature entering coil
TWB = wet bulb temperature entering coil.

The uncertainties in these values are known to be:

$W_{BAR.pr} = 0.05$ inHg
$W_{TWB} = 0.5^{\circ}F$
$W_{TDB} = 0.5^{\circ}F$

Now, a procedure suggested by Holman [] may be used to find the necessary partial derivatives. This procedure is suited for finding the derivative dependence of a value computed by several data reduction steps (such as a computer program) on a given input value. In the example at hand,

$$h_{in} = f(\text{TWB, TDB, Bar Pr}) \qquad \text{(B.5)}$$

The partial derivative are numerically approximated by:

$$\frac{\partial h_{in}}{\partial \text{TWB}} \simeq \frac{f(\text{TWB}+\Delta\text{TWB,TDB,Bar Pr}) - f(\text{TWB,TDB,Bar Pr})}{\Delta\text{TWB}}$$

$$\frac{\partial h_{in}}{\partial \text{TDB}} \simeq \frac{f(\text{TWB,TDB} + \Delta\text{TDB,Bar Pr} - f(\text{TWB,TDB,Bar Pr}))}{\Delta\text{TDB}} \qquad \text{(B.6)}$$

$$\frac{\partial h_{in}}{\partial \text{Bar Pr}} \simeq \frac{f(\text{TWB,TDB,Bar Pr} + \Delta\text{Bar Pr}) - f(\text{TWB,TDB,Bar Pr})}{\Delta\text{Bar Pr}}$$

The necessary values for Equations B.6 were obtained by perturbating each input value 0.1%, then running the code to find h_{in}, and then using the original input values to find h_{in}, and finally computing the partial derivatives. Then these were combined in Equation B.4 to find the uncertainty in h_{in}. Using this procedure, the following uncertainties were found:

$$W_{h\text{-}in} = 0.302 \text{ Btu/lb}$$
$$W_{h\text{-}out} = 0.314 \text{ Btu/lb}$$
$$W_{v\text{-}out} = 0.0268 \text{ ft}^3\text{/lb}$$

These uncertainties are increased by a 0.7% uncertainty resulting from the use of ideal gas laws to obtain psychrometric properties of moist air. This small uncertainty may be additively combined with those listed above to obtain:

$$W_{h\text{-}in} = 0.4 \text{ Btu/lbma}$$
$$W_{h\text{-}out} = 0.5 \text{ Btu/lbma}$$
$$W_{v\text{-}out} = 0.1 \text{ ft}^3\text{/lbm}$$

These uncertainties, along with the uncertainty in air flow rate (1.4% of 1249.5 cfm) can be used in equation B.3 to obtain an uncertainty in calculated air-side capacity of 12 percent. Or,

$$\text{ASCAP} \simeq 2.35 \pm .28 \text{ tons}$$

The calculated uncertainty in air-side capacity represents the maximum amount by which the capacity could be expected to be in error. Instantaneous heating capacity calculated from refrigerant side data at the indoor coil was 2.485 tons. Ideally, air-side and refrigerant side capacities should match (energy balance). The discrepancy of only 5.6% between air and refrigerant side capacities a smaller probable error in air side suggests capacity calculation than the 12% obtained in the analysis. This is expected because a number of steps were taken to reduce the error that is magnified in the uncertainty analysis by the enthalpy difference terms in equation B.3. Such small differential measurements greatly increase the error of the individual measures. Steps taken to reduce the error in the temperature measurements used to obtain the enthalpy difference but not recognized in the uncertainty analysis include calibration of thermocouple reference junctions to the freezing point of water, use of 16 point thermocouple grids to measure upstream and downstream air temperatures, use of uniform extension wire and grid wire lengths, use of thermocouple wire from a common wire spool, use of flow mixers and straighteners before temperature measurement and thermometer verification of thermocouple measurements. All experimental test data values retained were observed to have less than 6% difference between air and refrigerant-side

capacity calculations as indicated in Figure B.1 for the base case run from which data was taken for this analysis. This energy balance criteria satisfies ASHRAE standard 116-83 for testing of unitary air-conditioners and heat pumps.

Table B.1 - Summary of Uncertainty Calculation for Air-Side Capacity

QUANTITY	UNCERTAINTY	SYMBOL	SOURCE
Barometric Pressure	0.05 in HG	W_{EF}	1/2 Scale Increment (Calibrated as well)
Wet Bulb Temperature	$0.5^{o}F$	W_{WG}	1/2 Scale Increment (Dry Reading Check)
Dry Bulb Temperature	$0.5^{o}F$	W_{DB}	Data Calibration
Entering Air Enthalpy	0.4* Btu/lbma	W_{HI}	W_{WB}, W_{DB}, W_{BP} Kline & McClintock Eq
Exiting Air Enthalpy	0.5* Btu/lbma	W_{HO}	W_{WB}, W_{DB}, W_{BP} Kline & McClintock Eq
Specific Volume of Air	0.1 ft^3/lb	W_{V}	W_{WB}, W_{DB}, W_{BP} Kline & McClintock Eq
Air Flow Rate	1.4%	e_{Q}	ASME Flow Nozzles AMCA Calculation
Air-Side Capacity	12%	e_{AC}	W_{HI}, W_{HO}, W_{V}, e_{Q} Kline & McClintock Eq

* Includes 0.7% error from perfect gas equations

Note: W_X = Absolute uncertainty in X (with associated units)

e_X = Per unit uncertainty in X (expressed as a percentage)

$$= \frac{W_X}{X}$$

APPENDIX C

Equipment Used in the Testing Apparatus.

EQUIPMENT	SIZE/ RANGE	MAKE/MODEL	ACC.[1]
HEAT PUMP[2]	3 TON	PAYNE/544AJ036	
COMPRESSOR	3 TON	TECUMSEH/AV5535E	
ACCUMULATOR	163 OZ	TECUMSEH/51066-1	
OUTDOOR FAN	1/10 HP		
DATALOGGER	65 CHAN	ACUREX/AUTODATA	
WATT/WATT-HOUR TRANSDUCER	20 KW	OHIO SEMITRONICS/W-53	0.5%
PRESSURE TRANSDUCER	0-300psig	FOXBORO/1225-12G-K42	0.5%
DIFF.PRESSURE TRANSDUCER	0-2 INWG	CELESCO/LCCD 110 (CD) LCVR (TRANS)	0.1%
FLOW METER	0-26 LBPM	MICRO-MOTION/D-12	0.3%
DEW POINT SENS.	0-100°F	GENERAL EASTERN/DEW-10	0.5°F
THERMOCOUPLES	30 AWG	OMEGA/TYPE T	0.5°F

[1] Percentages are percent of span or range. Temperatures are deviations (+/-).

[2] Original unit supplied for testing. The modifications to the original unit included using a different indoor coil, installing a different accumulator, and replumbing of the refrigerant lines.